

Charles University
Faculty of Science

Biology
Immunology



Bc. Marta Šlaufová

The tumor immune microenvironment and its crosstalk with kallikrein-related peptidases
in mammary carcinoma of a mouse model

Vzájemné interakce mezi nádorovým mikroprostředím a kalikreinovými proteázami v
myším modelu karcinomu mléčné žlázy

Diploma thesis

Supervisor: Mgr. Petr Kašpárek, Ph.D.

Prague, 2021

Prohlášení:

Prohlašuji, že jsem závěrečnou práci vypracovala samostatně a že jsem uvedla všechny použité informační zdroje a literaturu. Tato práce ani její podstatná část nebyla předložena k získání jiného nebo stejného akademického titulu.

V Praze, 26. 04. 2021

Podpis:

Acknowledgments

I would first like to thank Petr Kasparek, whose expertise and research questions shaped this project. I also thank him for the opportunity to work under his leadership since my bachelor's studies and for the friendly environment he provided me with. I'm very grateful to Radislav Sedlacek, who let me work on my diploma project at the Czech Centre for Phenogenomics at the Institute of Molecular Genetics of the Czech Academy of Sciences. I want to express big thanks to Olga Zbodakova, Silvia Petrezselyova, and Jan Elias for their patience, critical comments, and help during the experimental part of this project. My thanks also belong to Jana Balounova and Kristina Vicikova for their kind help with tumor-infiltrating leukocytes analysis and Petra Kralova, Andrea Hojna, Ana Rita da Silva Oliveira, and Kristyna Hornova for their assistance while *in vivo* experiments. Finally, I would like to thank Daniel Palous and my loving family who supported me.

Abstract

Breast cancer is the most common cancer type with a high annual death rate. Finding meaningful tissue-related or body-fluid-accessible biomarkers is necessary to characterize cancer subtype, predict tumor behavior, choose the most effective therapy, predict severe treatment-related toxicities, and also the opportunity to personalize treatments for each patient. There is increasing evidence that various kallikrein-related peptidases (*Klk*) gene family members can modulate the immune response and are differentially regulated in breast cancer, and therefore are proposed to be potential prognostic biomarkers. This work established and validated an experimental setup to study the roles of selected kallikrein-related peptidases (KLK5, KLK7, KLK14) in breast cancer *in vivo* using gene-deficient mouse models previously generated in our laboratory. We used the CRISPR/Cas9 (clustered regularly interspaced short palindromic repeats) editing system to generate several E0771 cell line-based reporter and gene-deficient cell lines. These allowed enhanced monitoring of cancer progression *in vivo* and studying KLKs roles in tumor immune microenvironment of C57Bl/6N mice. Finally, we present the analysis of the initial *in vivo* experiments using these tools combined with established *Klk*-deficient mouse models. Our results support the evidence of KLK5, KLK7, and KLK14 roles in tumor progression and highlight the activation of the interleukin 1 β pathway in these processes.

Key words: mammary carcinoma, kallikrein-related peptidases, IL-1 β , PAR2, C57Bl/6, E0771, fluorescent proteins, nanoLuciferase, CRISPR/Cas9

Abstract (CZ)

Celosvětově je nejběžnějším typem rakoviny je rakovina prsu, jež je současně spojena s vysokou smrtností. Nalezení vhodných prognostických ukazatelů je důležitým aspektem pro bližší určení, o jaký typ rakoviny prsu se jedná a jaký průběh onemocnění lze u pacienta očekávat. Je známo, že kalikreinové proteázy jsou při rakovině prsu dysregulovány, a proto se spekuluje o jejich využití jako prognostických ukazatelů. Jejich schopnost ovlivňovat imunitní odpovědi včetně té protinádorové je též diskutována. Tento diplomový projekt využívá technologie CRISPR-Cas (clustered regularly interspaced short palindromic repeats) ke genetické editaci myší buněčné linie rakoviny prsu E0771. Geneticky modifikované linie E0771 jsou v projektu využívány ke studiu vzájemných interakcí mezi nádorovým mikroprostředím a kalikreinovými proteázami (KLK5, KLK7, KLK14) v C57Bl/6 myším modelu karcinomu mléčné žlázy. Diplomová práce přináší výsledky analýzy první části “*in vivo*” experimentů využívajících vytvořené geneticky modifikované buněčné linie v kombinaci se zavedenými myšími modely nesoucími mutace v genech pro zmíněné kalikreinové proteázy. Z předběžných výsledků tohoto diplomového projektu vyplývá, že zmíněné kalikreinové proteázy hrají roli při vývoji rakoviny prsu v použitém myším modelu a výsledky poukazují na možnou funkci těchto proteáz skrz aktivaci interleukinu 1 β .

Klíčová slova: karcinom mléčné žlázy, proteázy kalikreinového typu, PAR 2, IL-1 β , E0771, C57BL/6, fluorescenční proteiny, nanoLuciferáza, CRISPR/Cas9

Table of Contents

Acknowledgments	3
Abstract	4
Abstract (CZ).....	5
List of abbreviations.....	9
1 Introduction.....	11
2 Literature overview.....	12
2.1 Breast cancer	12
2.2 Experimental models in breast cancer.....	14
2.2.1 <i>In vitro</i> models in breast cancer.....	14
2.2.2 <i>In vivo</i> models in breast cancer.....	15
2.2.3 <i>In silico</i> models in breast cancer.....	18
2.3 Tumor microenvironment.....	18
2.3.1 Tumor non-immune microenvironment	19
2.3.2 Tumor immune microenvironment – cancer-immunity cycle.....	20
2.3.3 Proteinase-activated receptor 2.....	23
2.3.4 Interleukin-1 beta.....	26
2.3.5 Cathelicidin LL-37	28
2.4 Kallikreins – an overview.....	30
2.4.1 Physiological function.....	30
2.4.2 Pathophysiological function	31
2.4.3 Kallikreins as prognostic markers in breast cancer	31
2.4.4 Kallikreins influencing the immune system	34
2.5 Possible crosstalk of kallikreins, immune system, and tumor microenvironment.....	35
2.6 Breast cancer therapies	37
3 Materials and methods.....	39

3.1	Materials	39
3.1.1	Animals	39
3.1.2	Cell cultures	39
3.1.3	Antibodies	40
3.1.4	Primers	41
3.1.5	CRISPR guide RNAs	42
3.1.6	Plasmids	44
3.2	Methods	45
3.2.1	Transfection of E0771 cells	45
3.2.2	Isolation of tumor tissues	45
3.2.3	Flow cytometry	45
3.2.4	Subcutaneous injection of tumor cells	48
3.2.5	Mammary gland fat pad injection	48
3.2.6	Luminescence detection via plate reader	49
3.2.7	<i>In vivo</i> imaging	49
3.2.8	RNA isolation	49
3.2.9	Quantitative real-time polymerase chain reaction (qRT-PCR)	50
3.2.10	Protein isolation and detection – Western blot	51
3.2.11	PCR and PAGE	52
3.2.12	Fluorescence-activated cell sorting (FACS)	52
3.2.13	Statistical analysis	53
4	Results	54
4.1	The E0771 cell line is a suitable cell line model for orthotopic cell line-derived allograft experiments in C57Bl/6N mouse strain	55
4.2	Evaluation of various markers for <i>in vivo</i> imaging in murine breast cancer model	56
4.2.1	Fluorescent markers	57
4.2.2	Luminescent markers	63

4.3	Growth of Actb-mCH E0771 cell line in C57Bl/6N mice deficient for <i>Klk5</i> , 7, and 1467	
4.4	Analysis of tumor samples	67
4.4.1	qRT-PCR analysis	68
4.4.2	Western blot analysis.....	69
4.4.3	Flow cytometry analysis of tumor-infiltrating leukocytes (TIL).....	70
4.5	Generation of <i>Klk5</i> , <i>Klk7</i> , <i>Klk14</i> , <i>Il1b</i> , and <i>F2r11</i> deficient E0771 cell lines.....	74
4.5.1	Design and preparation of CRISPR/Cas9 vectors	74
4.5.2	Evaluation of randomly selected knock-out E0771 clones by PCR and PAGE	75
4.5.3	Evaluation of potential knock-out E0771 clones by sequencing.....	76
4.5.4	Evaluation of validated <i>Klk5</i> and <i>Klk7</i> knock-out E0771 clones by qRT-PCR analysis	78
5	Discussion.....	79
6	Conclusions, benefits, and prospects for the future	86
7	References.....	88

List of abbreviations

Actb - Beta-actin gene

BRCA - Breast Cancer gene

CAF - Cancer-associated fibroblast

CCL - C-C motif chemokine ligand

CRISPR/Cas9 - Clustered regularly interspaced short palindromic repeats / CRISPR-associated protein 9

CXCL – C-X-C motif chemokine ligand

CXCR - C-X-C motif chemokine receptor

DC - Dendritic cell

ECM - Extracellular matrix

EGFP –Enhanced Green Fluorescent Protein

ER - Estrogen Receptor

EYFP – Enhanced yellow fluorescent protein

F2rl1 – Protease-activated receptor 2 gene

GAPDH - Glyceraldehyde 3-phosphate dehydrogenase

GFP – Green fluorescent protein

HER2 - Human Epidermal Growth Factor Receptor 2

IFN- γ - Interferon-gamma

IL – Interleukin

IL-1 β - Interleukin-1 beta

Il1b - Interleukin-1 beta gene

I κ B- ζ - NF-kappa-B inhibitor zeta

iRFP670 – Near-infrared fluorescent protein 670

KLK - Kallikrein-related peptidase

Klk - Kallikrein-related peptidase gene

KO – Knock-out

LL-37 - Cathelicidin Antimicrobial Peptide LL 37

MAPK - Mitogen-activated protein kinases

mCherry – mCherry red fluorescent protein

mCRAMP – Mouse cathelicidin related antimicrobial peptide

MDSC - Myeloid-derived suppressor cell

MHC – Major histocompatibility complex

mTBFP2 – Blue fluorescent protein

NF- κ B - Nuclear factor kappa-light-chain-enhancer of activated B cells

NK - Natural killer cell

NKT - Natural killer T cell

NLSsfEGFP – Nucleus localization signal super folded enhanced green fluorescent protein

PAR2 - Protease-activated receptor 2

PD-L1 - Programmed death-ligand 1

PDX - Patient-derived xenograft

PR - Progesterone Receptor

Prdx1 - Peroxiredoxin 1 gene

PSA - Prostate-specific antigen

TAM - Tumour-associated macrophage

TAN - Tumour-associated neutrophil

TGF- β - Transforming growth factor- β

TIME - Tumour immune microenvironment

TIR - Toll-interleukin receptor

TME - Tumour microenvironment

Treg - Regulatory T cell

VEGF - Vascular endothelial growth factor

wt – Wild-type

1 Introduction

Breast cancer is the most frequent cancer in women, with an incidence of nearly 2.1 million cases worldwide in the year 2018 (Ferlay et al., 2019). Anyway, it should be mentioned that it affects even men, though it is with less frequency. Due to its heterogeneity, it shows highly variable clinical behavior and response to treatment, and thus the direction of therapeutic strategies leads up to a precision approach. Finding meaningful tissue-related or body-fluid-accessible biomarkers is necessary to characterize cancer subtype, predict tumor behavior, choose the most effective therapy, predict severe toxicity related to treatment, and better tailoring of treatment to patients.

Some of the kallikrein-related peptidases (KLK5 and KLK7) have clinical significance in breast cancer. Their dysregulation can be used as a prognostic biomarker in a clinic and subtype classification (Li et al., 2009). The same and even other kallikrein-related peptidases (KLK14) seem to have a role in modulating various immune responses and inflammation (Briot et al., 2009; Kasperek et al., 2017; Nylander-Lundqvist and Egelrud, 1997; Yamasaki et al., 2006). There is some evidence that the immune response is modulated by the proteolytic effect of these peptidases on some of the chain links in the immune signaling. Some of these links have an essential role in anti-tumor immune response in breast cancer, such as cytokine interleukin-1 beta (IL-1 β) (Kaplanov et al., 2019; Tulotta et al., 2019), by protease-activated receptor 2 (PAR2) (Carvalho et al., 2018; Su et al., 2009), and antimicrobial peptide cathelicidin (LL-37) (Chen et al., 2018; Filippou et al., 2016). There is a need to elucidate the anti-tumor immune response processes at the tumor site as the immunotherapy of this disease is on its rise.

This work aims to establish an experimental model for studying crosstalk of kallikrein-related peptidases with breast cancer tumor immune microenvironment (TIME). For these purposes, use the high translational value of E0771 cell-line derived orthotopic allograft in the established various kallikreins-deficient mouse models.

2 Literature overview

The literature overview highlights the most relevant processes and mechanisms for the crosstalk of kallikrein-related peptidases (KLKs) with breast cancer TIME. The outline is divided into seven main chapters. The first chapter briefly summarizes breast cancer disease characterization and classification. The second chapter describes the experimental models used for breast cancer research. The third chapter deals with the tumor immune TIME and anti-tumor immunity with an accent on selected immunomodulatory molecules (IL-1 β , PAR2, and LL-37). Chapter number four provides an overview of current knowledge about the function and prognostic value of KLKs in breast cancer. The last two chapters outline our hypothesis about possible crosstalk of KLKs, immune system, and tumor microenvironment (TME) and the existing therapies used in breast cancer patients.

2.1 Breast cancer

Cancers, including breast cancer, are very heterogeneous diseases characterized by the accumulation of an unpredictable number of genetic modifications and the deficit of standard cellular regulatory mechanisms (Tian et al., 2011). Thus, it requires distinct therapeutic strategies, and their use and efficacy still critically depend on further classification. Breast cancer can be divided into categories according to various criteria, such as the histopathological type, the number of regional lymph nodes with metastases, the grade, the stage, *BRC A* (Breast Cancer gene) mutations, and the molecular expression profile. (Fig. 1.) Such specification determines the most suitable therapeutic strategy and predicts the expected outcomes. For purposes of this diploma thesis, molecular characterization is the most relevant parameter.

Belonging to distinct immunophenotypes is mainly based on an assessment of the expression level of genes of three receptors: estrogen receptor (ER), progesterone receptor (PR), and human epidermal growth factor receptor 2 (HER2).

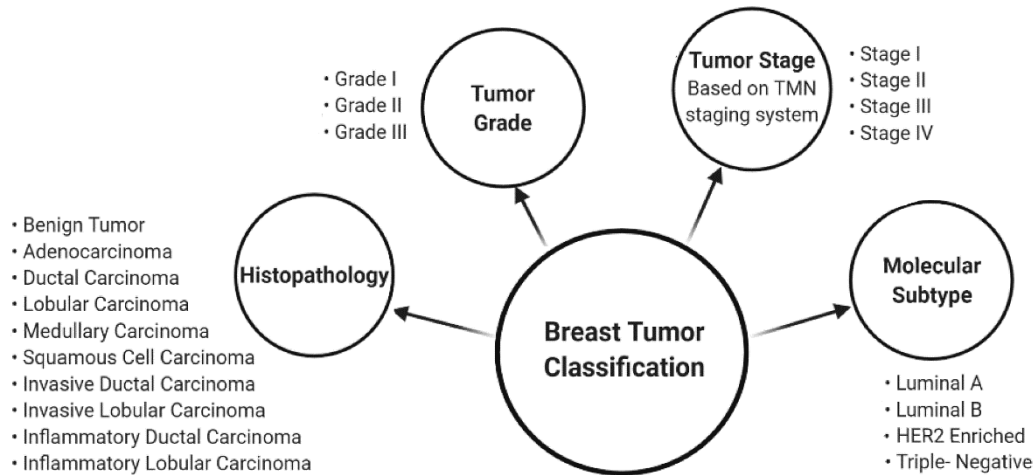


Figure 1. Schema of the breast cancer classification; HER2 - Human epidermal growth factor receptor 2; TMN - internationally accepted standard for cancer staging; (Costa et al. 2020)

ER and PR are both steroid receptors involved in developing mammalian breast epithelium, which undergoes multiple remodeling cycles during the reproduction period (Anderson and Clarke, 2004). ERs are responsible for ductal elongation and morphogenesis (Mallepell et al., 2006) and PRs for side-branching and lobuloalveolar development (Brisken et al., 1998). When these receptors are expressed on breast cancer cells, it indicates this subtype's responsiveness to hormonal therapy. Avoiding estrogen and progesterone from binding to the receptors can slow down tumor growth (Tsang and Tse, 2020). HER2 belongs to the ErbB family of receptor tyrosine kinases which are also essential regulators of mammary gland development (Gutierrez and Schiff, 2011). Its amplification was shown to be important in the pathogenesis and progression of human breast cancer (Slamon et al., 1987).

At least six molecular subtypes of breast cancer are distinguished according to their expression profile. These are normal breast-like, luminal A, luminal B, basal-like, claudin-low, and HER2 overexpressing subtypes (Testa et al., 2020). These subtypes can be further characterized using previously mentioned important functional markers ER, PR and HER2. (Tab. 1.)

Subtype	Gene Profile	Molecular Findings	IHC Phenotype
Luminal A	High expression of luminal epithelial genes and ER-related genes	Mutations in <i>PI3KCA</i> , <i>MAPK3K1</i> , and <i>GATA3</i>	ER ⁺ , PR ^{≥20%} , HER2 ⁻ , Ki67 ^{low}
Luminal B	Lower expression of luminal epithelial and ER-related genes, higher level of proliferation, and HER2-related genes than luminal A	Like luminal A but with a higher prevalence of p53 and RB pathways inactivation	ER ⁺ , PR ^{<20%} / or HER2 ^{+/or} Ki67 ^{high}
HER2-OE	High expression of HER2-related genes; low expression of ER-related genes	HER2 amplicon and EGFR/HER2 signal protein signature	ER ⁻ , PR ⁻ , HER2 ⁺
Triple-Negative	High expression of basal epithelial and proliferation genes; low expression of HER2-related and ER-related genes	Mutations in <i>TP53</i> ; losses in <i>RB1</i> and <i>BRCAl</i> ; amplification of <i>MYC</i> ; high PI3K/AKT activation	ER ⁻ , PR ⁻ , HER2 ⁻

Table 1. Overview of different molecular breast cancer subtypes; AKT - Protein kinase B (PKB); *BRCAl* - Breast cancer type 1 gene; EGFR - Epidermal growth factor receptor; ER - Estrogen receptor; *GATA3* - GATA3 transcription factor gene; HER2 - Human epidermal growth factor receptor 2; HER2-OE - HER2 overexpressing; Ki67 - Proliferation-associated nuclear antigen; *MAPK3K1* - Mitogen-activated protein kinase kinase kinase 1 (MAP3K1) gene; *MYC* - Myc family of proto-oncogenes; *PI3KCA* - Phosphatidylinositol 3-kinase (PI3K) gene; PR - Progesterone receptor; p53 - Tumor protein p53; RB - Retinoblastoma protein; *RB1* - Retinoblastoma protein gene; *TP53* - Tumor protein p53 gene; (Tsang and Tse, 2020)

2.2 Experimental models in breast cancer

The understanding of breast cancer pathology is dependent on the ability to mimic its features accurately. This can be achieved through various experimental models that can be divided into three main categories. These are *in vitro*, *in vivo*, and *in silico* experimental models. All these models have specific properties (described below) contributing to their pros and cons for utilization in particular breast cancer research. However, the cons of one experimental model can be partially compensated by combination with other experimental models. This is the strategy that my supervisor and I decided to use in this diploma project. We combine one of *in vitro* models with a famous *in vivo* model. More specifically, we combine the E0771 mouse breast cancer cell line with C57Bl/6N mouse strain animal model.

2.2.1 *In vitro* models in breast cancer

In vitro models enable studying various cellular processes in highly controllable conditions. They are used for studying cellular signaling pathways, metabolism, metastasis, and proliferation. Compared to *in vivo* models, maintain these is much easier, cheaper, and with fewer ethical concerns. On the other hand, these models lack the context of the microenvironment and immunological response. Thus, they are considered basic models that cannot cover all the attributes and heterogeneity of cancer disease.

Cell line cultures are the most frequently used *in vitro* models nowadays. The first breast cancer cell line (BT-20; triple-negative invasive ductal carcinoma) was established in 1958 (Lasfargues and Ozzello, 1958). Fifteen years later, the Michigan Cancer Foundation described the MCF-7 (luminal A invasive ductal carcinoma) cell line, which remains the most commonly used human cell line in breast cancer research (Soule et al., 1973). Since then, there are many cell lines derived from distinct species and assigned to various breast cancer subtypes (Dai et al., 2017; Zeng et al., 2020). The 4T1 cell line is the most popular murine mammary carcinoma cell line due to its high tendency to metastasize to bone, liver, brain, and lungs. It was isolated from a spontaneous mammary tumor in a BALB/cfC3H mouse (Dexter et al., 1978).

3D *in vitro* models represent the next step to higher complexity and enable a more realistic view of tumor formation, progression, and metastasizing. This category includes organoids, spheroids, scaffold-based models, and tissue slice models. Such 3D models can be obtained from established cell lines or collected from patients' biopsies (Costa et al., 2020).

2.2.1.1 E0771 cell line

E0771 cell line is a mouse breast cancer cell line derived initially from spontaneous mammary adenocarcinoma of C57Bl/6 mouse (Casey et al., 1951). The results of the molecular characterization of this cell line vary, so the molecular subtype status of this cell line remains unclear. Some articles consider it triple-negative, while others state it is a luminal B subtype (Johnstone et al., 2015; Le Naour et al., 2020a). We must keep in mind both possibilities of belonging to a specific breast cancer subtype during obtained data evaluation. For this diploma project's purposes, we decided to choose the E0771 cell line due to its origin in the C57Bl/6 mouse strain, which corresponds with the strain of mice used as an *in vivo* experimental model in this project.

2.2.2 *In vivo* models in breast cancer

Tumors present heterogeneous structures whose growth and proliferation depend on complex crosstalk between various cell types and the neighboring environment. This fuels the need for more complex experimental models. Animal models used for breast cancer research are of different animal species, mainly including mammals (reviewed in Zeng, Li,

and Chen 2020). Mice are the most popular animal model not only in breast cancer research due to their small size, low cost, short generation time, advanced gene-editing technologies, and availability of many inbred strains. The breast cancer pathogenesis in animal models can be spontaneous without artificial treatment or induced chemically by drug administration, physically by radiation, or biologically by lentivirus infection. Another approach to creating an animal breast cancer model is to transplant cancer cells in experimental animals. Finally, it is possible to prepare a genetically engineered animal with active oncogenes or inactive tumor suppressor genes (Zeng et al., 2020).

For purposes of this diploma project, we will focus further on murine transplantation models. These models can be divided into allografts and xenografts or cell line-derived and tumor-derived, depending on the origin of the transplant, or into orthotopic and ectopic, depending on the transplantation site. Most frequently used xenografts are derived from established breast cancer cell lines – cell line-derived xenografts (CDX) or patient tumor tissue - patient-derived xenografts (PDX). Xenografts must grow in immunodeficient mice, such as nude mice which lack T lymphocytes, nonobese diabetic (NOD) - severe combined immunodeficiency (SCID) mice that lack T lymphocytes as well as B lymphocytes, and NOD-SCID IL-2 receptor common gamma chain null (NSG) mice which lack T and B lymphocytes, natural killer cells (NKs) and macrophages (Hirenallur-Shanthappa et al., 2017). However, immunodeficient mice cannot faithfully mimic the microenvironment and immune response of human cancer, making it inappropriate for immunotherapy research. For these purposes, the humanized PDX model was established recently (Meraz et al., 2019).

Compared to that, allografts can be transplanted into commonly used immunocompetent mouse strains, such as BALB/c mouse strain or C57Bl/6 mouse strain, depending on the origin of the transplant. C57Bl/6 mice show a more robust Th1-type immune response, whereas BALB/c mice prevail more toward a Th2- response (Sellers et al., 2012). It should be mentioned that most genetically engineered mice have been generated on the C57Bl/6 strain background, which increases the value of transplantation models in this strain. Mouse breast cancer cells transplanted into the same genetic mouse strain with normal

immune function represents an allograft experimental model with fast growth and metastasizing, and most importantly, an immunocompetent microenvironment.

This diploma project establishes the high translational value experimental model of E0771 cell line-derived orthotopic (mammary fat pad) allograft in immunocompetent C57Bl/6 mouse strain.

2.2.2.1 *Fluorescent markers in cancer models*

Imaging of fluorescent protein-transfected tumor cell lines is an exciting tool for monitoring tumor behavior *in vivo*. They enable the distinction of the host from the tumor on the single-cell resolution level. Fluorescent proteins of many different colors have now been characterized, and one has to think over which of these markers is the most suitable one for his research purposes (Shaner et al., 2005). These, from the green fluorescent protein (GFP) family, are the most commonly used fluorescent proteins in cancer research using optical imaging. Some variants emit light at longer wavelengths, being more suitable for *in vivo* animal studies. One of them is mCherry red fluorescence protein (mCherry) which is even more photostable. Various colors can be used for color-code experiments in a single examined organism (Suetsugu et al., 2010). Most cancer studies using fluorescent proteins are performed on immunodeficient mice. However, some experiments require using immunocompetent animals, such as in this diploma project, where the used animal model is based on C57Bl/6 mouse strain background. In these cases, the immunogenicity of fluorescent proteins may play a crucial role (Day et al., 2014). The immune response depends on various aspects, such as the difference between the transgene and endogenous protein, the type of cell expressing the transgene, and the MHC (Major Histocompatibility Complex) inventory of the host. Experiments using various reporter markers have to deal with the induction of immune responses to introduced transgene products limiting the duration of marker gene expression *in vivo* (Gambotto et al., 2000). However, there are diverging opinions on the levels of immunogenicity of various fluorescent proteins across multiple animal models (Aoyama et al., 2018; Bresser et al., 2020; Gossa et al., 2015; Ombrato et al., 2019; Skelton et al., 2001; Stripecke et al., 1999).

When using fluorescent proteins in experimental models, there are usually some sources of auto-fluorescent noise, including feces, skin, or fur (Jun et al., 2017). That can be

reduced by precise animal preparation before imaging, but it cannot be eliminated. Luminescent markers, on the contrary, do not undergo such limitations and give a cleaner signal.

2.2.2.2 Luminescent markers in cancer models

In vivo bioluminescence imaging is another approach used in cancer research. Contrary to fluorescent proteins, a specific substrate must be administered to the animal to initiate the luciferase reaction. There are more than 30 different luciferases available (Kaskova et al., 2016). Most of these enzymes emit in the blue and green regions of the UV-vis spectra. However, these wavelengths are strongly absorbed and scattered by adjacent tissue (Cheong et al., 1990). However, emission of greater than 600 nm in wavelength is less absorbed, and thus red-shifted luciferases are more popular for *in vivo* imaging (Miloud et al., 2007). Besides fluorescent proteins, the immune response can be induced even against luciferase markers (Aoyama et al., 2018; Bresser et al., 2020). It was found that the decline of tumor growth and decline of the metastasize ability correlates with the level of *in vivo* luciferase expression (Baklaushev et al., 2017).

2.2.3 *In silico* models in breast cancer

In silico models are computational models that use IT techniques and high computational power to simulate biological mechanisms. Using these models avoids caring about the living entities, the various species' natural variability, and ethical concerns (Jean-Quartier et al., 2018). The development of machine learning allows us to simulate breast cancer pathology and predict new targeted drugs' efficacy. However, data obtained from databases and already published works using *in vivo* and *in vitro* models are necessary to develop such computational models (Benzekry et al., 2014; Madhukar et al., 2019).

2.3 Tumor microenvironment

Primary tumors, in general, are complex heterogeneous organs, which contain neoplastic cancer cells together with various non-transformed cells. These two subsets of cells together with multilevel interactions between them create the TME. In the subset of non-transformed cells, we can find infiltrate of some of the immune system representatives, fibroblasts, vasculature and pericytes, and lymphatics or adipocytes. (Fig. 2.)

2.3.1 Tumor non-immune microenvironment

Cancer-associated fibroblasts (CAFs) are the dominant cell type within a solid tumor mass. They are likely of mesenchymal lineage origin and differentiate from resting fibroblasts residential at the tumor site or mesenchymal stem cells as a response to the injury triggered by the progressing neoplasm (Kalluri, 2016). Trans-differentiation of other cell types, such as pericytes, endothelial and epithelial cells, is another way how CAFs arise (Kalluri and Weinberg, 2009; Potenta et al., 2008). It is a dynamic component that arranges the interaction between the malignant cells and the host stromal response. They play a role in producing extracellular matrix (ECM) as well as metabolic and immune reprogramming of the TME. CAFs secrete various mitogenic growth factors that promote tumor growth, such as hepatocyte growth factor, fibroblast growth factor (Sun et al., 2017), and transforming growth factor- β (TGF- β) (Yu et al., 2014). They also secrete some chemokines and cytokines with a similar pro-tumorigenic function, for instance, CXCL12, CCL7, CCL2, or IL-6 (Han et al., 2015). However, the recent findings show CAFs don't have only pro-tumorigenic functions but also function as anti-tumor immunity regulators (Harper and Sainson, 2014).

Cancer-associated adipocytes are another producer of chemokines, cytokines, and growth factors in tumor tissue. They secrete CCL2, CCL5, IL-1 β , IL-6, TNF- α , and vascular endothelial growth factor (VEGF), promoting cancer progression (Wu et al., 2019).

Vascular endothelial cells and pericytes play an essential role in the vascularization and nutrition of tumor mass. Neovascularization is stimulated when blood vessels sense angiogenic signals or due to hypoxic conditions in the TME. VEGF is one of the main angiogenic factors produced by malignant cells and some of the immune cells (Carmeliet and Jain, 2011).

The omnipresent cell type, which we can find in the tumor mass, is a lymphatic endothelial cell. Lymphatic vessels drain the tumor to sentinel lymph nodes, which are important sites of immune regulation, and have an essential role as a route for dissemination of malignant cells (Swartz and Lund, 2012).

Surrounding ECM provides a dynamic scaffold for all stated cells. Apart from mentioned growth factors, chemokines and cytokines, it contains increased levels of collagen and

elastin fibers which make tumors typically stiffer than the nearby normal tissue. ECM can be degraded by matrix metalloproteases secreted and activated by neoplastic cells, tumor-associated macrophages (TAMs), or CAFs. ECM degradation further releases the stored chemokines, cytokines, and growth factors and promotes the malignant cells dissemination (Levental et al., 2009).

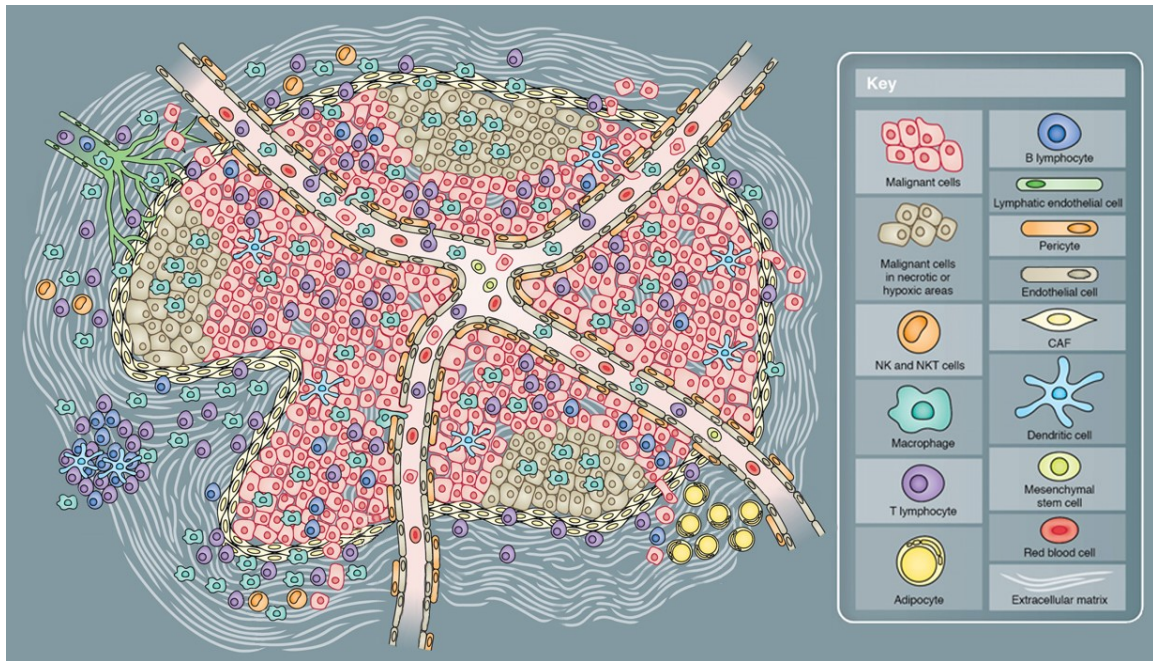


Figure 2. The TME components (taken and edited from Balkwill, Capasso, and Hagemann 2012)

2.3.2 Tumor immune microenvironment – cancer-immunity cycle

The immune system within the TME is represented by T lymphocytes, B lymphocytes, dendritic cells (DCs), TAMs, tumor-associated neutrophils (TANs), NKs, natural killer T cells (NKTs), and myeloid-derived suppressor cells (MDSCs) and complement system (Balkwill et al., 2012). A sequence of self-sufficient stepwise anti-cancer immune response processes leading to the effective elimination of cancer cells is called the cancer-immunity cycle (Chen and Mellman, 2013).

The cycle is activated by the administration of tumor neo-antigens to DCs that present the captured antigens on MHC-I and MHC-II molecules to prime and activate tumor-specific T-lymphocytes (most importantly CD8⁺ T-lymphocytes) in lymph nodes. The immune response outcome is determined by the ratio of anti-tumorigenic T effector cells versus pro-tumorigenic regulatory T cells (Tregs) infiltrating the tumor site. Activated effector T

cells migrate and infiltrate the tumor stroma, where subsequently identify and eradicate tumor cells. T cell-mediated killing of tumor cells releases new tumor neo-antigens and further stimulates the cancer-immunity cycle (Chen and Mellman, 2013). (Fig. 3.)

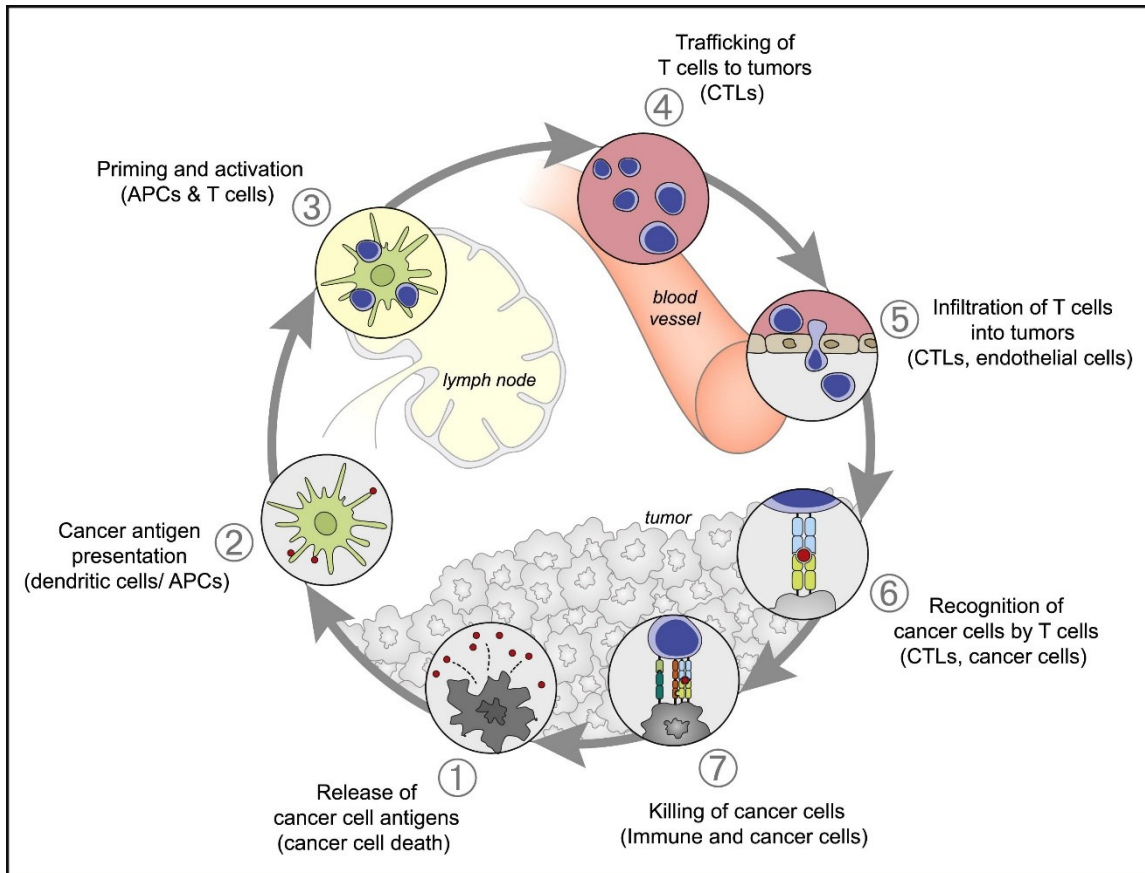


Figure 3. The cancer-immunity cycle; APCs - antigen-presenting cells; CTLs - cytotoxic T lymphocytes (Chen and Mellman, 2013)

However, this cycle does not have to function optimally. Tumor neo-antigens may be detected by DCs and T cells as “self”, and thereby Tregs are activated. Another obstacle is when T cells cannot correctly infiltrate tumors because of the TME factors suppressing them (Motz and Coukos, 2013).

Among mentioned immune cells, TAMs and MDSCs are the most abundant tumor-infiltrating immune cells. TAMs can change their phenotype according to the surrounding stroma's signals to either anti-tumorigenic (M1) or pro-tumorigenic (M2). M1 macrophages release pro-inflammatory cytokines, such as TNF and IL-2, as well as reactive nitrogen and oxygen intermediates. On the contrary, M2 macrophages produce high amounts of cytokines that inhibit infiltration and function of anti-tumor CD8⁺ T-cells,

stimulate angiogenesis, and promote tumor cell proliferation and metastasis (Noy and Pollard, 2014).

MDSCs are heterogeneous immature myeloid cells suppressing the anti-tumor immune response. They are classified as monocytic and granulocytic. Monocytic MDSCs express inducible nitric oxide synthase and generate nitric oxide (NO), while granulocytic MDSCs produce reactive oxygen species (ROS) and hydrolase arginase 1. ROS and NO production induce T cells apoptosis. Moreover, MDSCs secrete immunosuppressive cytokines, such as IL-10 and TGF- β inducing Tregs, and increase the expression of programmed death-ligand 1 (PD-L1) and thus suppress the effector T cell function. In breast cancer patients, MDSC levels are increased, and their level correlates with the clinical stage and metastatic burden. MDSCs interact with NK cells at the tumor site and significantly reduce NK cells' cytotoxicity against tumor cells described below (Cha and Koo, 2020).

TANs are related to aggressiveness and a poor prognosis with human cancers. As well as TAMs, TANs undergo polarization under the influence of cytokines within the TME. They become either pro-tumorigenic (N2) or anti-tumorigenic (N1) (Fridlender et al., 2009). However, the relevance of TAN in breast cancer has not been fully elucidated yet.

Besides cytotoxic T cells, NK cells were also defined as cytotoxic against neoplastic tumor cells. They can exclusively distinguish abnormal cells from healthy ones, leading to more specific anti-tumor cytotoxicity. Moreover, they can inhibit proliferation, migration, and colonization of distant body parts and have been reported to produce a large amount of interferon- γ (IFN- γ), by which they modulate adaptive immune responses and participate in other related signaling pathways (Wu et al., 2020).

The subpopulation of T cells, Tregs, is the essential population for enduring tolerance to „self“. Different subpopulations of Tregs are characterized, and some have been reported to play a role in breast cancer. The CD4⁺ Tregs present in the tumor tissue significantly suppress the immune response leading to an induction of immune tolerance (Wang and Wang, 2007).

NKT cells are a subset of T cells with regulatory function, which has been associated with both up- and down-regulation of immune responses. They can produce Th1, Th2, or Th17

cytokines upon cell-cell interaction or interaction with signaling molecules, working as a controlling switch turning on and off the innate and adaptive immune responses. In cancer, NKT cells have been associated with both increasing and suppressing immunosurveillance above the tumor progression. Th1-like type I NKT cells are more anti-tumorigenic, while Th2- and Th17-like type I NKT cells are more pro-tumorigenic. Type II NKT cells are primarily responsible for immunosuppression by producing IL-13 and subsequent TGF- β production by MDSCs (Krijgsman et al., 2018). However, NKT cell-mediated immune response mechanisms include complex signaling pathways and remain to be specified.

The complement system, an essential player in innate immunity, seems to be one of the major cancer regulators too. Its components, such as C1q, C3a, and C5a, have been associated with inhibition of anti-tumor T-cell response by the enrolment and activation of immunosuppressive cell subpopulations such as MDSCs, Tregs, or M2 TAMs (Pio et al., 2019).

2.3.3 Proteinase-activated receptor 2

PAR2 belongs to membrane G protein-coupled receptor's superfamily. Instead of classical ligand-receptor interaction, PAR2 is activated by various proteases, such as trypsin, tryptase, coagulation factor VIIa and Xa, matriptase MT-SP1, bacterial gingipains, and KLKs. Furthermore, recent studies show that PAR2 can also be cleaved by thrombin (Mihara et al., 2016; Oldham and Hamm, 2008). These proteases cleave an extracellular N-amino terminus between arginine and serine. The new exposed N-terminus serves as a tethered ligand, which binds a region on the second extracellular loop of the receptor and activates it. Once activated, PAR2 experiences conformational changes of the transmembrane helices on the inner cytoplasmic surface. These changes enable interaction with the heterotrimeric G-protein (Vu et al., 1991). (Fig. 4.) Besides, PAR2 can signal via interaction with β -arrestin, a multifunctional adaptor protein, and other adaptor proteins to promote cellular responses (DeFea et al., 2000). The arrestin-dependent mechanism activates an anti-inflammatory response in contrast to the G-protein-dependent signaling mechanism, which triggers an inflammatory response (Zoudilova et al., 2007).

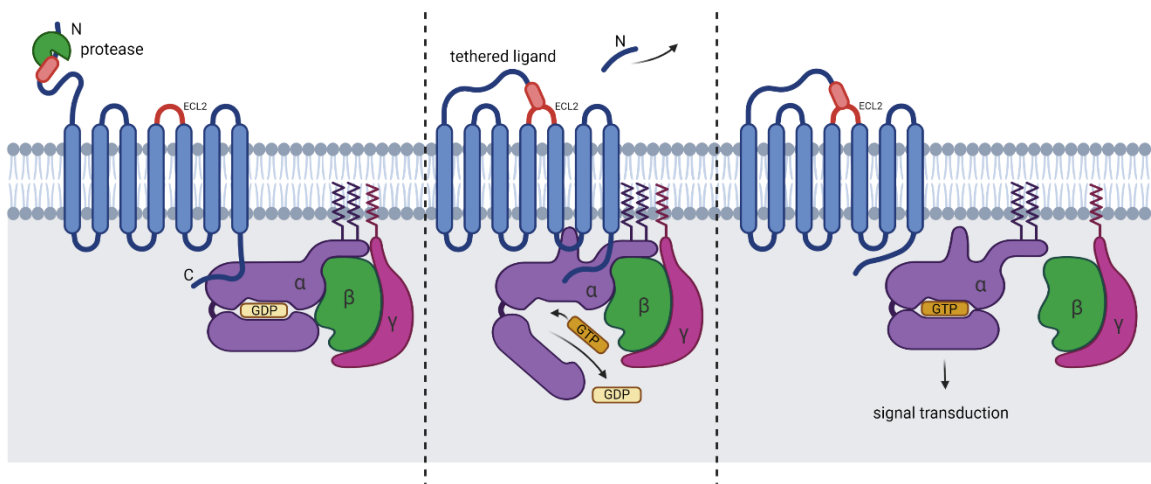


Figure 4. G protein-coupled signaling induced by PAR2 activation; ECL2 – second extracellular loop (Created with BioRender.com)

Some synthetic peptides can mimic the tethered ligand sequence and activate PAR2 without its proteolytic cleavage (Kakarala and Jamil, 2016). On the other hand, some proteases, including metalloproteinases, disable PARs activation by its downstream cleavage from the potential tethered ligand sequence. This mechanism reveals an essential way of regulating PAR2 signaling (Ludeman et al., 2004). Moreover, PAR2 can also be transactivated by cleaved PAR1 (Lin et al., 2013)

PAR1 induces activation of mitogen-activated protein kinases (MAPK), the release of intracellular Ca^{2+} , Rho and Rac signaling, and other effectors' regulation to promote diverse cellular responses coupling to G_q , G_i , and $\text{G}_{12/13}$ subtypes of G-protein (Steinhoff et al., 2005). Equally, PAR2 activation increases inositol tris-phosphate release along with diacyl-glycerol and subsequently elevates intracellular Ca^{2+} (Nystedt et al., 1995). PAR2 was also reported to activate the MAPK cascade and nuclear factor kappa-light-chain-enhancer of activated B cells (NF- κ B) DNA binding (Belham et al., 1996; Buddenkotte et al., 2005). Furthermore, factor Xa-mediated activation of extracellular signal-regulated kinases and activation of Rho and Rac (GTPases) leading to the regulation of p21-activated kinase was also shown to be PAR2 mediated (Belham et al., 1996; Koo et al., 2002).

Generally, PAR2 promotes inflammation and cellular migration. It is involved in the recruitment of leukocytes to the inflammation sites by rapid induction of leukocyte rolling mediated by P-selectin secretion on endothelial cells. In the absence of PAR2, the onset of inflammation is delayed (Lindner et al., 2000). Specifically, it promotes eosinophil pro-inflammatory functions, such as cytokines secretion, superoxide production, and degranulation (Bolton et al., 2003). Likewise, PAR2 is involved in DC maturation, their trafficking to the lymph nodes, and finally, T-cell activation (Csernok et al., 2006; Ramelli et al., 2010). On top of that, PAR2 stimulates enhanced neutrophil migration and increases secretion of the cytokines IL-1 β , IL-8, and IL-6 by neutrophils and monocyte chemoattractant protein 1 from neutrophils and monocytes (Shpacovitch et al., 2004, 2011). As mentioned above, PAR2 activation causes intracellular Ca²⁺ mobilization, which is involved in the degranulation and activation of mast cells and macrophages (D'andrea et al., 2000; Rayees et al., 2020). (Fig. 5.)

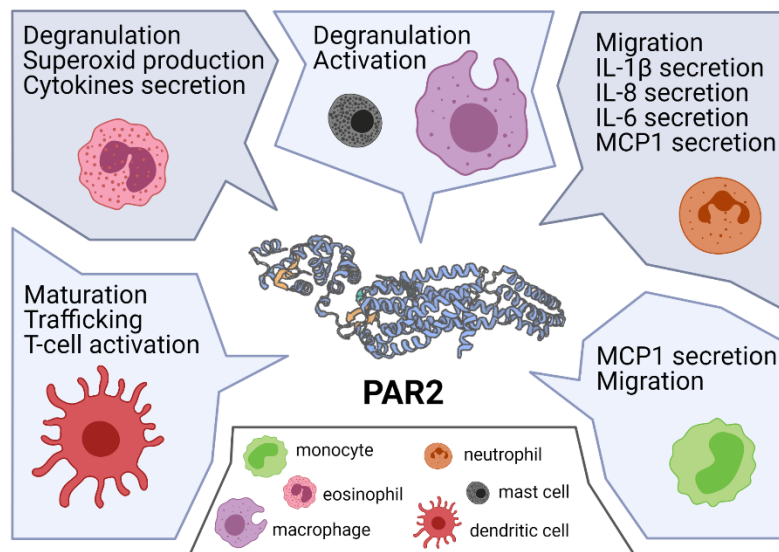


Figure 5. Immunomodulatory function of PAR2; (Created with BioRender.com)

The role of PAR2 in breast cancer pathogenesis and metastasis has been determined in *in vitro* and *in vivo* experimental studies of breast cancer tumor samples as well as breast cancer cell lines (Morris et al., 2006; Su et al., 2009). These publications claim the elevation of PAR2 protein level in breast tumor specimens compared to physiological breast tissue specimens and higher PAR2 levels in breast cancer cell lines than in normal breast cells and non-cancerous breast cell lines. PAR2 agonists seem to be potent tumor growth

enhancers and chemoattractants to breast cancer cells (Su et al., 2009). Versteeg et al. demonstrated in 2008 that PAR2 blocking monoclonal antibodies could effectively suppress tumor growth in xenograft models and thus may represent an attractive therapeutic strategy for breast cancer patients (Versteeg et al., 2008).

2.3.4 Interleukin-1 beta

IL-1 β is an endogenous pyrogen initially described in 1985 as a part of an interleukin 1 family (Van Damme et al., 1985). To date, it is the most studied member of the IL-1 family due to autoinflammatory diseases (Dinarello, 2011). IL-1 β is expressed in a wide range of tissues and cells, most preferably in hematopoietic cells, including blood monocytes and macrophages in lymphoid organs. However, it is also expressed by cells in non-lymphoid organs, such as in tissue macrophages in the lung, digestive tract, and liver. Except for macrophages, they are also expressed by other cell types, including neutrophils, lymphocytes, epithelial and endothelial cells, smooth muscle cells, fibroblasts, brain microglia, skin DCs, and keratinocytes (Dinarello, 2011; Takács et al., 1988).

The IL-1 β precursor gathers in the cytosol until the trigger initiates activation of the inflammasome, various nucleotide-binding domain and leucine-rich repeat pyrin-containing proteins (NLRP) and caspase-1 which process the precursor into an active cytokine (Franchi et al., 2009). The active cytokine then exits the cell and induces various pro-inflammatory responses. The binding of IL-1 (IL-1 α or IL-1 β) to the IL-1R1 receptor promotes conformational changes that allow IL-1R1 to bind to its coreceptor, IL-1R3. Such a conformation mediates Toll-interleukin receptor (TIR) domains approximation. Myeloid differentiation primary response 88 protein (MyD88) then attaches to the TIR domain doublet and triggers a cascade of kinases producing a strong pro-inflammatory signal leading in the end to activation of NF κ B, c-Jun N-terminal kinases, extracellular signal-regulated kinases, p38 mitogen, and MAPKs (Dinarello, 2018; Dunne and O'Neill, 2003).

It activates T-cells and their cytokine production. When generated by activated antigen-presenting cells, it induces type 1 immune response producing CD8⁺ T-lymphocytes, and it leads to the polarization of CD4⁺ T-lymphocytes towards T-helper cell type 17 (Th17) (Acosta-Rodriguez et al., 2007). It was recently reported that IL-1 β results in increased numbers and effector function of antigen-specific T cells (Ben-Sasson et al., 2013). It

induces prostaglandin synthesis, fibroblast proliferation, and collagen production. In secondary lymphoid organs, IL-1 β promotes differentiation of immature NK cells to conventional IFN- γ -producing NK cells (Hughes et al., 2010). In general, it induces neutrophil influx and activation, differentiation of monocytes into conventional DCs and M1-like macrophages, and, last but not least, B-cell activation and antibody production (Dinarello, 2009; Schenk et al., 2014).

It was already shown a long time ago that in breast cancer, higher expression of IL-1 β correlates with higher tumor invasiveness and aggressiveness (Jin et al., 1997). It has been shown that the expression of IL-1 β and their receptors in human breast malignant tissue causes activation of various cell populations and consequently participates in tumor progression (Pantschenko et al., 2003). Furthermore, there have been found clear associations between IL-1 β and neovascularization in various tumors (Nakao et al., 2005). Not surprisingly, IL-1 β has also been shown to play a crucial role in enhancing tumor cell metastasis (Weichand et al., 2017). IL-1 β contributes to the suppression of effective adaptive anti-tumor immune responses by recruiting tumor-infiltrating MDSCs and extension of the immunosuppressive activity of TAMs (Mantovani et al., 2018). (Fig. 6.)

Due to mentioned evidence, IL-1 β is considered an attractive therapeutical target in breast cancer patients. Various therapeutics on this base are already available, including Anakinra (IL-1Ra; inhibitor of IL-1 α and IL-1 β signaling), Canakinumab (neutralizing antibodies to IL-1 β), and various inflammasome inhibitors (Dinarello et al., 2012).

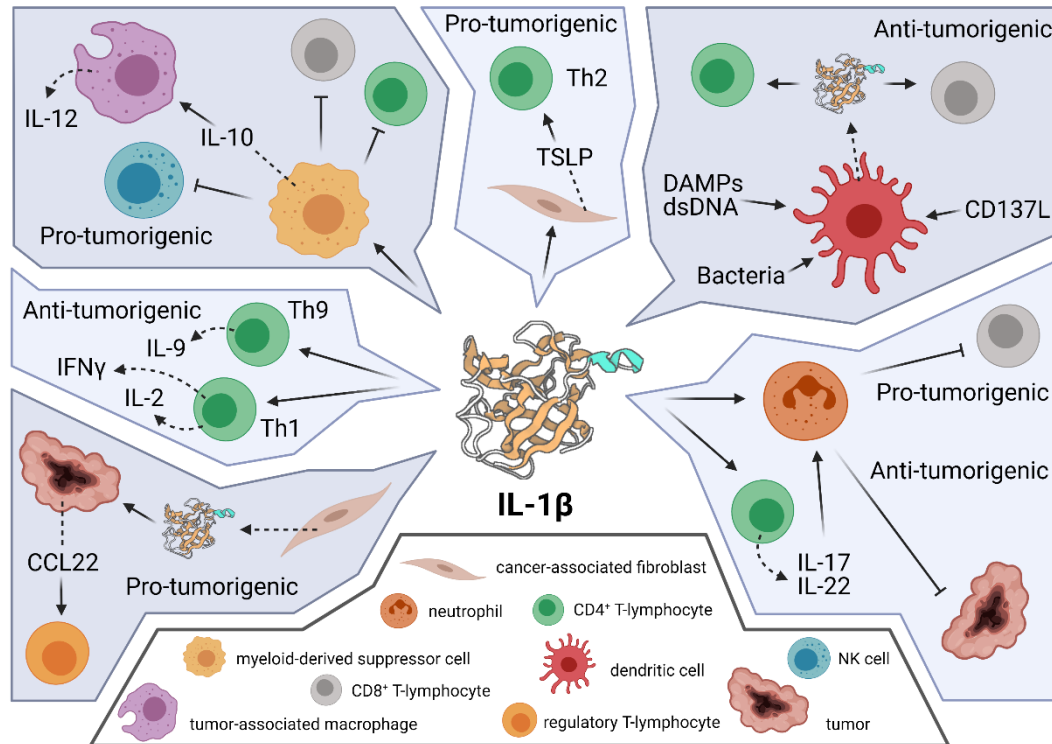


Figure 6. Immunomodulatory function of IL-1 β on pro- and anti-tumorigenic immune response; Based on (R  b   and Ghiringhelli, 2020) (Created with BioRender.com)

2.3.5 Cathelicidin LL-37

Cathelicidin proteins are composed of the N-terminal and C-terminal domains. In humans, neutrophils are the primary source of these peptides. The neutrophil synthesizes inactive hCAP18 (human cationic anti-microbial protein of 18 kDa), the precursor of a mature peptide LL-37 (37 amino acids long peptide with two N-terminal Leu residues), and store it in secondary particles. Toll-like receptors, activated by damage-associated molecular pattern molecules (DAMPs), pathogen-associated molecular pattern molecules (PAMPs), or cytokines, can stimulate neutrophils' degranulation. The hCAP18 protein (LL-37 precursor) is during degranulation released from secondary particles extracellularly, where it is enzymatically processed with proteinase 3 to a mature peptide LL-37 (S  rensen et al., 2001).

Besides neutrophils, other cells of the immune system, such as DCs, monocytes, and macrophages, are proved to produce LL-37 as well (Lowry et al., 2014). However, LL-37 is not expressed only in immune cells. It is also expressed in many other tissue cells, such as keratinocytes, epithelial cells, myelocytes, mesenchymal stromal cells, and in cells of testes

(Agerberth et al., 1995). LL-37, produced by these cells, can directly recruit immunocompetent cells (Vandamme et al., 2012). Antigen-presenting cells then present the antigen to the specific T lymphocytes, and the cells of the adaptive immune system are instantly attracted and activated. The immunomodulatory functions of LL-37 are expressed in Figure 7. based on the information from a recent review (Yang et al., 2020).

The N-terminal domain of LL-37, known as the cathelin-like domain, has anti-microbial activity toward gram-negative and gram-positive bacteria as it binds to bacterial lipopolysaccharides (Turner et al., 1998). It serves as a chemotactic agent for neutrophils, monocytes, and T cells using the formyl peptide receptor 1 (Yang et al., 2000).

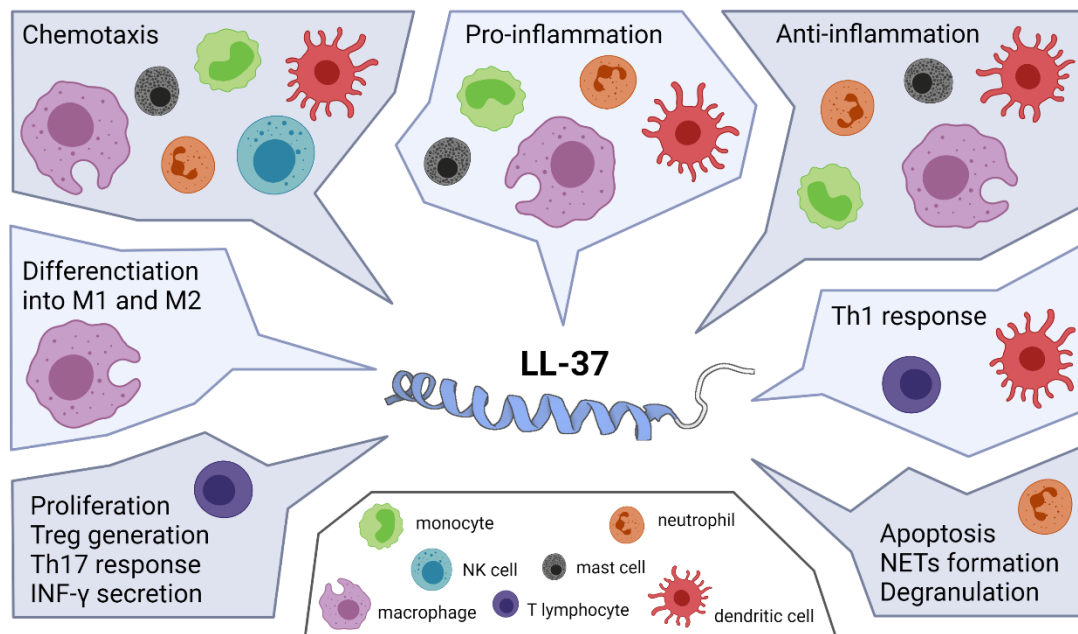


Figure 7. Immunomodulatory function of LL-37 (Created with BioRender.com)

Overexpression of LL-37 is found in various cancers, such as ovarian cancer, lung cancer, breast cancer, malignant melanoma, and prostate cancer. On the other hand, it is reported to be downregulated in gastrointestinal cancers (colon cancer and gastric cancer) and hematological malignancies (Piktel et al., 2016). Although LL-37 is an essential factor in the mammary gland epithelium's innate immune defense system contributing to the anti-infectious properties of breast milk (Armogida et al., 2004), its higher expression was observed in breast cancer cells, and its expression level seems to correlate with malignancy grade (Heilborn et al., 2005). LL-37 promotes tumor progression by affecting

mesenchymal cells activating the following pathways: formyl peptide receptor 1, formyl peptide receptor 2, insulin-like growth factor 1 receptor, HER2, and CXCR4 (Girmita et al., 2012; Pan et al., 2018; Weber et al., 2009; Xiang et al., 2016). Additionally, LL-37 promotes tumor formation by polarizing macrophages into M2 type (Cha et al., 2016).

Mouse cathelicidin-related anti-microbial peptide (mCRAMP), an orthologue of LL-37 in mice, shows significant similarities to LL37, making it a valuable model to investigate the function and mechanism of regulation of human cathelicidin (Pestonjamas et al., 2001).

2.4 Kallikreins – an overview

KLKs consist of a large family of secreted serine proteases divided into two categories. Plasma KLKs are released from the pancreas into the bloodstream, and tissue KLKs are expressed in various tissues into ECM. These two categories differ significantly. However, this work considers selected tissue KLKs (KLK5, KLK7, and KLK14) as prognostic biomarkers in cancer patients, and plasma KLKs are not studied in this project. KLK1 was the first described tissue KLK. So far, the remaining 14 tissue KLKs are called kallikrein-related proteases (KLK2 – KLK15). All of them are encoded by a cluster of genes located on chromosome 19q13.4 (Yousef and Diamandis, 2001).

2.4.1 Physiological function

KLKs play roles in a wide range of physiological processes, such as general protein turnover, cell signaling, cell proliferation, semen liquefaction, immune response, neural development, blood pressure, skin desquamation, tooth enamel formation, and related pathological conditions (Stefanini et al., 2015). They are synthesized and secreted to the ECM as a pre-pro-protein form activated by the trypsin-like cleavage (Yoon et al., 2007). Tissue-specific inhibitors, such as these of the SPINK/LEKTI family, are the primary reducers of KLK activity in tissue (Deraison et al., 2007). Gene dysfunction of these inhibitors is further correlated with several inherited diseases, where KLK excessive activity is the leading cause. One such condition is Netherton syndrome, where *Spink5* gene dysfunctions lead to a severe skin disease caused by dysregulation of epidermal proteases (mainly KLK5, KLK7, and KLK14). These proteases' unregulated activity further leads to disruption of the skin barrier (Kasperek et al., 2017).

2.4.2 Pathophysiological function

Various *in vitro* and *in vivo* strategies have been used to understand the molecular mechanisms of KLK activity during cancer progression. Modification of *Klk* expression in cancer cell lines using overexpression vectors, knockdown of endogenous expression with small interfering RNA (siRNA), and miRNA or exogenous treatments with recombinant KLKs and specific inhibitors suggested that KLKs modulate cancer cell proliferation, migration, invasion, and chemo-resistance. However, these outcomes are frequently criticized because KLK activity *in vitro* may not represent their actual function in cancer progression. In this diploma project, we would like to utilize the mouse models deficient for various *Klks*, which are already established in our laboratory, and contribute to the elucidation of KLKs' pathophysiological function in breast cancer malignancies.

Proteolytic activity against the ECM's proteins, cell junction, and cell adhesion proteins is the primary mechanism causing KLKs' pro-invasive and pro-migratory function. In cooperation with other proteases such as urokinase-type plasminogen activator, plasmin, matrix metalloproteases, and cathepsins, various KLKs are able to disrupt *membrana basalis*, nearby ECM, and thus release growth factors to boost cancer progression and metastasizing. Participation of KLKs in epithelial to mesenchymal transition is another process that is associated with the increased invasiveness of cancer cells. However, some studies suggested even a negative effect of KLKs on cancer cell migration and invasion, corresponding to the fact that downregulation of various *Klks* is observed in some cancers. These processes are reviewed in more detail by Kryza et al. (Kryza et al., 2016).

2.4.3 Kallikreins as prognostic markers in breast cancer

Prognostic biomarkers are used to describe potential breast cancer development and progression, and they contribute to more optimal patient clustering and thus choosing the most suitable treatment. Histological information, such as lymph node status, tumor size, and tumor stage, is not sufficient to accurately assess individual risks. Many molecular markers have already been identified as predictors of disease prognosis or responsiveness to therapy. Commonly used prognostic and predictive molecular markers are ER and PR, HER2, plasminogen activators and inhibitors (uPA, PAI), markers of proliferation (Ki-67), angiogenesis-related prognostic markers (VEGF), and apoptosis-related prognostic

markers (Bcl-2, p53) (Esteva and Hortobagyi, 2004). In addition to the already mentioned markers, many others are evaluated as potential prognostic factors. Expression levels of tissue *Klks* are one of them.

Talking about mRNA levels, all *Klks* are more or less expressed in normal breast tissue. However, there is no consistent conclusion about *Klks* expression in breast cancer, and so it is not significantly conclusive to consider them as valuable biomarkers in clinics. Differences in published data may be caused by misinterpretation of results obtained by various scientists, examining different types of samples, and applying diverse technical approaches with distinct sensitivity and specificity. Moreover, specific tissue KLKs have specific tissue regulators that make the obtained data even more challenging to interpret (Kryza et al., 2016; Schmitt et al., 2013). KLKs are dysregulated in a majority of solid human tumors, especially in hormone-dependent cancers. The consequence between dysregulation of *Klks* and breast cancer pathogenesis is supported by the fact that *Klks* are regulated mainly by estrogen and progesterone, two hormones playing a significant role in breast tissue development and breast cancer progression (Kryza et al., 2016).

2.4.3.1 *KLK1 and KLK2*

In particular, there is insufficient evidence on KLK1 playing an essential role in breast cancer biology, and just a few studies were focused on the KLK2.

2.4.3.2 *KLK3*

On the contrary, much research is concentrated on KLK3 due to its evident prognostic value in various prostate disorders. KLK3 is better known under the name prostate-specific antigen (PSA). It is secreted by epithelial cells of the prostate gland where it liquefies semen, and its levels are elevated in the presence of prostate cancer, prostatitis, or prostatic hyperplasia (Velonas et al., 2013). In women, the breast tissue seems to be the source of PSA, and its levels have been found higher in the serum of patients with breast cancer than in healthy controls (Mashkoo et al., 2013).

2.4.3.3 *KLK4*

Klk4 mRNA levels show an increase in breast cancer tissue compared to normal breast tissue. In the late stage of this disease, *Klk4* mRNA expression lowers, suggesting that *Klk4* expression is modulated during cancer progression (Papachristopoulou et al., 2009).

2.4.3.4 *KLK5*

The *KLK5* is almost undetectable in sera (Yousef et al., 2003a), while in breast tissue, it is present in high concentration (Shaw and Diamandis, 2007). However, in malignant breast tumors, the expression of *Klk5* mRNA is reduced, and so it is considered a biomarker indicating the malignant or benign character of breast tumors (Avgeris et al., 2011).

2.4.3.5 *KLK6*

KLK6 is elevated in breast cancer patient serum compared to healthy non-cancerous controls which nominate it for valuable cancer-specific and body-fluid-accessible biomarker (Mangé et al., 2016).

2.4.3.6 *KLK7*

The research outcomes, according to *Klk7* expression in breast cancer, are contradictory. According to the research of Talieri et al., patients with breast cancer tumors positive for *Klk7* mRNA have relatively shorter disease-free survival and overall survival than patients with *Klk7* negative tumors. It suggests that *KLK7* could be used as a marker of unfavorable prognosis (Talieri et al., 2004). Contrariwise, Holzscheiter et al., in their study, showed that high expression levels of *Klk7* are associated with a decreased relapse risk or death and may be favorable prognostic markers in breast cancer (Holzscheiter et al., 2006). Moreover, Ejaz et al. reported low levels of *KLK7* protein in breast cancer patients' sera (Ejaz et al., 2017). However, *KLK7* can cleave fibronectin, and this way enhance metastasis by degrading ECM components (Ramani and Haun, 2008).

2.4.3.7 *KLK8, KLK9, and KLK10*

Klk8, Klk9, and Klk10 are highly expressed in the breast tissue, and their levels are low in breast cancer, which corresponds with the phenomenon that has been described in other *Klks* (Yousef et al., 2003b, 2004; Zhang et al., 2006).

2.4.3.8 *KLK11, KLK12, and KLK15*

Data concerning a prognostic or predictive value for *Klk11, Klk12, and Klk15* in breast cancer and whether they have any role in breast cancer pathology has not been reported so far.

2.4.3.9 *KLK13*

According to a study by Chang et al., *Klk13* over-expression is related to a significant reduction in relapse and death risk supporting its utilization as an independent, favorable prognostic marker (Chang et al., 2002).

2.4.3.10 *KLK14*

KLK14 was initially described as a peptidase operating in the central nervous system but later described as a predictor of lower disease-free survival and overall survival in breast cancer patients. Its higher level has been associated with increased tumor grade, meaning that *Klk14* mRNA levels could be an unfavorable biomarker in breast cancer (Papachristopoulou et al., 2011).

Up till now, several *KLKs* have been found to increase or decrease various tumor progression. The majority of data regarding mRNA and protein expression levels of *KLKs* in solid tumors is available for ovarian cancer. Most *Klks* seem to be overexpressed in ovarian cancer, and thus they can be used to distinguish the normal and the malignant phenotype (Loessner et al., 2018). For breast cancer, the majority of *Klks* seem to be down-regulated. However, more studies are necessary to validate these peptidases' function as biomarkers or regulators of pathogenesis in breast cancer. There is also a demand for the elucidation of *KLKs*' physiopathological role before they are considered relevant therapeutic targets for breast cancer therapy.

2.4.4 Kallikreins influencing the immune system

KLKs, as a family of multifunctional proteases with pleiotropic (patho)physiological roles, are revealed to have a function even in innate immunity and inflammatory processes (Sotiropoulou and Pampalakis, 2010). These mechanisms are described further. *KLKs* directly impact various immunomodulatory molecules, such as PAR2, IL-1 β , and LL-37, having multiple immune functions, including anti-tumorigenic and pro-tumorigenic.

2.4.4.1 *PAR2* activation by kallikreins

As already mentioned, *PAR2* can be cleaved by various *KLKs*. In 2006 Oikonomopoulou et al. found that *KLK5*, *KLK6*, and *KLK14* cleave near *PAR* protein N-terminus representing the activation motif of human *PAR1* and *PAR2* and so can activate their downstream signaling (Oikonomopoulou et al., 2006). These findings correspond with

Briot et al., who demonstrate the direct impact of KLK5 hyperactivity in activating a proallergic signaling pathway by PAR2 and NF- κ B pathway activation. This led to overexpression of intercellular adhesion molecule 1, IL8, TNF- α , and thymic stromal lymphopoietin in keratinocytes in Netherton syndrome (genetic skin disease) (Briot et al., 2009). KLK14, as a potent promoter of PAR2 signaling, can also trigger the activation of extracellular signal-regulated kinase -1 and -2 (ERK1/2), members of the mitogen-activated protein kinase family affecting cell proliferation and apoptosis (Gratio et al., 2011).

2.4.4.2 IL-1 β activation by kallikreins

The IL-1 β precursor is also processed by other serine proteases than only caspase 1 (Netea et al., 2015). KLK7 has also been shown to cleave and activate pro-IL-1 β (Nylander-Lundqvist and Egelrud, 1997).

2.4.4.3 LL-37 activation by kallikreins

According to research in dermatology in humans, KLK5 controls activation of the cathelicidin precursor protein and thus the formation of LL-37. KLK7, on the other hand, cleaves the cathelicidin precursor to multiple various products. Besides, both KLK5 and KLK7 can further process LL-37 to smaller peptides, such as RK-31, KS-30, LL-29, KS-27, KS-22, and KR-20, which can have even higher anti-microbial activity. However, these smaller peptides are degraded in a short time, and thus we can talk about the mechanism of activation/deactivation of this anti-microbial defense (Yamasaki et al., 2006).

2.5 Possible crosstalk of kallikreins, immune system, and tumor microenvironment

Interaction of stromal cells with cancer cells is essential for cancer progression. It establishes a potential microenvironment for tumor growth mainly by secretion of protumorigenic factors. KLKs and their cooperation with other signaling molecules may play a crucial role in such communication. Possible crosstalks between KLKs and tumor progression are mentioned below.

KLKs can modulate signaling molecules essential for tumor growth. It has been found that KLK2, 3, 4, 5, and 14 can cleave various insuli-like growth factor-binding proteins, making

it accessible for cancer cell receptors activating mitogenesis, differentiation, and overall neoplastic cell survival (Matsumura et al., 2005; Michael et al., 2005; Sutkowski et al., 1999).

It is already well described that steroid hormones, such as estrogen and progesterone, play a significant role in several hormone-related malignancies. They also regulate *Klks* expression, giving a straight suspicion of KLKs' possible participation in these malignancies. It is known from RT-PCR and Western blot experiments that mRNA and protein levels of KLK5, 6, 8, 9, 10, 11, 12, 13, 14, and 15 are stimulated by estrogen in breast cancer cells. These and other steroid hormone regulations of *Klks* are well described and summarized in a review by Mitchell G. Lawrence et al. (Lawrence et al., 2010). It was shown that KLK3 could enhance androgen receptor-dependent suppression of p53 function, leading to decreased apoptosis and increased cell survival of prostate cancer cells (Niu et al., 2008). Another possible crosstalk could be between steroid hormones, KLKs, and telomerase activity since estrogen and progesterone have been shown to enhance telomerase activity and promote replicative immortality (Mocellin et al., 2013).

Angiogenesis is another vital hallmark of cancer progression, supplying nutrients and oxygen to rapidly growing tumors. KLKs are critical to ECM degradation and remodeling, which is necessary for neoangiogenesis. They regulate matrix metalloproteinases and urokinase-type plasminogen activator pathways which in turn mediate the degradation of ECM components (Lu et al., 2011). Moreover, some reports showed that the KLKs could release the membrane-bound precursor of platelet-derived growth factor-beta, promoting the VEGF-A secretion. VEGF-A is, in turn, essential for new capillaries formation (Kryza et al., 2014). Additionally, blood vessels penetrating primary tumors provide a path for cancer metastasizing. The contribution of KLKs to angiogenesis is mainly associated with KLK1 because of its role in the KLK-kinin system (Spinetti et al., 2011).

Another critical feature of KLKs is their ability to promote the epithelial-to-mesenchymal transition. For instance, KLK3, 4, and 7 can cleave E-cadherin, leading to a loss of epithelial phenotype and subsequently transition, necessary for cancer cells to get into an invasive phenotype (Cui et al., 2017; Haddada et al., 2018).

Except for the already mentioned immunomodulatory molecules that KLKs can process, they can affect anti-cancer immunity in various other ways. They can play a role during the complement network activation via C3 processing (Oikonomopoulou et al., 2013).

In general, distinct KLKs' ability to function as tumor suppressors or tumor promoters depend on the specific microenvironment where they are expressed, released, or activated. However, it seems that targeting these pathways associated with cancer hallmarks could allow the development of novel anti-cancer therapies.

2.6 Breast cancer therapies

The selection of suitable therapy for breast cancer patients is based on the clustering of these patients according to specific clinical characteristics. Therapeutic strategies can be divided into local approaches, such as tumor surgery and radiotherapy, and systemic approaches, associating drug administrating strategies, including chemotherapy, hormone therapy, and immunotherapy. Following this diploma thesis's aim, this chapter will focus mainly on reviewing the immunotherapeutic approaches in breast cancer. In general, cancer immunotherapy aims to induce a self-sufficient process of the cancer-immunity cycle by induction of individual steps of the cycle.

The first step of the cancer-immunity cycle, the tumor neoantigens release, can be supported by more traditional therapeutical approaches, such as chemotherapy, radiation therapy, and targeted therapies (Zitvogel et al., 2013). The cancer antigen presentation can then be initiated through vaccines (Palucka and Banchereau, 2013). However, cancer vaccines' preparation is challenging because cancer cells' expression profiles might differ in patients or even in cells within one tumor mass. Chimeric antigen receptors T cell (CAR T) therapy is another approach to support antigen presentation and thus anti-tumor immune response activation (Bajgain et al., 2018). Most of the developing therapies are targeted into the third step of the cycle, supporting T cells priming and activation. These therapies contain various approaches, including anti-CTLA4 antibodies blocking the binding of ligands B7.1 and B7.2 (CD80 and CD86) to the inhibiting receptor of T cells, cytotoxic T lymphocyte antigen-4 (CTLA4) (Solinas et al., 2017). Anti-PD-L1 and anti-PD-1 antibodies are used in immunotherapies targeting other inhibitory molecules, the

programmed death-1 (PD-1), a T cell inhibitory receptor and its PD-L1, expressed by both tumor and immune cells (Solinas et al., 2017). (Fig. 8.)

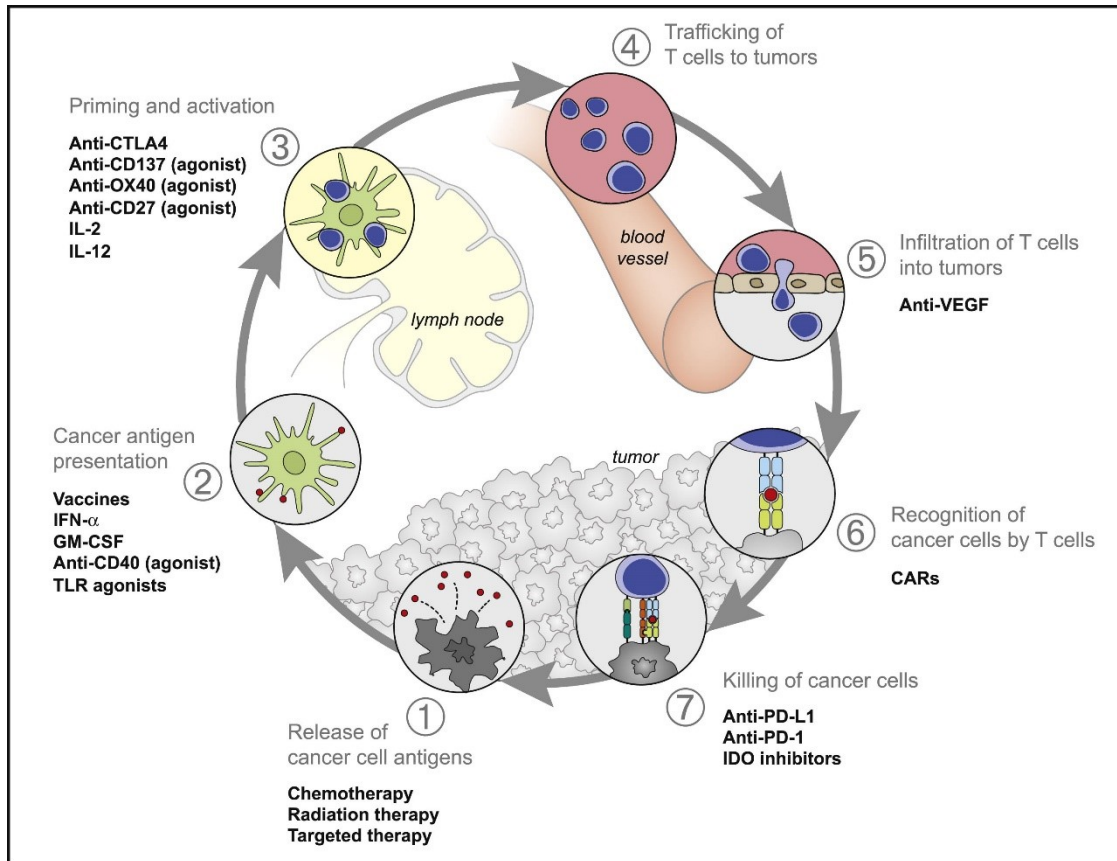


Figure 8. Therapies affecting the cancer-immunity cycle; GM-CSF, granulocytic macrophage colony-stimulating factor; CARs, chimeric antigen receptors; Indoleamine 2,3-Dioxygenase (Chen and Mellman, 2013)

Many therapies target various cancer-immunity cycle steps. Their combination may provide significant benefits. It is necessary to understand the crosstalk between cancer cells and the immune response components to be able to choose the best combination of these therapies for a specific cancer subtype.

It must be kept in mind that multiple systemic factors can affect immune therapy's success or failure in each patient. Immune-related biomarkers in particular patients may let us map their tumors' cancer-immunity cycle and tailor suitable immune therapies or their combinations to them.

3 Materials and methods

3.1 Materials

3.1.1 Animals

All animal experiments were ethically reviewed and performed following European directive 2010/63/EU and were approved by the Czech Central Commission for Animal Welfare. Animals were bred under specific-pathogen-free conditions in individually ventilated cages in the animal facility of The Institute of Molecular Genetics AS CR, v.v.i. in BIOCEV.

Wild type BALB/c and C57BL/6N female mice used in this study came from the animal facility of The Institute of Molecular Genetics AS CR, v.v.i. in BIOCEV. Mutant C57BL/6N mice (*Klk14^{-/-}*, *Klk7^{-/-}*, and *Klk5^{-/-}Klk7^{-/-}*) used in the experimental part of this project, were produced in Czech Centre for Phenogenomics by Mgr. Petr Kaspárek, Ph.D. (Horn et al., 2018; Kaspárek et al., 2017) If possible, in experiments with these mutant mice, wild-type littermates were used as controls. Animals were monitored and weighed regularly during the experiments, and tumor growth was measured with a caliper. For tumor volume determination, two diameters were measured with a caliper, and the lower one was taken as the third diameter. Signs of Pain, Quality of Stool, Wound Healing, and Body Condition Score was monitored regularly during all experiments.

3.1.2 Cell cultures

E0771 cell line, Murine Breast Cancer Cell Line (Cat. No. 94A001; CH3BioSystems LLC), was maintained in RPMI 1640 medium (Cat. No. R8758; SAFC - Sigma-Aldrich) supplemented with 10 mmol/L HEPES, 10% fetal bovine serum (Gibco™) and 100 units/ml Penicillin-Streptomycin (Cat. No. 15140148; Gibco™). 4T1-Red-FLuc cell line (Cat. No. BW124087; Bioware) was maintained in RPMI 1640 medium (Cat. No. R8758; SAFC - Sigma-Aldrich) supplemented with 10% fetal bovine serum (Gibco™) and 100 units/ml Penicillin-Streptomycin (Cat. No. 15140148; Gibco™). Both cell lines were maintained in a humidified atmosphere of 5% CO₂ at 37 °C. Cells were passaged every 3-6 days depending upon confluency. While passaging, cells were washed by Phosphate Buffered Saline, treated with Trypsin-EDTA (0.5%) (Cat. No. 15400054; Gibco™), and

then harvested with a complete medium. Cells were preserved in fetal bovine serum (Gibco™) supplemented with 10% dimethyl sulfoxide (Cat. No. D8418; Sigma Aldrich®) at -80 °C.

3.1.3 Antibodies

Marker	Fluorochrome	Clone	Manufacturer	Catalog number	c (g/L)	Dilution
CD5	BV421	53-7.3	BD Biosciences	562739	0.2	200x
Ly6G	BV421	1A8	BD Biosciences	562737	0.2	100x
CD19	BV510	1D3	BD Biosciences	562956	0.2	400x
CD8a	BV605	53-6.7	BioLegend	100744	0.2	600x
GITR	BV711	DTA-1	BD Biosciences	563390	0.2	500x
CD4	FITC	RM4-5	BD Biosciences	553047	0.5	800x
CD11b	PerCPCy5.5	M1/70	Biolegend	101228	0.2	1000x
Ly6C	PE	HK1.4	BioLegend	128007	0.2	1000x
CD11c	PE-Cy7	HL3	BD Biosciences	558079	0.2	200x
CD161	APC	PK136	BD Biosciences	550627	0.2	300x
CD45	A700	30-F11	Invitrogen™	56-0451-82	0.2	300x
MHCII	APC-Cy7	M5/114.15.2	BioLegend	107628	0.2	1000x
Fc block	*	2G4	BD Biosciences	553142	0.5	200x
CD5	BV421	53-7.3	BD Biosciences	562739	0.2	200x

Table 3.1. List of antibodies used in flow cytometry experiments. * it is not labeled; it blocks Fc receptors on immune cells that would bind antibodies non-specifically

Name	MW (kDa)	Dilution	Host	Reactivity	Cat. No.	Manufacturer
Primary antibodies						
Anti-GAPDH	36	1:10000	Rabbit	Mouse, Human, Rat	G9545	Sigma Aldrich®
Anti-IκB-ζ	75, 85	1:1000	Rabbit	Mouse	93726	Cell Signaling Technology
Anti-IL-1β (D3H1Z)	17,31	1:1000	Rabbit	Mouse	12507	Cell Signaling Technology
Anti-PAR2	44	1:1000	Rabbit	Mouse, Rat, Human	ab180953	Abcam
Secondary antibody						
Anti-rabbit (HRP)	-	1:10000	Goat	Rabbit	ab205718	Abcam

Table 3.2. List of primary and secondary antibodies used in protein detection experiments.

3.1.4 Primers

ID	Target gene	Target gene Ensembl ID	Size of PCR product	Sequence (5'-3')	
				Forward	Reverse
pKlk5	<i>Klk5</i>	ENSMUSG0000074155	743 bp	AATCTCTCCCTCCCTTCC A	CCATGAATCCTCCCCTCA T
pKlk7.2	<i>Klk7</i>	ENSMUSG0000030713	599 bp	CTGATCCTGTGACTCTGCG G	GGGAGGGAGGGAAAGTG AGA
pKlk14	<i>Klk14</i>	ENSMUSG0000044737	856 bp	GTGCTGGTGTGTGCTGAG AT	ATGTGCTCCGAAGTGGATT C
pIl1bi	<i>IL1b</i>	ENSMUSG0000027398	764 bp	TATGGGAAGCCATTGAGA GC	TGGCATCGTGAGATAAGC TG
pF2r1l	<i>F2r1l</i>	ENSMUSG0000021678	954 bp	TCACCAACTGCCCTGTGTA G	CGTGACAGGTGGTGTATGT TC

Table 3.3. List of primers used in KO clones detection. Primers were designed using The Primer3Plus software (Untergasser et al., 2007).

Target gene name	Target gene Ensembl ID	Sequence (5'-3')	
		Forward	Reverse
rtpKlk14	ENSMUSG0 0000044737	AACCATAGCCAGTCCCATTG	GATTCCAGGGTAGGCTCGAT
rtpKlk7	ENSMUSG0 0000030713	TGCAAAATGGGTCAGTACCA	GACGTGGGTCTTTGTGGAGT
rtpKlk5	ENSMUSG0 0000074155	CTGTTCTTGCTGGGGATGTT	ATCCGTGCTGAGGTCTCTGT
rtpmActb	ENSMUST0 0000100497	ACCTTCTACAATGAGCTGCG	CTGGATGGCTACGTACATGG
rtpmF2r1l	ENSMUSG0 0000021678	TGCTGGGAGGTATCACCCCTT	CGCTGGGTTTCTAATCTGCCA
rtpPrdx1	ENSMUST0 0000135573	AATGCAAAAATTGGGTATCCTGC	CGTGGGACACACAAAAGTAAAGT
rtpmGAPDH	ENSMUST0 0000117757	CGTCCCGTAGACAAAATGGT	TTGATGGCAACAATCTCCAC
rtpmI11b	ENSMUSG0 0000027398	GCCACCTTTTGACAGTGATGAG	GACAGCCCAGGTCAAAGGTT

Table 3.4. List of primers used in the qRT-PCR.

3.1.5 CRISPR guide RNAs

Synthetic, desalted, and lyophilized DNA oligonucleotides were ordered from Sigma Aldrich® and, after delivery, diluted to 100 µM and 10 µM concentration with ddH₂O. The DNA oligonucleotides sequence corresponds to the coding sequence for gRNA targeting the gene of interest. 5'CACC and 5'AAAC overhangs were added for ligation into the pair of BbsI sites in pSpCas9(BB)-2A-GFP plasmid. pSpCas9(BB)-2A-GFP (pX458) was a gift from Feng Zhang (Addgene plasmid # 48138 ; <http://n2t.net/addgene:48138> ; RRID:Addgene_48138) (Ran et al., 2013).

Delivered oligonucleotides were annealed after dilution. The reaction was performed using 1 µl of each (forward and reverse strand) oligonucleotide (100µM), 1 µl of T4 Polynucleotide Kinase (10 U/µl; Cat. No. EK0031; Thermo Scientific™), 1 µl of T4 Ligase buffer (10X; Cat. No. B0202S; New England BioLabs®) and 6 µl of ddH₂O. The reaction

was incubated in a thermocycler (BIO-RAD T100™ Thermal Cycler) for 10 minutes at 95 °C, and then slow cooling down from 85 °C to 4°C (ramp rate 0.1 °C / 1 s). The ligation of annealed CRISPR guides into a pX458 plasmid was performed using so cold Golden gate ligation with 1 µl of annealed oligos (0.5µM), 100 ng of pX458 plasmid, 2 µl of T4 Ligase buffer (10X; Cat. No. B0202S; New England BioLabs®), 1 µl of T4 DNA ligase (10 U/µl; Cat. No. M0202L; New England BioLabs®), 1 µl of BbsI enzyme (10 U/µl; Cat. No. ER1012; Life technologies) and 14 µl of ddH₂O. The reaction was incubated in a thermocycler (BIO-RAD T100™ Thermal Cycler) for 5 minutes at 37 °C, for 5 minutes at 16 °C, these steps repeated ten times, then for 5 minutes at 37 °C, for 10 minutes at 60 °C, for 10 minutes at 80 °C and then cooled down at 4 °C.

Prepared plasmids were amplified in competent *E. coli* strain XL1-Blue. 2 µl of plasmids were added to bacteria and heat-shocked at 42 °C for 90 seconds. After shaking incubation in 400 µl of LB medium (BIOCEV media) at 37 °C for 30 minutes, the transfected bacteria were centrifuged for 1 minute at 800 g and then the pellet was resuspended in 100 µl volume of LB, plated on 19 mm LB agar plates (BIOCEV media) containing 100 ng/µl ampicillin and incubated at 37 °C overnight. After overnight incubation, one colony was selected, inoculated in 4 ml of LB medium (BIOCEV media) containing 100 µg/ml ampicillin (Cat. No. A0166-25G; Sigma Aldrich®), and incubated shaking at 37 °C overnight. The bacteria were centrifuged at 8000 g for 5 minutes at room temperature using a microcentrifuge (Eppendorf 5415R). The supernatant was discarded, and the plasmid DNA was isolated using the GeneJET Plasmid Miniprep Kit (Cat. No. K0503; Thermo Scientific™) according to the manufacturer's protocol. DNA concentration was measured using a UV-Vis Spectrophotometer (NanoDrop 2000c, Thermo Scientific™).

ID	Target gene	Target gene Ensembl ID	Sequence (5'-3')	
			Forward	Reverse
gKlk5	<i>Klk5</i>	ENSMUSG0000074155	CACCGCAGCTCTCGAATTGTGAT	AAACATTCACAATTCGAGAGCTGC
gKlk7	<i>Klk7</i>	ENSMUSG0000030713	CACCGTAAAGAAGGCTCGCACCA	AAACTGGGTGCGAGCCTTCTTTAC
gKlk14	<i>Klk14</i>	ENSMUSG0000044737	CACCGAGTCCTGTTGTCAGATCAAT	AAACATTGATCTGACAACAGGACTC
gIl1bi	<i>IL1b</i>	ENSMUSG0000027398	CACCGCATCAACAAGAGCTTCAGGC	AAACGCCTGAAGCTCTTGTTGATGC
gF2r1l	<i>F2r1l</i>	ENSMUSG0000021678	CACCGCGCCGTGATTTACATGGCCA	AAACTGGCCATGTAAATCACGGCGC

Table 3.5. List of CRISPR guide RNAs used for genome editing of E0771 cell using CRISPR-Cas9 editing system

3.1.6 Plasmids

Publicly available plasmids used in this diploma project:

pGL4.18 CMV-Luc was a gift from Lee Helman (Addgene plasmid # 100984 ; <http://n2t.net/addgene:100984> ; RRID:Addgene_100984)

pSpCas9(BB)-2A-GFP (pX458) was a gift from Feng Zhang (Addgene plasmid # 48138 ; <http://n2t.net/addgene:48138> ; RRID:Addgene_48138)

Other plasmids used in this diploma thesis were previously prepared by Mgr. Petr Kasparek, Ph.D. and are so far unpublished.

3.2 Methods

3.2.1 Transfection of E0771 cells

Transfection of E0771 cells was performed with Lipofectamine™ 3000 Transfection Reagent (Cat. No. L3000008; Invitrogen™), following the manufacturer's protocol. For one well of 12-well plate was used 100 µl of Opti-MEM™ Reduced Serum Medium (Cat. No. 31985062; Gibco™), 1.8 µl of Lipofectamine 3000 reagent, 1.5 µl of P3000 reagent, and 1 µg of prepared DNA. The transfection mixture was added to the well with cells in 75% confluency and left in a culture incubator for 4 hours. After that time, the medium was discarded, cells were washed with Phosphate Buffered Saline, and a new complete medium was added. Transfected cells were selected by 5 µg/ml of Blasticidin (Cat. No. ant-bl-05; Invitrogen™) or 800 µg/ml of Geneticin™ Selective Antibiotic (G418 Sulfate) (Cat. No. 10131019; Gibco™) and/or sorted using a fluorescence microscope or FACS.

3.2.2 Isolation of tumor tissues

Grown tumors were harvested after 17 – 20 days after tumor cells injection, or at the time one of the tumor diameters reached 15 mm. For flow cytometry experiments, up to 0.2 g of fresh tissue was dissociated in single-cell suspension using The Tumor Dissociation Kit, mouse (Cat. No. 130-096-730; Miltenyi Biotec) in combination with RPMI 1640 according to manufacturer's instructions. In protocol were used gentleMACS C Tubes (Cat. No. 130-096-334; Miltenyi Biotec), gentleMACS Dissociator (Cat. No. 130-093-235; Miltenyi Biotec), MACSmix™ Tube Rotator (Cat. No. 130-090-753; Miltenyi Biotec) in combination with an incubator at 37 °C, and CellTrics® 100 µm strainer (Cat. No. 04-0042-2318; Sysmex Partec). For protein and RNA isolation, tumors were cut into pieces (approx. 5 mm³) and stored at -80 °C.

3.2.3 Flow cytometry

To remove red blood cells from cell suspension, the cell pellet was resuspended in 1 ml of ACK buffer (150 mM NH₄Cl, 10 mM KHCO₃, 0.1 mM Na₂EDTA in ddH₂O to reach pH 7.2 – 7.4) and incubated for 3 minutes at room temperature. Afterward, HBSS (Hanks Balanced Salt Solution) to final volume 5 ml was added, and the suspension was then filtered through a 100 µm cell strainer. Cell concentration was measured diluted 1:1 in Trypan blue stain in Nexcelom Cellometer Auto T4 using the Cellometer Disposable

Counting Chambers SD100 (Cat. No. CHT4-SD100-014; Nexcelom Bioscience LTD). For fluorescence-activated cell sorting (FACS) analysis, the single-cell suspension of 10^7 viable cells was stained with specific antibodies directly conjugated with fluorochromes. The list of antibodies used for staining is provided in Tab. 3.1. For viability, cells were resuspended in 100 μ l Ghost dye UV450 (Cat. No. 13-0868-T500; Tonbo Bioscience) diluted 1:400 in HBSS and incubated 20 minutes at 4 °C. During the staining procedure, FACS buffer (2% FCS, 10 mM HEPES, 2 mM EDTA, 0.1 % NaN₃ in HBSS without Ca²⁺ and Mg²⁺) was used, and cells were incubated with 100 μ l of staining cocktail of antibodies for 30 minutes at 4 °C. Prepared cells were analyzed by BD LSR Fortessa™ SORP (BD Biosciences), and up to 300 000 CD45⁺ events were acquired. Obtained data were analyzed in FlowJo™ Software (Becton, Dickinson and Company; 2019). The gating strategy is shown in Figure 3.1.

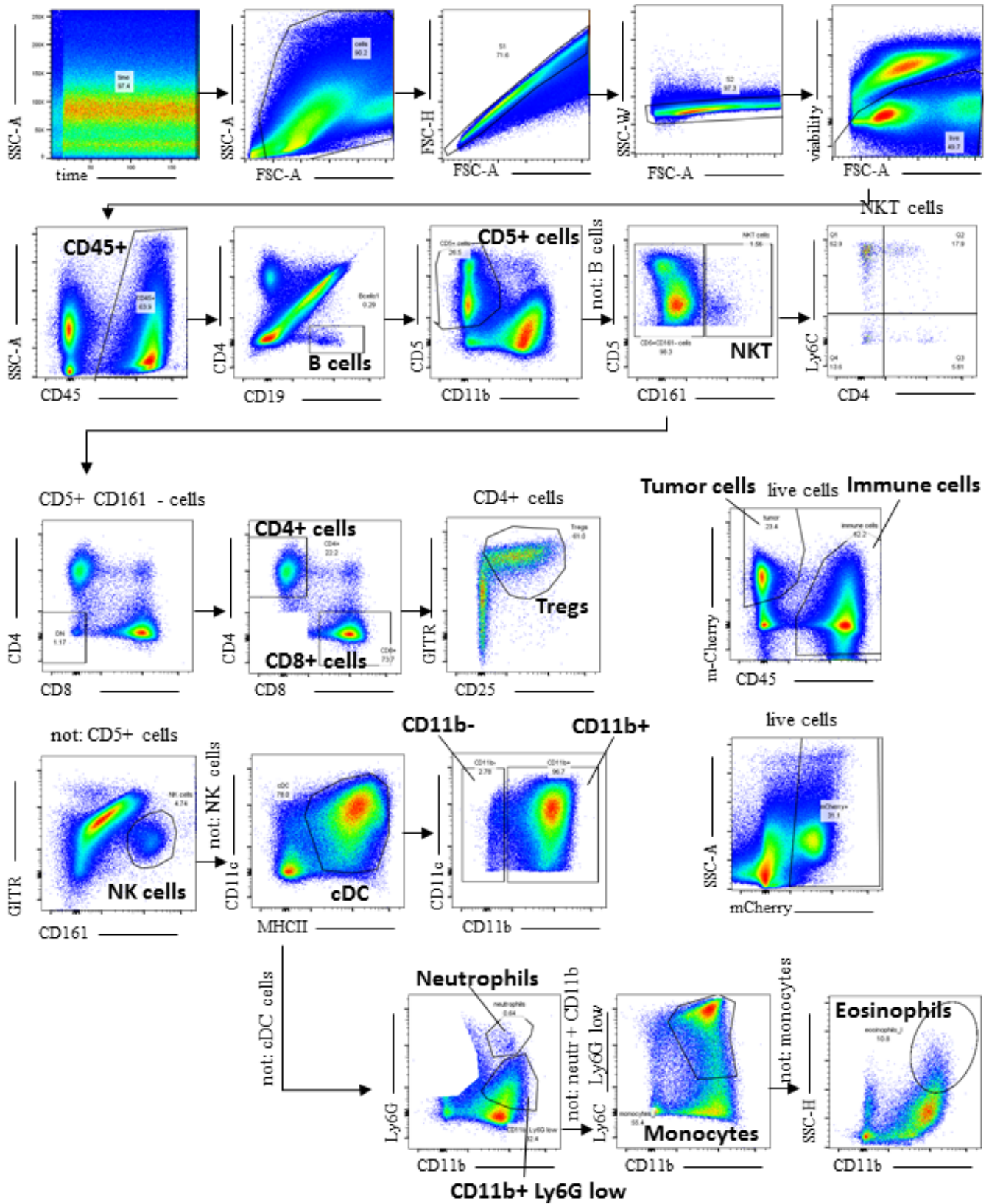


Figure 3.1 Gating strategy

3.2.4 Subcutaneous injection of tumor cells

Cells were counted in the Bürker chamber, and 10^6 cells were resuspended in 100 μ l of phosphate buffered saline. 80 μ l of cell suspension was injected with an insulin syringe subcutaneously in the shaved abdomen area of sacrificed C57Bl/6N mice. Fluorescent cells were visualized immediately. To cells expressing nanoLuciferase, Furimazine (1 μ g/ml) (kind gift from Mgr. Jan Procházka Ph.D.; Institute of Molecular Genetics of the Czech Academy of Sciences) or Coelentrazine (1 μ g/ml) (kind gift from Mgr. Jindřich Sedláček Ph.D.; Institute of Organic Chemistry and Biochemistry of the Czech Academy of Sciences) were added to microtubes with cells before injection. D-Luciferine (150 μ g/ml) (Cat. No. 122799-5; PerkinElmer) was added to cells expressing firefly luciferase and red-shifted firefly luciferase before injection. Fluorescence and luminescence were visualized in Lago X optical imaging systems (Spectral Instruments Imaging). For the fluorescence detection set, as seen in Tab. 3.6. The excitation was turned off for the luminescence detection, the emission filter was open, and the exposure time was 5 s.

Detection of	Optimal excitation wavelength	Optimal emission wavelength	Set excitation wavelength	Set emission filter wavelength	Exposure time
EGFP	488 nm	507 nm	465 nm	510 nm	5 s
mCherry	587 nm	610 nm	570 nm	610 nm	5 s
EYFP	513 nm	527 nm	500 nm	550 nm	5 s
mTBFP2	399 nm	454 nm	405 nm	490 nm	5 s
iRFP670	643 nm	670 nm	605 nm	670 nm	5 s
NLSsfEGFP	488 nm	507 nm	465 nm	510 nm	5 s

Table 3.6. Optimal excitation and emission wavelengths of used fluorescent proteins and the nearest possible setting of the imaging system. EGFP – enhanced green fluorescent protein; mCherry – mCherry red fluorescent protein; EYFP – enhanced yellow fluorescent protein; mTBFP2 – blue fluorescent protein; iRFP670 – near-infrared fluorescent protein emitting light in wavelength 670 nm; NLSsfEGFP – nucleus localization signal super folded enhanced green fluorescent protein

3.2.5 Mammary gland fat pad injection

Cells for mammary gland fat pad injection were counted in the Bürker chamber. Cells were resuspended in 20.25 μ l of ice-cold Phosphate Buffered Saline, and 20.25 μ l of Matrigel® growth factor reduced basement membrane matrix (Cat. No. 356238; Corning) and stored

on the ice up to 1 hour maximum before injection into a mammary gland fat pad of anesthetized mice. Mice were anesthetized with a combination of Rometar (Bioveta): Zoletil (Biopharm) 1:4 (5 mg/kg), and 30 µl of the prepared cells-Matrigel solution was injected with an insulin syringe into a fourth mammary gland fat pad.

3.2.6 Luminescence detection via plate reader

The level of luminescence of cells was detected at plate reader CLARIOstar® Plus (BMG LABTECH). Luminescence was measured after the addition of an appropriate luciferase substrate. Coelentraine (1 µg/ml) (kind gift from Mgr. Jindřich Sedláček Ph.D.; Institute of Organic Chemistry and Biochemistry of the Czech Academy of Sciences) was added to cells expressing nanoLuciferase. D-Luciferine (150 µg/ml) was added to cells expressing firefly luciferase and red-shifted firefly luciferase.

3.2.7 *In vivo* imaging

In vivo imaging was performed in Lago X optical imaging systems (Spectral Instruments Imaging). Mice were anesthetized while imaging by Aerrane (Isofluranum; Cat. No. 4DG9621; Baxter). For luminescence and various fluorescence visualization, Lago X optical imaging system was set as seen in the tab. 3.6. Before luminescence detection, mice were injected by insulin syringe intraperitoneally with 5 µg of Furimazine (kind gift from Mgr. Jan Procházka Ph.D.; Institute of Molecular Genetics of the Czech Academy of Sciences) dissolved in 100 µl of PBS. *In vivo* imaging of nanoLuciferase positive tumors in mice was performed regularly once in three days after tumor cells injection into a mammary gland fat pad.

3.2.8 RNA isolation

For the RNA extraction from cell cultures, 600 µl of TRI Reagent® (Cat. No. T9424; Sigma Aldrich®) was added, and the cell suspension was harvested. For the RNA extraction from frozen (-80 °C) tumor samples, 600 µl of TRI Reagent® (Cat. No. T9424; Sigma Aldrich®) was added, and the tissue was lysed using iron balls and vibration in Qiagen TissueLyser II (30 Hz for 2 minutes). The mixtures were then incubated for 5 minutes at room temperature, and 120 µl of chloroform was added to each sample. After 15 minutes of incubation at room temperature, mixtures were shaken repeatedly and centrifuged with a microcentrifuge (Eppendorf™ 5424 R) at 12000 g for 15 minutes at 4

°C. The aqueous phase (containing the RNA fraction) was collected, and 300 µl of isopropyl alcohol was added. The samples were mixed and incubated for 30 minutes at -20 °C. Samples were then centrifuged 12000 g for 15 minutes at 4°C, and the supernatant was discarded afterward. The pellet was washed twice in 1000 µl of 75% ethanol and centrifuged at 7500 g for 5 minutes at 4 °C. The supernatant was discarded, and after drying up of a pellet, the RNA was dissolved in 100 µl of ddH₂O. RNA concentration was measured using an Implen NanoPhotometer® N50. RNA quality was verified by rRNA band detection using gel electrophoresis on a 1% agarose gel prepared from SeaKem® LE Agarose (Cat. No. 50004; Lonza) and TAE buffer (40 mM Tris, 20 mM acetic acid, 1 mM EDTA) run at 100V fixed voltage setting for 30 minutes.

3.2.9 Quantitative real-time polymerase chain reaction (qRT-PCR)

In vitro reverse transcription was performed using M-MLV Reverse Transcriptase (Cat. No. M1705; Promega) following the manufacturer's protocol. For the reaction, 2 µg of RNA, 2 µl of oligo(dT)₂₃ primer (35µM), purchased as a synthetic, desalted, and lyophilized DNA oligonucleotides from Sigma Aldrich®, 1.25 µl of deoxynucleotide mix (10 mM, Sigma Aldrich®), 5 µl of M-MLV RT buffer (5X; Cat. No. M5313; Promega), 25 units of RNasin® ribonuclease inhibitor (Cat. No. N2515; Promega) and 200 units of M-MLV Reverse Transcriptase (Cat. No. M1705; Promega) were combined with ddH₂O to 25 µl total reaction volume. The reaction mix was incubated in a thermocycler (BIO-RAD T100™ Thermal Cycler) at 42 °C for 1 hour, and 75 µl of ddH₂O was added to the sample afterward. The expression levels of genes of interest were determined by qRT-PCR. The measurements were performed in duplicates or triplicates on Light cycler® 480 (Roche). PCR reactions were performed using 3 µl of cDNA, 5 µl of LightCycler® 480 SYBR Green I Master (Cat. No. 4887352001; Roche s.r.o.) and 0.25 µl of each primer (10µM) (Tab. 3.4) and 1.5 µl of ddH₂O. The qRT-PCR reaction was performed as seen in the tab. 3.7. Relative mRNA levels of interest were calculated using three housekeeping genes normalization (*Prdx1*, *Actb*, and *GAPDH*) and the $2^{-\Delta C_t}$ analysis method.

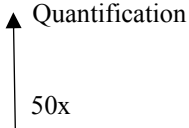
Temperature (°C)	Time (s)	Ramp (°C/s)	Mode
95	120	4.8	
95	15	4.8	
60	20	2.5	
72	20	4.8	
95		0.1	Melting curve

Table 3.7. qRT-PCR cycle

3.2.10 Protein isolation and detection – Western blot

For protein isolation, cell cultures and frozen (-80 °C) tumor samples were lysed in RIPA-buffer (150 mM NaCl, 1 % Triton X-100, 0.5 % sodium deoxycholate, 0.1 % sodium dodecyl sulfate and 50mM Tris, pH 8.0) supplemented with 1:100 cOmplete™, Mini Protease Inhibitor Cocktail (Cat. No. 04693124001; Roche s.r.o.) The protein concentration was quantified using Pierce™ BCA Protein Assay Kit (Cat. No. 23225; Thermo Scientific™) and plate reader EPOCH Microplate Spectrophotometer (BioTek). Forty micrograms were used for each sample loaded onto 15% separating gel prepared from Akrylamid/bisakrylamid 30% Rotiphorese® (Cat. No. R 30291; CARL ROTH), TEMED (Cat. No. T9281-50ml; Sigma Aldrich®), 10% ammonium persulfate (Cat. No. A3678-100G; Sigma Aldrich®), 10% Sodium dodecyl sulfate and 1.5 M Tris-HCl, pH 8.8. 1.5 M Tris-HCl, pH 6.8 was used for the stacking gel. The proteins were separated by SDS-PAGE electrophoresis and blotted on nitrocellulose membrane (Cat. No. 10600002; Amersham™). Used primary and secondary antibodies are seen in the tab. 3.2. SuperSignal™ West Pico PLUS Chemiluminescent Substrate (Cat. No. 34580; Thermo Scientific) was used for visualization with Chemidoc MP imaging system, and images were captured using Image Lab 6.0.1 software (Bio-Rad). PageRuler™ Plus Prestained Protein Ladder, 10 to 250 kDa (Cat. No. 26619; Thermo Scientific™) was used as a molecular weight marker. ImageJ 1.50b software (National Institutes of Health, Bethesda, MD, USA) was used to quantify each protein's band intensity followed by normalization to its corresponding GAPDH control.

3.2.11 PCR and PAGE

DNA isolation from various prepared E0771 single clones transfected with CRISPR-Cas9 system targeting selected genes (Tab. 3.5) was performed by QuickExtract DNA Extraction Solution (Cat. No. QE09050; GeneTiCA). The targeted locus was then amplified by polymerase chain reaction (PCR) using primers in Tab. 3.3. For the PCR, 3 μ l of DNA from each sample, 1 μ l of each primer (10mM), 0.5 μ l of deoxynucleotide mix (10 mM, Cat. No. D7295; Sigma Aldrich®), 2.5 μ l of DreamTaq Green Buffer (10X; Cat. No. EP0714; Thermo Scientific™) and 0.2 μ l DreamTaq DNA Polymerase (5 U/ μ L; Cat. No. EP0714; Thermo Scientific™) were combined with ddH₂O to 25 μ l total reaction volume and incubated in a thermocycler (BIO-RAD T100™ Thermal Cycler) at 95 °C for 3 min, for 35 cycles at 95 °C for 30 seconds, 60 °C for 30 seconds, 72 °C for 1 minute, followed by 72 °C final extension time for 5 minutes.

The amplified PCR reaction mix was separated by agarose gel electrophoresis on a 2 % agarose gel prepared from SeaKem® LE Agarose (Cat. No. 50004; Lonza) and TAE buffer (40 mM Tris, 20 mM acetic acid, 1 mM EDTA) at 90 V fixed voltage setting for 40 minutes. The amplified PCR reaction mix was also separated by polyacrylamide gel electrophoresis (PAGE) on a 5% polyacrylamide gel prepared from Akrylamid/bisakrylamid 30% Rotiphorese® (Cat. No. R 30291; CARL ROTH), TEMED (Cat. No. T9281-50ml; Sigma Aldrich®), ammonium persulfate (Cat. No. A3678-100G; Sigma Aldrich®) and 10X TBE buffer (1 M Tris, 1 M boric acid, 20 mM EDTA) at 90 V fixed voltage setting for 45 minutes. GeneRuler 1 kb Plus DNA Ladder (Cat. No. SM1331; Thermo Scientific™) was used to size a double-stranded DNA.

PCR products from various prepared E0771 single clones were purified using ExoSAP-IT™ PCR Product Cleanup (Cat. No. 78200.200.UL; Applied Biosystems™) following the manufacturer's protocol and send for direct Sanger sequencing (Eurofins Genomics).

3.2.12 Fluorescence-activated cell sorting (FACS)

For fluorescence-activated cell sorting (FACS), transfected E0771 cells were treated with Trypsin-EDTA (0.5%) (Cat. No. 15400054; Gibco™) and resuspended in complete medium with 1% fetal bovine serum (Gibco™). Cells were sorted by BD Influx Cell Sorter (BD Biosciences;) or FACSAria IIu (BD Biosciences), both in the facility of flow

cytometry in the Institute of Molecular Genetics of the Czech Academy of Sciences. Cells were sorted into a conditional medium made from 50% of their collected and filtered complete medium and 50% of a new complete medium in one collection tube or as single clones in a 96-well plate.

3.2.13 Statistical analysis

All statistical analyses and graphs present in this diploma thesis were created using GraphPad Prism (GraphPad Software, version 9.1.0 (221), March 15, 2021). While analyzing leukocyte fractions, the unpaired 2-tailed Student's t-test and Mann-Whitney test, justified by fulfillment of their assumptions, were used for statistical significance evaluation. The box plots represent medians with 1st and 3rd quartile; whiskers present minimal and maximal values. GP: ≥ 0.05 (ns), 0.01 to 0.05 (*), 0.001 to 0.01 (**), 0.0001 to 0.001 (***), < 0.0001 (****). For correlation analysis, Pearson product-moment correlation coefficient "r" was measured.

4 Results

This work aims to establish experimental models for studying the expected crosstalk of selected kallikrein-related peptidases (KLK5, KLK7, and KLK14) with breast cancer TIME and for validation of their function as prognostic biomarkers in breast cancer disease. To fulfill this goal, the diploma project included the following steps:

- Selection of suitable cell line for cell-line derived orthotopic allograft experiments in a mouse model based on C57Bl/6N mouse strain background
- Validation of various fluorescent and luminescent markers for *in vivo* imaging of cancer progression
- Generation of selected *Klks* (*Klk5*, *Klk7*, and *Klk14*) and *Il1b* “knock-out” cell lines
- Analysis of KLK roles in tumorigenesis and anti-tumor immune response using the generated experimental models (Fig. 4.1)

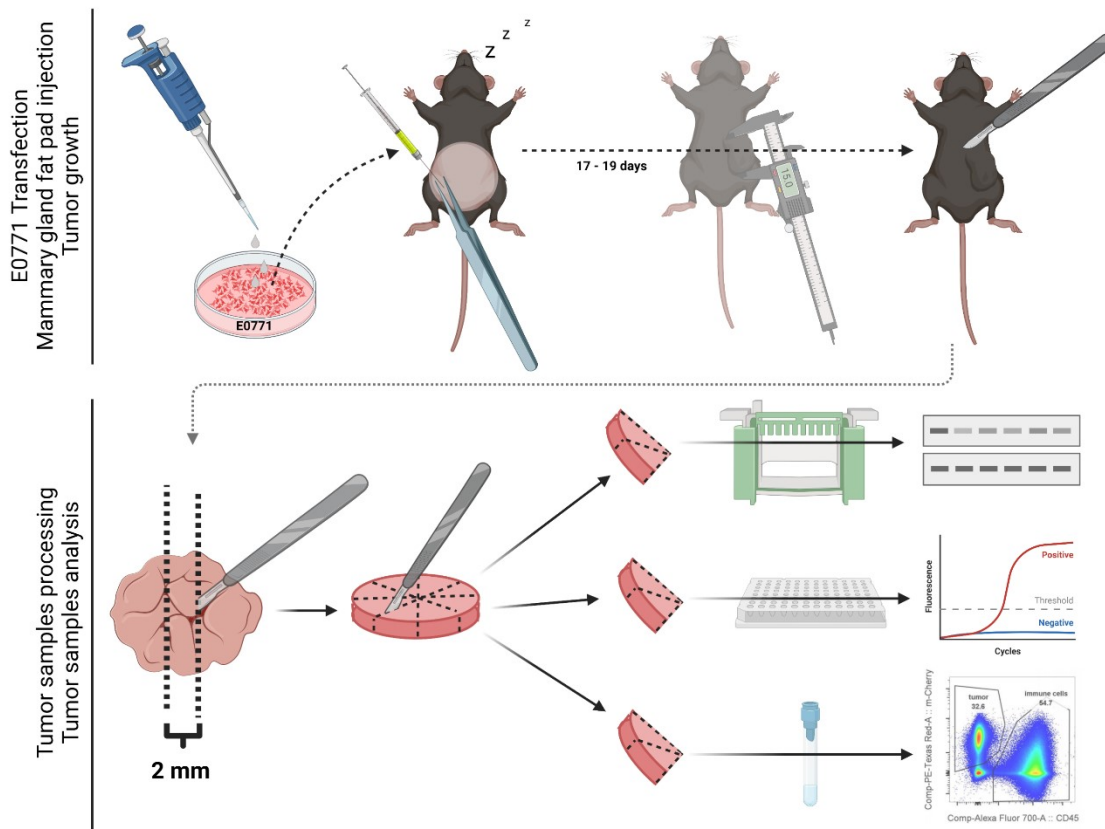


Figure 4.1 Schema of the final *in vivo* experiment of Actb-mCherry E0771 cell line inoculation into mammary gland fat pads of various *Klks* gene-deficient C57Bl/6N mice (Created with BioRender.com)

4.1 The E0771 cell line is a suitable cell line model for orthotopic cell line-derived allograft experiments in C57Bl/6N mouse strain

Two murine breast cancer cell lines were used to compare their growth in two popular experimental mouse strains, BALB/c and C57Bl/6N mouse strains. 4T1-Red-FLuc, derived from mouse mammary gland adenocarcinoma cell line 4T1 bearing red-shifted firefly luciferase gene from *Luciola Italica* (*Red-FLuc*) and it has been already used in our laboratory. On the contrary, the E0771 cell line was purchased and established newly in our laboratory. It is a murine breast adenocarcinoma cell line initially isolated from spontaneous mammary gland tumor from C57Bl/6N mouse (Casey et al., 1951). 2.0×10^5 and 4.0×10^5 of 4T1-Red-Fluc and wt E0771 cells, respectively, were injected each in mammary gland fat pad of three mice of BALB/c mouse strain and three mice of C57Bl/6N mouse strain. All female mice were seven weeks old. The efficiency of generating tumors from these two cell lines under the regular monitoring of mouse weight and tumor size were compared. None of the mice, injected with 4T1-Red-Fluc cells, developed tumors by 20 days (0 of 6, 0%). None of the mice of BALB/c strain, injected with wt E0771 cells, developed tumors by 20 days (0 of 3, 0%). All three C57Bl/6N mice, injected with wt E0771 cells, developed tumors with at least 1.5 cm in diameter by 20 days (3 of 3, 100%). Tumors growth is seen in figure 4.2.A. During the whole experiment, Signs of Pain = 1, Quality of Stool = 1, Wound Healing = 1, and Body Condition Score = 3 in all animals.

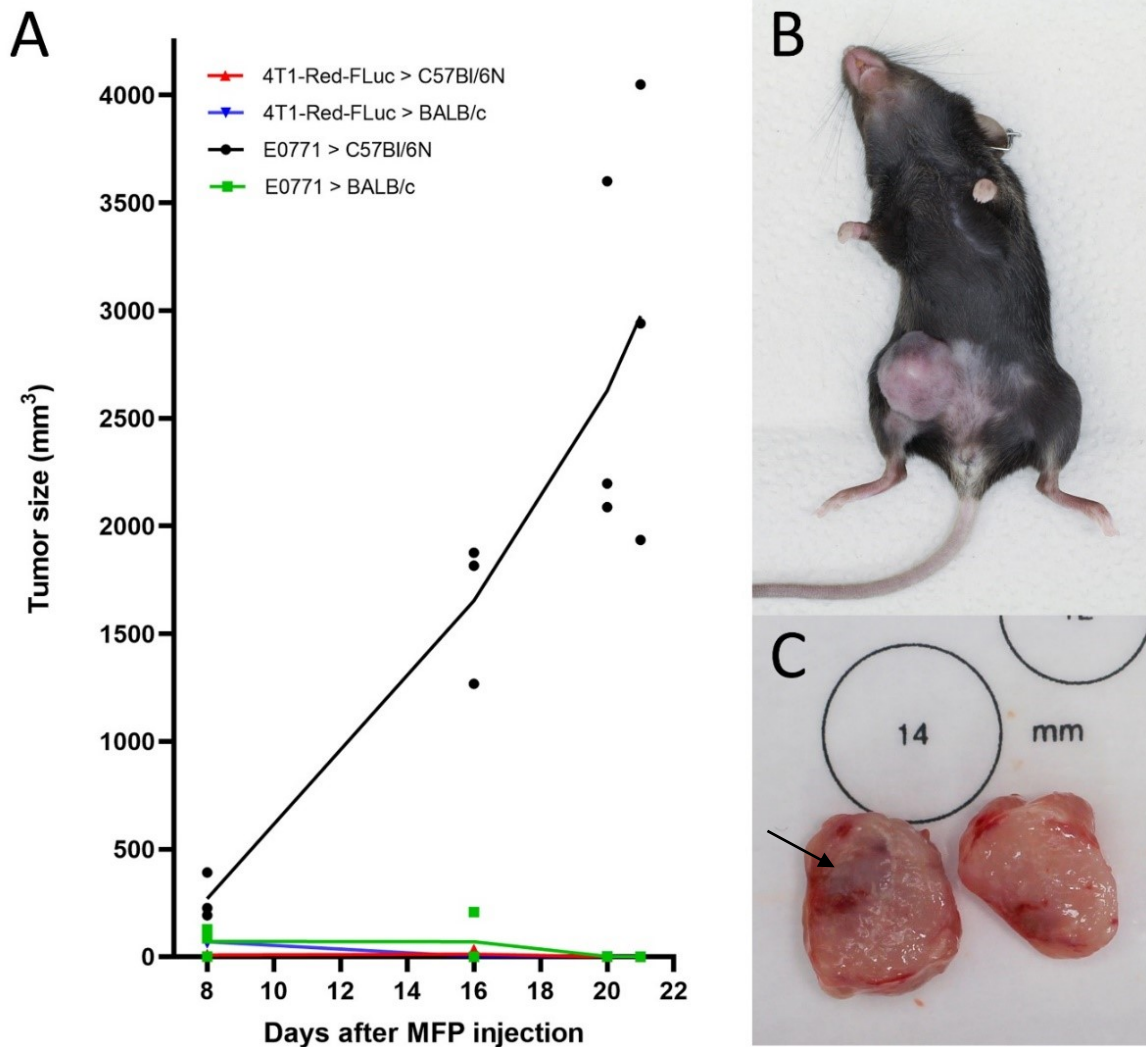


Figure 4.2. Tumor growth in BALB/c and C57Bl/6N female mice injected in mammary gland fat pad with 4T1-Red-FLuc and wt E0771 cells (A); 7-weeks-old C57Bl/6 female mouse with mammary gland tumor 20 days postinjection (B); wt E0771 cell-line-initiated tumor cut in half (C); beginning necrosis indicated by an arrow; MFP – mammary gland fat pad

4.2 Evaluation of various markers for *in vivo* imaging in murine breast cancer model

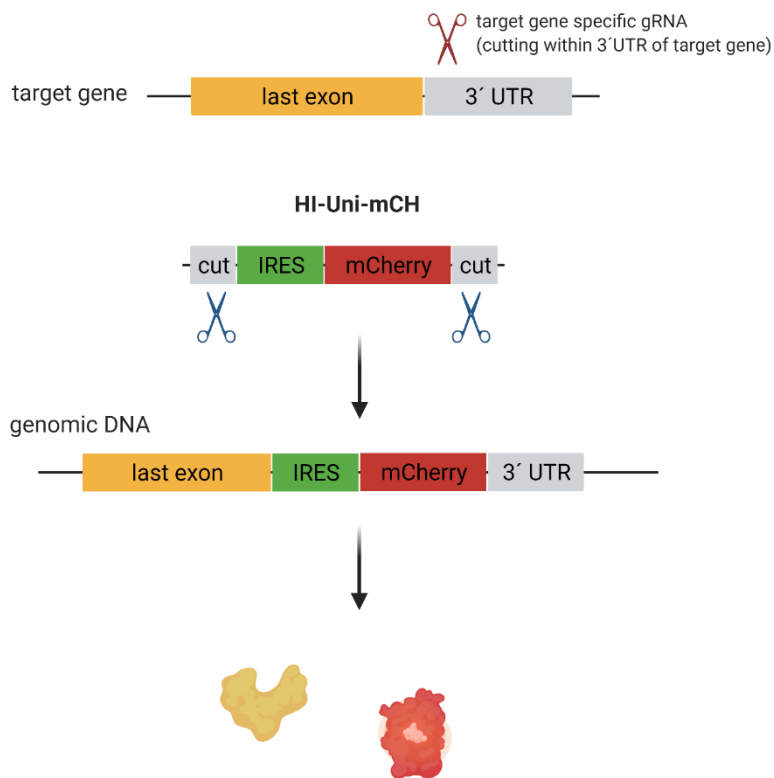
Monitoring and analyzing disease progression real-time *in vivo* in animal models are a valuable tool for its research. It has an enormous benefit, especially in cancer, where the disease progression is based on the forming of redundant pathological tissue or metastasizing. As a part of this project were prepared reporter cell lines with various fluorescent and luminescent markers under the beta-actin gene (*Actb*) promoter.

4.2.1 Fluorescent markers

Six fluorescent proteins were chosen to prepare mutant cell lines carrying a fluorescent marker driven by the endogenous *Actb* promoter: EGFP, mCherry, EYFP, mTBFP2, iRFP670, and NLSsfEGFP.

4.2.1.1 Generation of E0771 cell lines carrying various fluorescent markers

The transfection of the E0771 cell line was performed with a combination of three plasmids. The first plasmid harbors sequences of fluorescent proteins listed in the tab. 3.6 (EGFP, mCherry, EYFP, mTBFP2, iRFP670, and NLSsfEGFP). The second plasmid carries a CRISPR/Cas9 editing system cutting out the fluorescent protein sequence from the first plasmid. The third plasmid bears a CRISPR/Cas9 editing system with gRNA specific for 3'UTR of the *Actb*. When all three plasmids are present in one cell, the fluorescent protein sequence is cut out of the first plasmid and inserted by a non-homologous end joining (NHEJ) repair mechanism into 3'UTR of the *Actb* (Fig. 4.3) (Suzuki and Izpisua Belmonte, 2018). Transfection of the E0771 cell line was performed as written in the 3.2.1 chapter of this thesis. Upon Blasticidin (5 µg/ml) selection, clones producing fluorescent proteins were sorted as single positive clones by FACS according to



their emission spectra (Tab. 3.6). For each reporter line, three to four positive clones were co-cultivated to obtain a heterogeneous population. Reporter lines were clearly detectable from wild-type cells (Fig. 4.4).

Figure 4.3. Mechanism of *Actb*-reporter lines generation; 3'UTR - the three prime untranslated region; IRES - An internal ribosome entry site

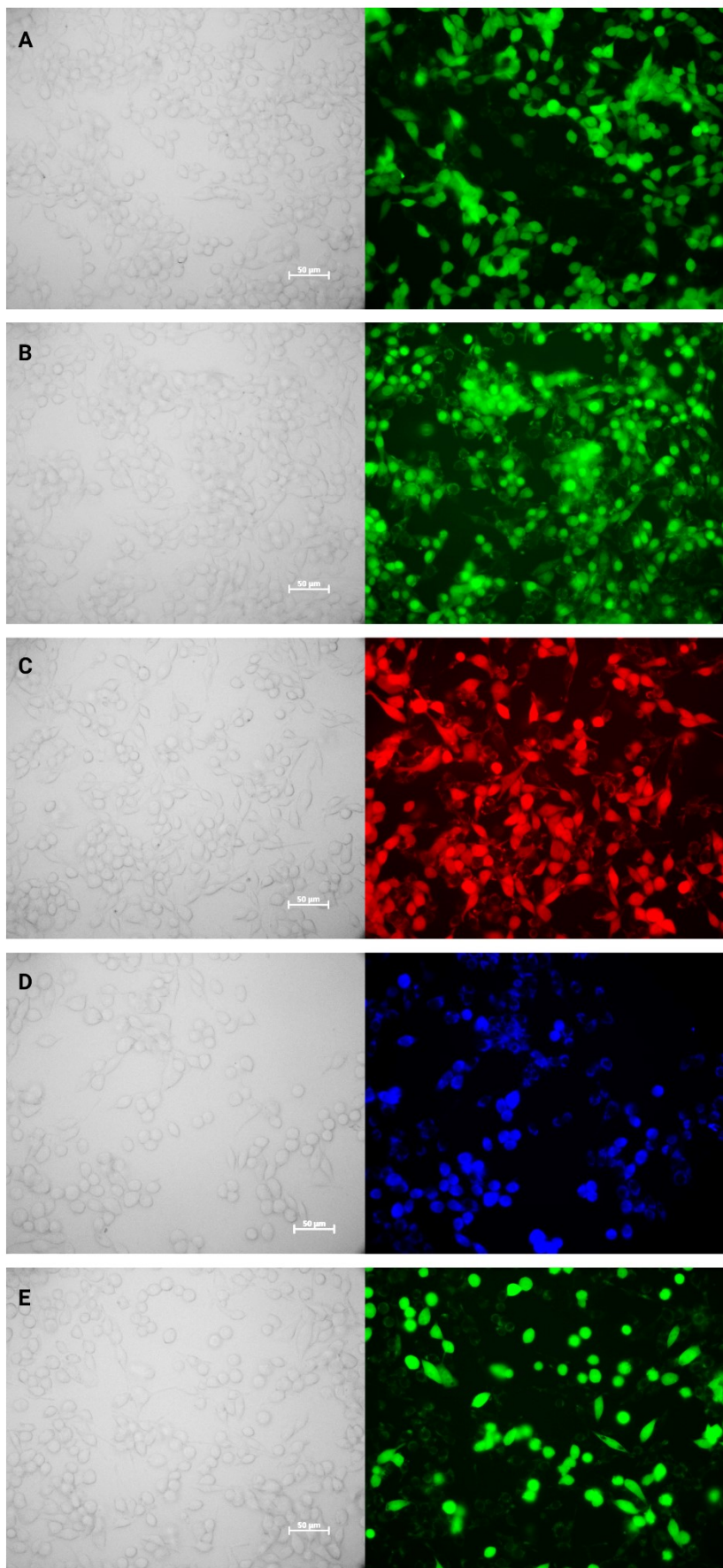


Figure 4.4. Detection of generated heterogeneous reporter E0771 cells; Reporter cells were co-cultivated with wt cells on glass slides. Slides were gently washed by PBS and immediately visualized using a fluorescent imaging microscope; Actb-EGFP E0771 reporter line (A); Actb-NLSsfEGFP E0771 reporter line (B); Actb-mCherry E0771 reporter line (C); Actb-mTbfp2 E0771 reporter line (D); Actb-EYFP E0771 reporter line (E); left side of the figure shows bright-field views and right side shows their corresponding fluorescent signals.

Various combinations of two generated fluorescent reporter lines were co-cultivated on glass slides to exclude the possibility of spectral overlap. Slides were gently washed by PBS and immediately visualized using a fluorescent imaging microscope (Fig. 4.5).

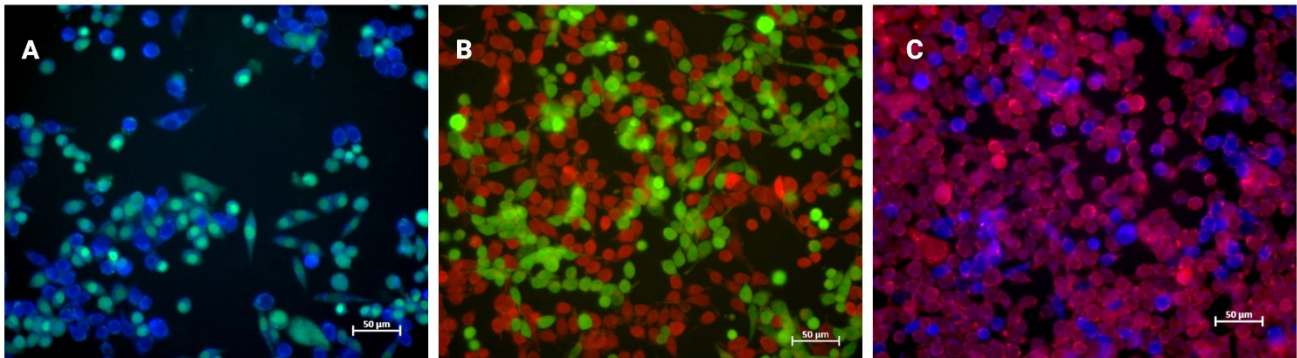


Figure 4.5. Visualisation of various reporter cell lines co-cultivation using a fluorescent imaging fluorescent microscope; Actb-mTBFP2 E0771 + Actb-NLSsfEGFP E0771 (A); Actb-EGFP E0771 + Actb-mCherry E0771 (B); Actb- mTBFP2 E0771 + Actb-mCherry E0771 (C)

4.2.1.1 Characterization of E0771 reporter lines in vivo

Each generated reporter cell line was injected in three C57Bl/6 female mice. 3×10^5 cells were injected into the mammary gland fat pad unilaterally. None of the mice, injected with Actb-iRFP670 E0771 and Actb-EYFP E0771 cells, developed tumors by 28 days (0 of 6, 0%). Two mice, injected with Actb-EGFP E0771 cells, developed tumors with at least 1.5 cm in diameter by 28 days (2 of 3, 66%). All mice, injected with Actb-mTBFP2 E0771, Actb-mCherry E0771, Actb-NLSsfEGFP E0771 or wt E0771 cells, developed tumors with at least 1.5 cm in diameter by 28 days (12 of 12, 100%). Tumors growth is seen in figure 4.6. During the whole experiment, Signs of Pain = 1, Quality of Stool = 1, Wound Healing = 1, and Body Condition Score = 3 in all animals.

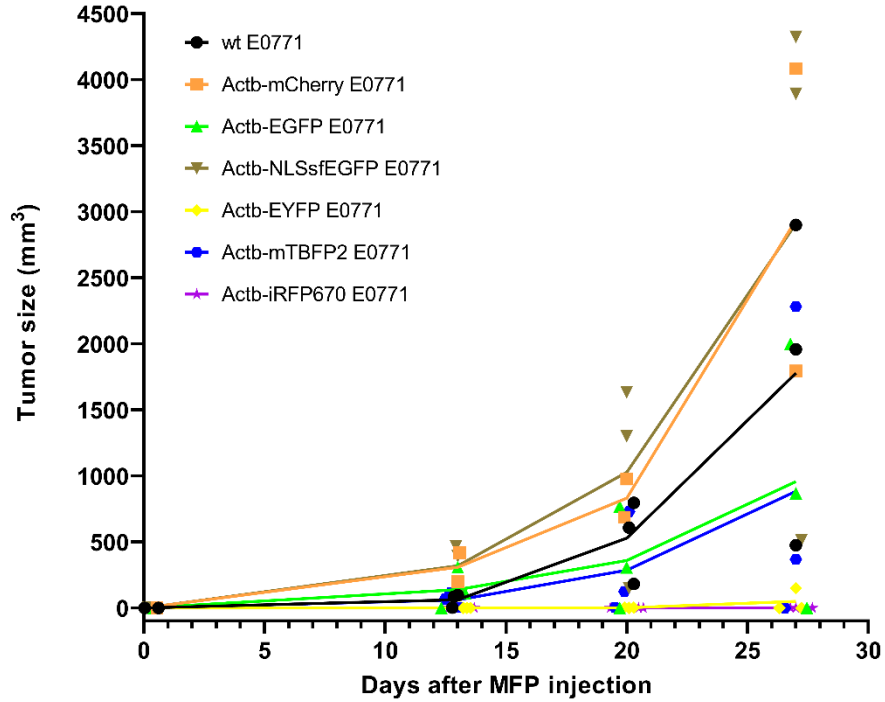


Figure 4.6 Tumor growth in C57Bl/6N female mice injected with generated fluorescent cell lines into a mammary gland fat pad (MFP).

To verify the potential of generated reporter lines to be used as a tool for real-time tumor progression imaging, the cells were injected subcutaneously in the shaved abdomen area of sacrificed C57Bl/6N mice. A fluorescent signal was monitored right after injection in the Lago X optical imaging systems (Spectral Instruments Imaging) (Fig. 4.7)

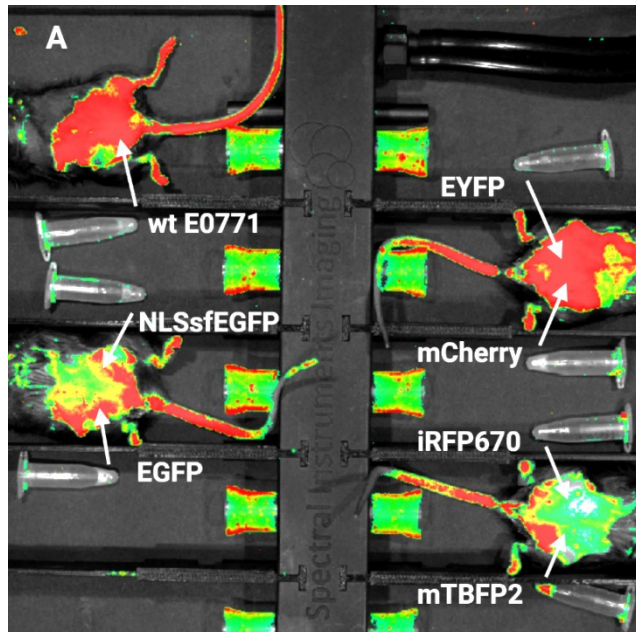


Figure 4.7 Detection of fluorescent signal of generated reporter lines by Lago X optical imaging system; excitation and emission filters were set according to individual fluorescent proteins spectra (Tab. 3.6); the signal was detected in microtubes with Actb-mTBFP2 E0771 cells but was not detected in place of injection (A)

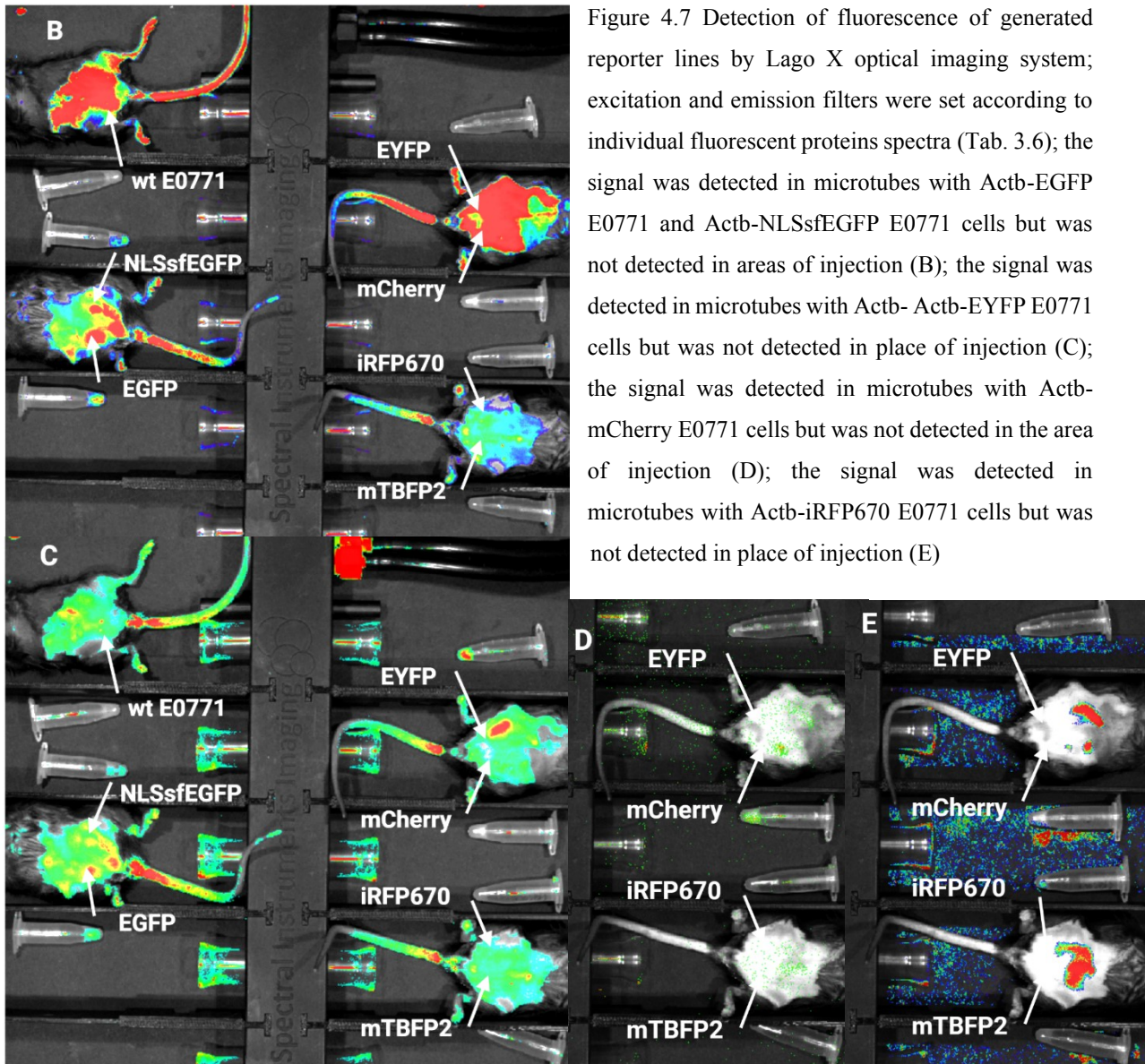


Figure 4.7 Detection of fluorescence of generated reporter lines by Lago X optical imaging system; excitation and emission filters were set according to individual fluorescent proteins spectra (Tab. 3.6); the signal was detected in microtubes with Actb-EGFP E0771 and Actb-NLSsfEGFP E0771 cells but was not detected in areas of injection (B); the signal was detected in microtubes with Actb- Actb-EYFP E0771 cells but was not detected in place of injection (C); the signal was detected in microtubes with Actb-mCherry E0771 cells but was not detected in the area of injection (D); the signal was detected in microtubes with Actb-iRFP670 E0771 cells but was not detected in place of injection (E)

Even though we detected the fluorescence signal of cells resuspended in PBS in Eppendorf tubes, we could not see the fluorescence signal using *in vivo* imaging system available in our facility.

4.2.1.2 *Generated EGFP, NLSsfEGFP, YFP, and mCherry expressing E0771 cell lines develop in tumors in C57Bl/6N mouse strain*

Once tumors reached 1.5 cm in diameter, animals were sacrificed and tumors dissected. Fresh pieces of tumors were visualized by the fluorescence microscope (Fig. 4.8)

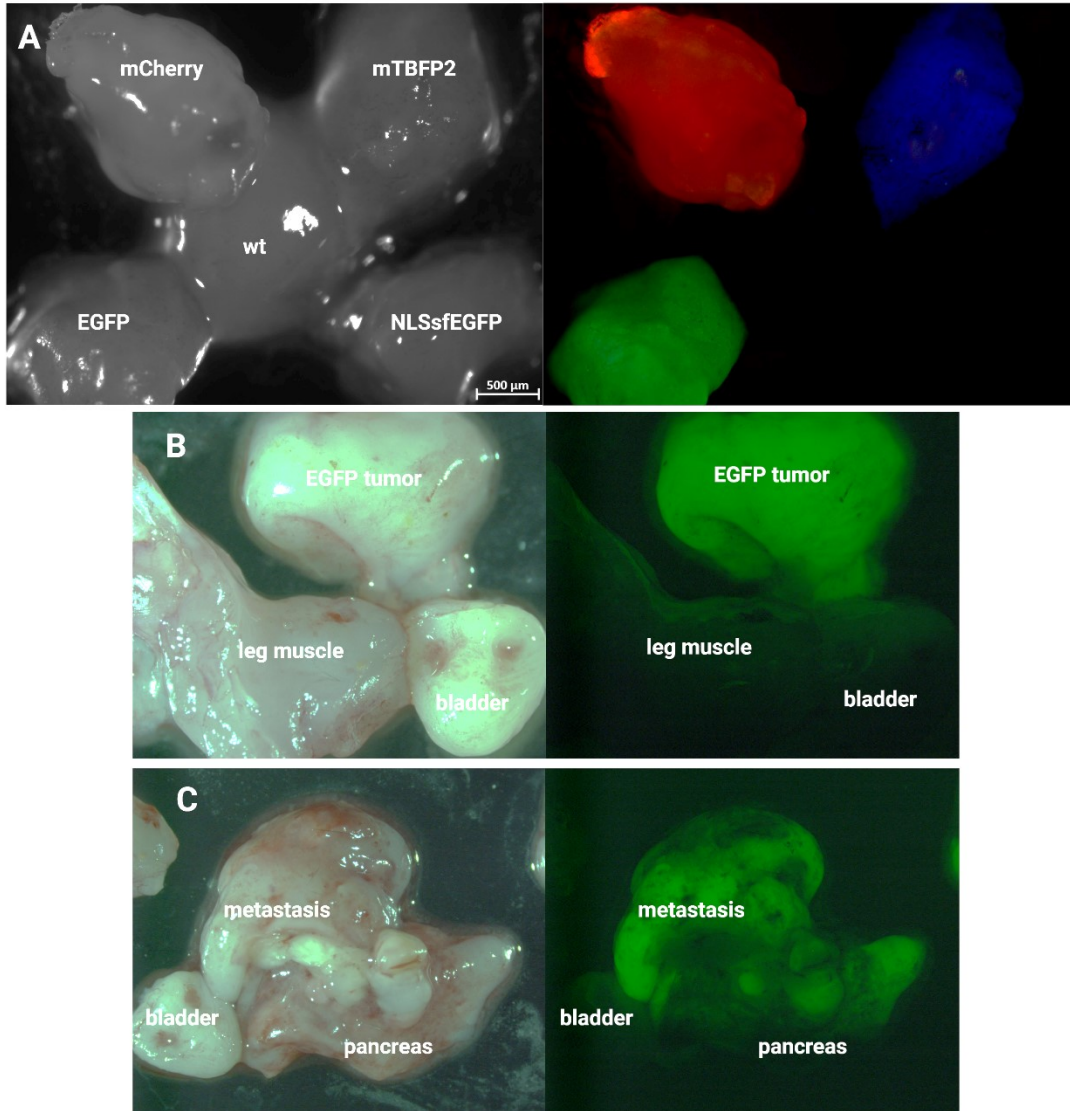


Figure 4.8 Detection of fluorescence in fresh pieces of tumors developed from injected reporter fluorescent cells. Fresh chunks of tumors (A); EGFP expressing tumor with other samples of tissue from one mouse injected with Actb-EGFP E0771 cells (B); Metastasis in the pancreas of a mouse injected with Actb-EGFP E0771 cells (C)

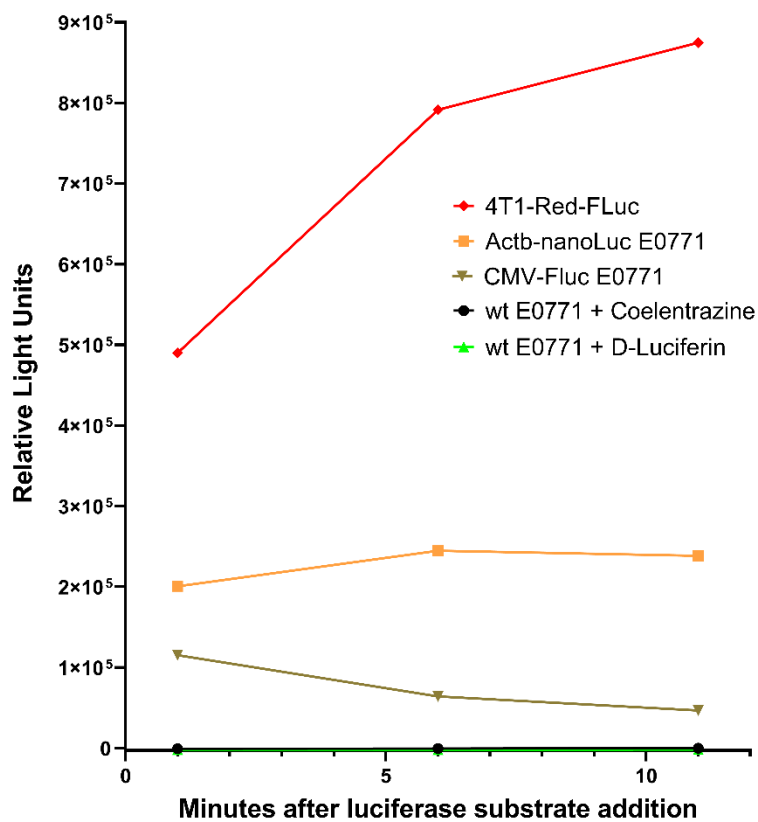
Presented results show the sustainability of fluorescence in developing tumors initiated by mammary gland fat pad injection of generated Actb-mTBFP2 E0771, Actb-mCherry E0771, and Actb-EGFP E0771 cell lines.

4.2.2 Luminescent markers

Two luminescent markers were selected to prepare mutant cell lines carrying a luminescent marker: nanoLuciferase and Firefly Luciferase.

4.2.2.1 NanoLuciferase under the β -Actin promoter combined with its substrate Coelentrazine gives a stronger signal than Firefly Luciferase under the CMV promoter with its substrate D-Luciferin.

Transfection of the E0771 cell line was performed as described in chapter 3.2.1 of this thesis. NanoLuciferase gene was inserted under the endogenous *Actb* promoter by combining three plasmids similar to those described in the 4.2.1.1 chapter, and positive clones were selected by Blasticidin (5 μ g/ml). Firefly luciferase driven by exogenous CMV promoter was transfected into cells in pGL4.18 CMV-Luc plasmid, and positive clones were selected by Geneticin (800 μ g/ml). (Grohar et al., 2011) Upon antibiotics selection, the luminescence intensity of selected Actb-nanoLuc E0771 and CMV-Luc E0771 clones was determined on a plate reader after adding the corresponding luciferase substrate. As a positive control were used already mentioned 4T1-Red-FLuc cells and as negative control

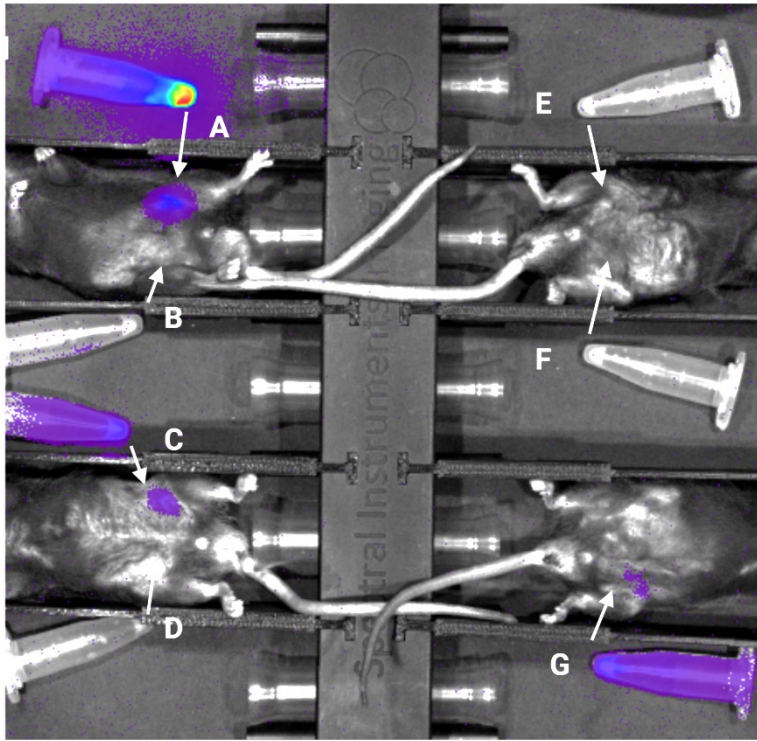


wt E0771 cells. Complete medium with luciferases substrates was used as a blank. The dynamic luminescence curves of all analyzed samples are seen in Fig. 4.9.

Figure 4.9 Dynamic luminescence curve of 4T1-Red-FLuc cells with 150 μ g/ml of D-Luciferin, Actb-nanoLuc E0771 with 1 μ g/ml Coelentrazine, CMV-FLuc E0771 with 150 μ g/ml of D-Luciferin, wild-type E0771 cells with 1 μ g/ml of Coelentrazine, wild-type E0771 cells with 150 μ g/ml of D-Luciferin; Luminescence intensity is given in relative light units.

4.2.2.2 *NanoLuciferase is a suitable luminescence marker for real-time in vivo imaging in C57Bl/6N mice*

To verify the potential of generated luminescent reporter lines to be used as a tool for real-time *in vivo* imaging, the cells were injected with their substrates subcutaneously in the abdomen area of sacrificed C57Bl/6N mice. Contrary to previous similar experiment results with fluorescent markers, the luminescence signal was detected right after injection



in the Lago X optical imaging system in mice injected with 4T1-Red-FLuc cells and Actb-nanoLuc E0771 cells with both used substrates. (Fig. 4.10)

Figure 4.10 Detection of luminescence of generated reporter lines by Lago X optical imaging system. The excitation was turned off for the luminescence detection, the emission filter was open, and the exposure time was set to 5 s; 4T1-

Red-FLuc + D-Luciferin (A); wt E0771 + D-Luciferin (B); Actb-nanoLuc E0771 + Furimazine (C); wt E0771 + Furimazine (D); CMV-FLuc E0771 + D-Luciferin (E); wt E0771 + Coelentrazine (F); Actb-nanoLuc E0771 + Coelentrazine (G); Arrows indicate area of injection.

4.2.2.3 *Generated Actb-nanoLuc E0771 cell line is sustainable in luciferase expression, and its signal can be detected while the tumor progression*

Generated Actb-nanoLuc reporter cells were injected in three C57Bl/6 female mice. 3×10^5 cells were injected into the mammary gland fat pad bilaterally. All mice developed tumors bilaterally (3 of 3, 100%). Mice were monitored regularly, and tumors were visualized in Lago X optical imaging system. Besides visualization, tumors were measured by caliper at the same time point (Fig. 4.11). During the whole experiment, Signs of Pain = 1, Quality of Stool = 1, Wound Healing = 1, and Body Condition Score = 3 in all animals.

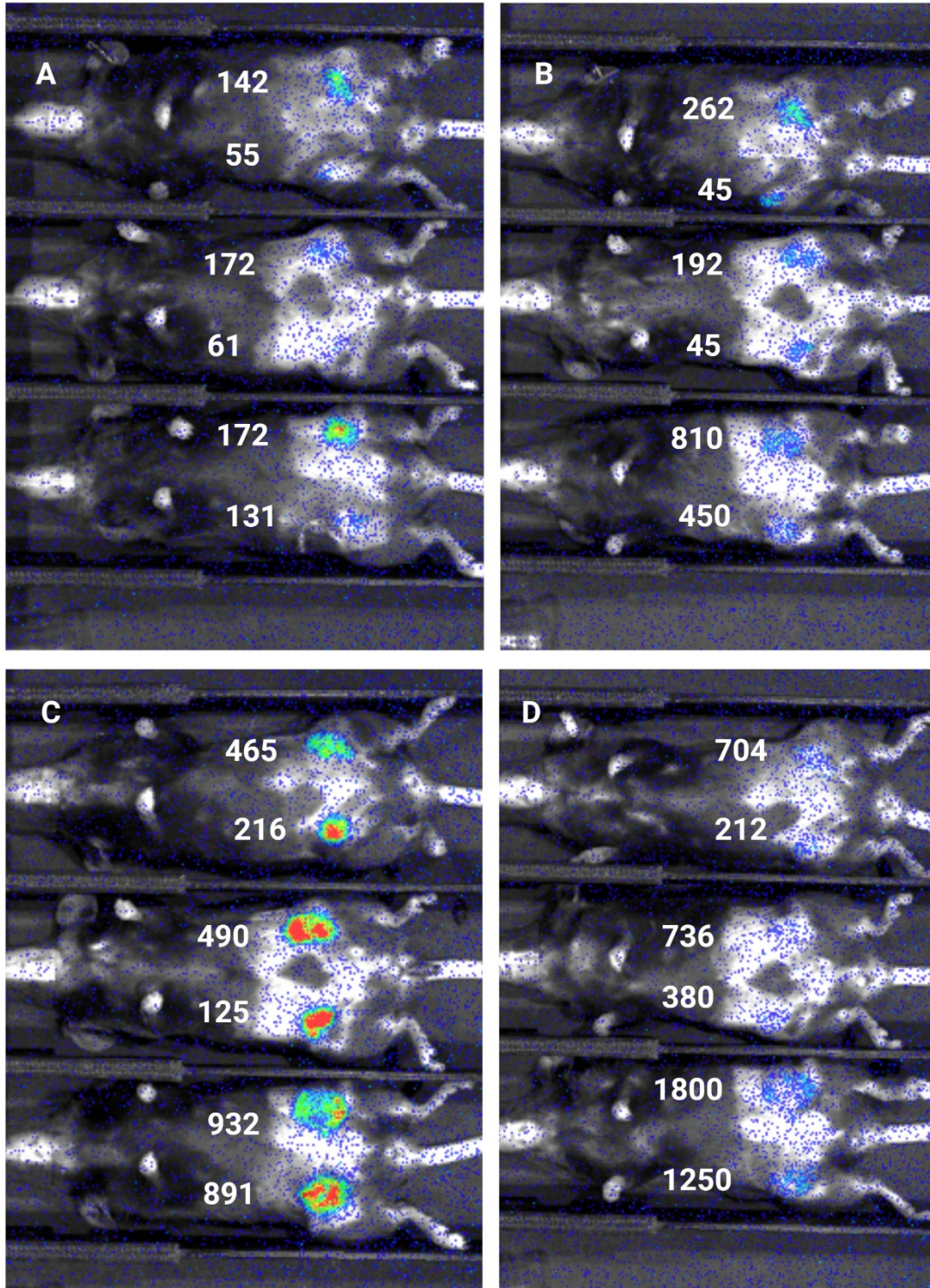


Figure 4.11 Detection of luminescence luminescent tumors by Lago X optical imaging system. The excitation was turned off for the luminescence detection, the emission filter was open, and the exposure time was set to 2 s. Tumors were monitored 7. (A), 12. (B), 14 (C) and 16. (D) day post-injection of Actb-nanoLuc cells in mammary glands fat pad bilaterally. The layout of mice is uniform in each picture. Numbers indicate tumor sizes measured by caliper on the same day.

The growth of tumors grown from generated Actb-nanoLuc cells in C57Bl/6N female mice was compared to the growth of wild-type E0771 tumors in C57Bl/6N female mice. 3×10^5 cells of both cell lines were injected into the mammary gland fat pad of three C57Bl/6N mice bilaterally. All mice developed tumors bilaterally (6 of 6, 100%). The tumor growth in both cohorts is seen in Figure 4.12. Mice were monitored regularly, and tumors were measured by caliper. During the whole experiment, Signs of Pain = 1, Quality of Stool = 1, Wound Healing = 1, and Body Condition Score = 3 in all animals.

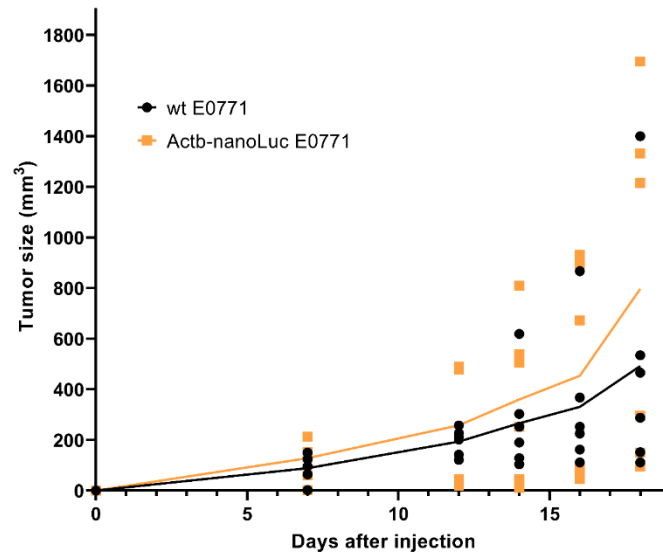


Figure 4.12 Tumor growth in C57Bl/6N female mice injected into a mammary gland fat pad with generated luminescent Actb-nanoLuc E0771 cell line and original wt E0771 cell line.

4.3 Growth of Actb-mCH E0771 cell line in C57Bl/6N mice deficient for *Klk5*, 7, and *14*

Generated Actb-mCherry E0771 reporter cell line was injected in twelve C57Bl/6 female mice ($3 \times \text{wt}$, $3 \times Klk7^{-/-}$, $3 \times Klk5^{-/-}Klk7^{-/-}$, $3 \times Klk14^{-/-}$). Each mouse was injected bilaterally with 3×10^5 cells into the mammary gland fat pad. Except for one *Klk14*^{-/-} mouse, who developed tumor unilaterally, all mice developed tumors bilaterally. The mouse weight and the tumor growth were monitored regularly. Tumors growth is shown in figure 4.13. During the whole experiment, Signs of Pain = 1, Quality of Stool = 1, Wound Healing = 1, and Body Condition Score = 3 in all animals.

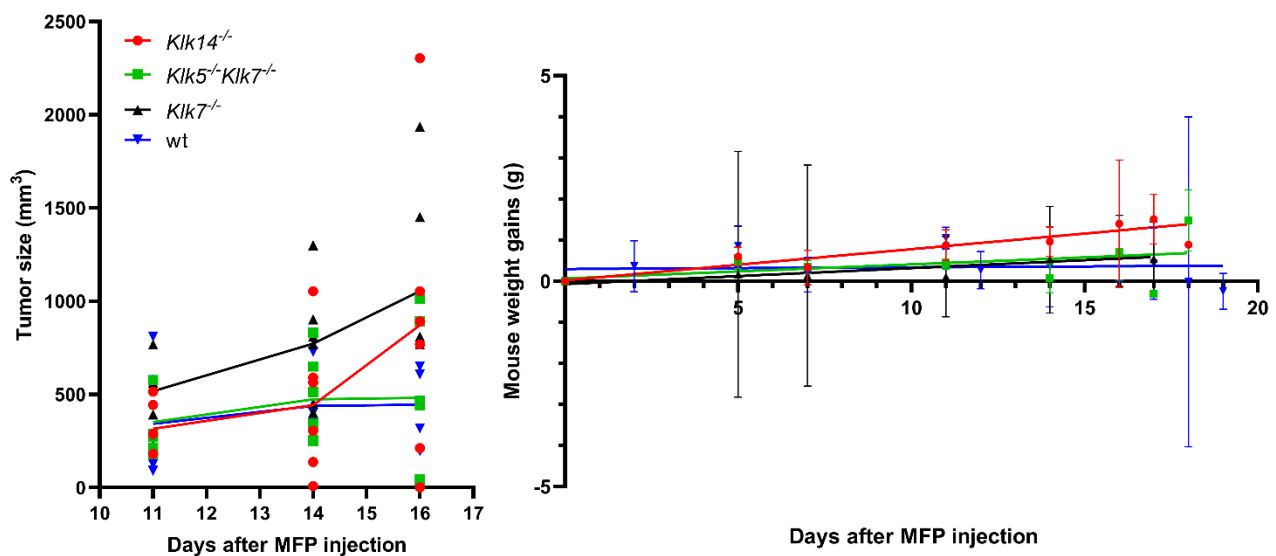


Figure 4.13 Tumor growth and mouse weight gains of C57Bl/6N female mice: *Klk7*^{-/-}, *Klk5*^{-/-}*Klk7*^{-/-}, and *Klk14*^{-/-}, injected into a mammary gland fat pad with generated Actb-mCherry E0771 cell line; MFP – mammary gland fat pad

4.4 Analysis of tumor samples

Mice from the experiment in chapter 4.3 were sacrificed, and the tumors dissected 17 – 18 days post-injection of tumor cells. Dissected tumors were further analyzed. Expression levels of selected genes (*Klk5*, *Klk7*, *Klk14*, *Il1b*, and *F2r1l*) in the TME were measured by qRT-PCR as described in chapter 3.2.9. Relative protein levels of IL-1 β , I κ B ζ , and PAR2 were determined by Western blot as described in chapter 3.2.10. The immune infiltrates fractions in the tumor tissue were analyzed by flow cytometry, as explained in chapter 3.2.3.

4.4.1 qRT-PCR analysis

Expression levels of *Klk5*, *Klk7*, *Klk14* in the TME of *Klk5*, *7*, and *14* deficient C57Bl/6N mice seem to be affected by their deficiency in the host organism. However, relative mRNA levels of these genes are not significantly changed in the tumor tissue (Fig. 4.14)

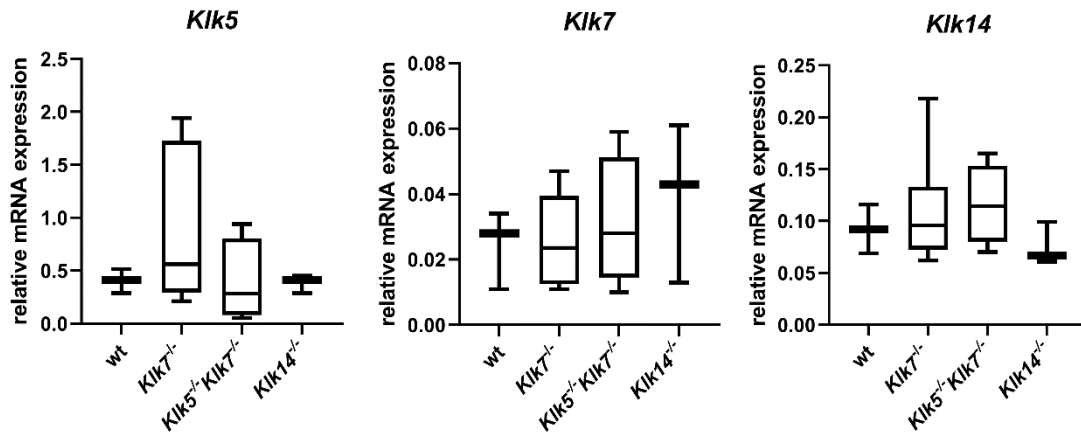


Figure 4.14 Relative mRNA expression of *Klk5*, *Klk7*, and *Klk14* in the tumor tissue of wt, *Klk7*^{-/-}, *Klk5*^{-/-} *Klk7*^{-/-}, and *Klk14*^{-/-} mice injected with Actb-mCherry E0771 cells into a mammary gland fat pad. Three housekeeping genes normalization (*Prdx1*, *Actb*, and *GAPDH*) and the 2^{-ΔCt} analysis method was used.

As previously mentioned, KLKs directly impact various immunomodulatory molecules, such as PAR2, IL-1β. Relative mRNA expression of their genes was also analyzed in harvested tumor samples (Fig. 4.15). The relative expression level of *Camp* (gene for mCRAMP - mouse analog of human LL-37) was intended to be measured as well. However, none of the used primer pairs reprinted from (Kin et al., 2011) and (Guesdon et al., 2020) worked for our samples.

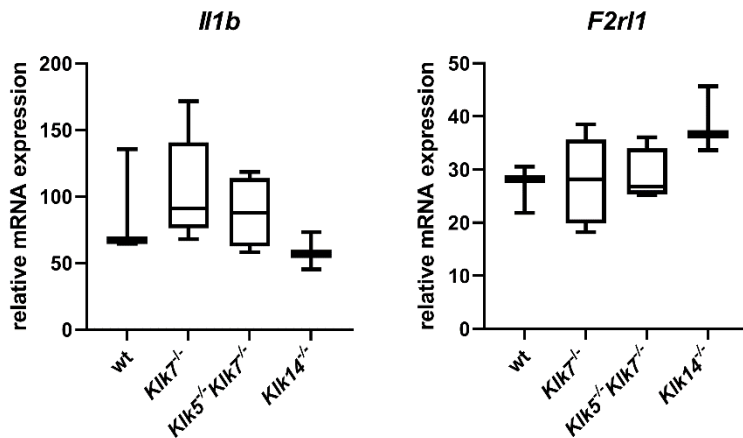


Figure 4.15 Relative mRNA expression of *Il1b*, and *F2r1* in the tumor tissue of wt, *Klk7*^{-/-}, *Klk5*^{-/-} *Klk7*^{-/-}, and *Klk14*^{-/-} mice injected with Actb-mCherry E0771 cells into a mammary gland fat pad. Three housekeeping genes normalization (*Prdx1*, *Actb*, and *GAPDH*) and the 2^{-ΔCt} analysis method was used.

4.4.2 Western blot analysis

Both by qRT-PCR-analyzed immunomodulatory molecules can be processed and activated by KLKs. To determine their presence in tumor tissue on the protein level, relative protein levels of IL-1 β , I κ B ζ , and PAR2 were defined (Fig. 4.16). NF-kappa-B inhibitor zeta (I κ B ζ) is an NF- κ B cofactor, which is selectively induced by IL-1 β (Cowland et al., 2006). I κ B ζ was used in this experiment as a downstream indicator of IL-1 β activation.

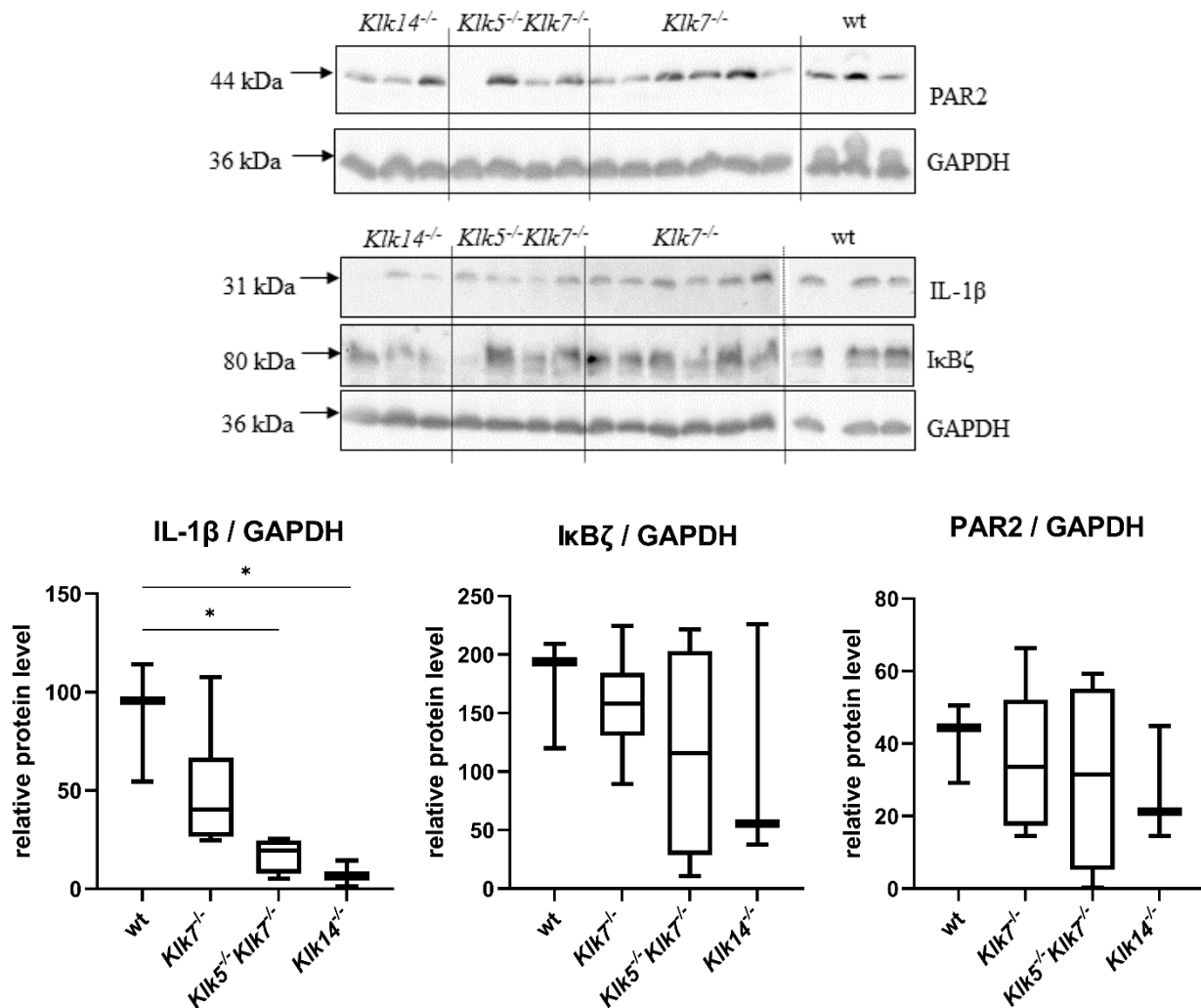


Figure 4.16 Relative protein levels of PAR2, IL-1 β , and I κ B- ζ determined by Western blot in the tumor tissue of wt, *Klk7*^{-/-}, *Klk5*^{-/-}*Klk7*^{-/-}, and *Klk14*^{-/-} mice injected with Actb-mCherry E0771 cells into a mammary gland fat pad. Statistical significance was measured by unpaired Student's t-test.

4.4.3 Flow cytometry analysis of tumor-infiltrating leukocytes (TIL)

Generated Actb-mCherry E0771 reporter cell line allows exact measurement of tumor cell fraction by flow cytometry due to its endogenous expression of mCherry fluorescent protein. In general, all *Klks* deficient mice cohorts developed bigger tumors than wild-type cohort, and the fraction of immune cells was lower. Compared to the wt cohort, the statistical significance was reached only for the *Klk7^{-/-}* and *Klk14^{-/-}* cohort, respectively (Fig 4.17).

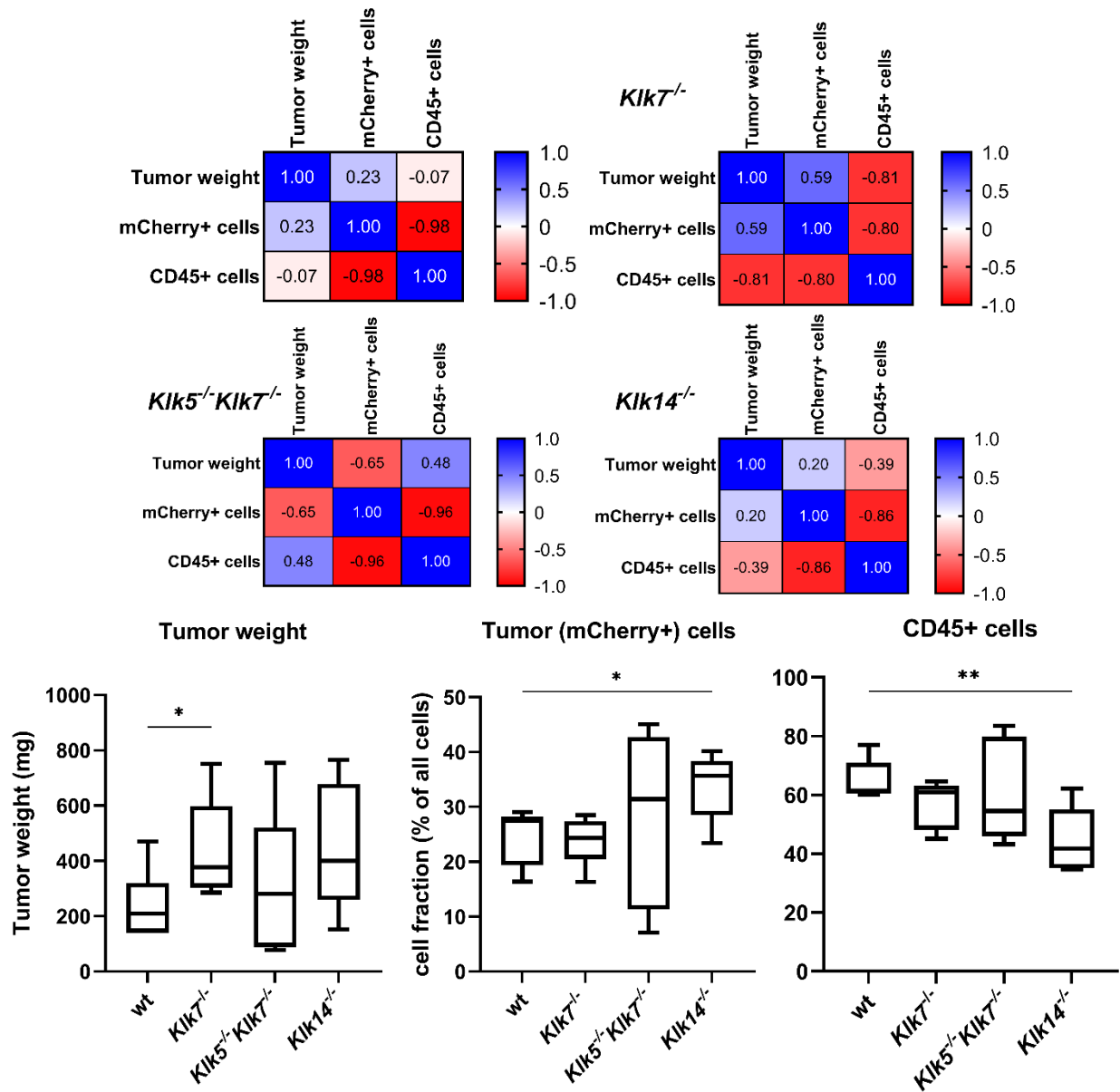


Figure 4.17 Correlation matrices and box plots of harvested tumor weights with and fractions (%) of tumor and immune cells present in the tumor tissue of wt, *Klk7^{-/-}*, *Klk5^{-/-}Klk7^{-/-}*, and *Klk14^{-/-}* mice with Actb-mCherry E0771 tumors. Unpaired Student's t-test measured statistical significance.

Besides tumor cells, particular infiltrating immune cell fractions were measured in harvested tumor samples. The gating strategy for immune cell population determination is shown in Fig. 3.1. Box plots of populations without the statistical significance of fraction proportions are supplemented in Fig. S.1.

Three T-cell populations (CD4⁺ helper T cells, CD4⁺ regulatory T cells, and CD8⁺ cytotoxic T cells) were evaluated, and proportions in the wild-type cohort were compared to each KO cohort. CD4⁺ regulatory T cells were significantly increased in tumor tissue of *Klk5^{-/-}Klk7^{-/-}* mice whose overall T cell fraction was raised. (Fig. 4.18)

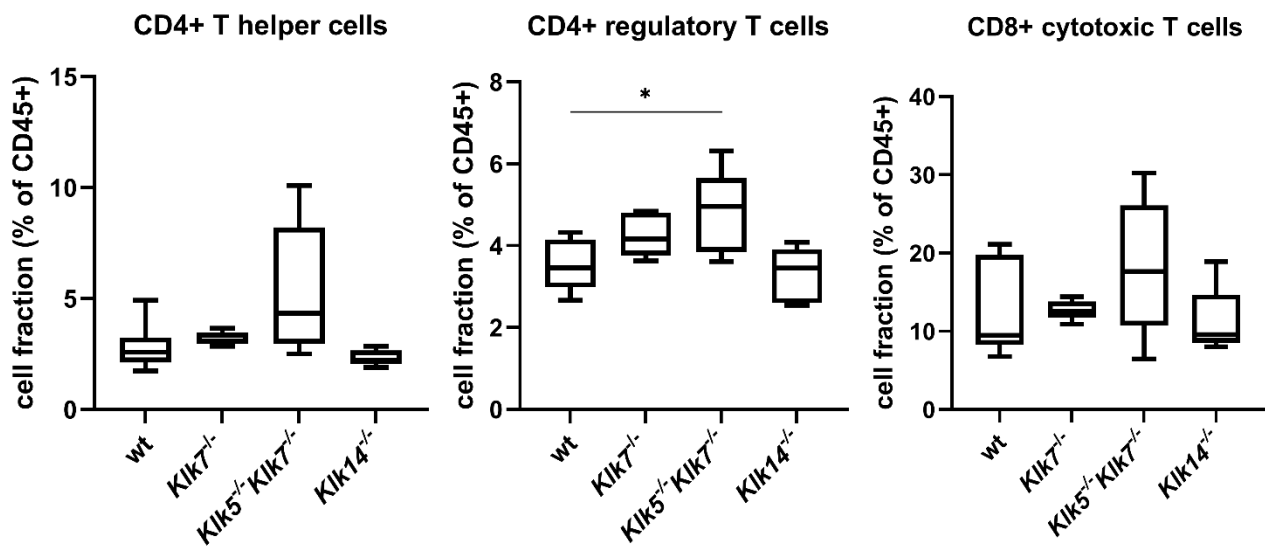


Figure 4.18 Box plots of CD4⁺ helper T cell, CD4⁺ regulatory T cell, and CD8⁺ cytotoxic T cell fractions (% of all CD45⁺ cells) infiltrated in tumor tissue harvested from wt, *Klk7^{-/-}*, *Klk5^{-/-}Klk7^{-/-}*, and *Klk14^{-/-}* mice with Actb-mCherry E0771 tumors. Unpaired Student's t-test measured statistical significance.

Four populations of NKT cells were determined in the collected tumor tissue. Differences in their proportions are shown in Fig. 4.19. However, their total fraction in all examined tumors did not exceed 1 % of all CD45+ cells, and this fact has to be considered during interpretation.

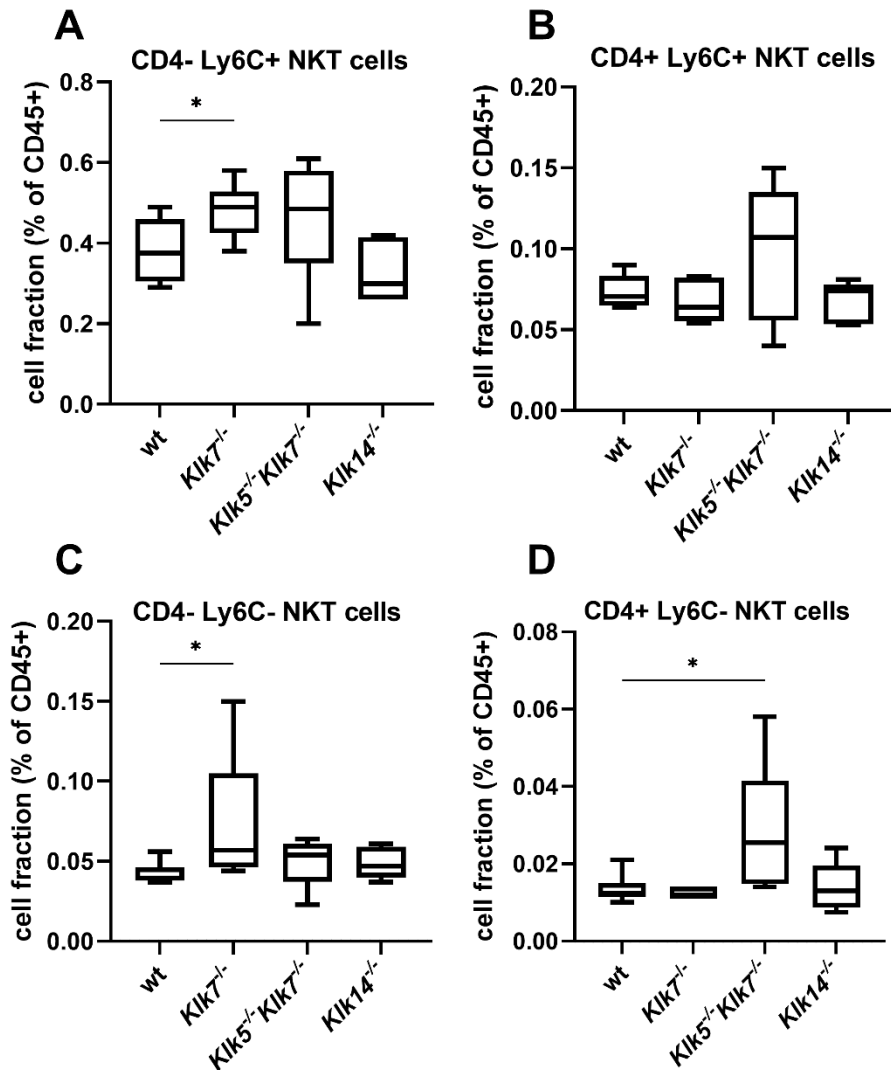


Figure 4.19 Box plots of four populations of NKT cell fractions (% of all CD45+ cells) infiltrated in tumor tissue harvested from wt, *Kik7*^{-/-}, *Kik5*^{-/-}*Kik7*^{-/-}, and *Kik14*^{-/-} mice with Actb-mCherry E0771 tumors. For calculation of statistical significance was used Mann-Whitney test (D) and the Unpaired Student's t-test (A, C).

Two myeloid cell populations reached statistical significance in the dataset: CD11b+, Ly6G low cells, and eosinophils (Fig 4.20)

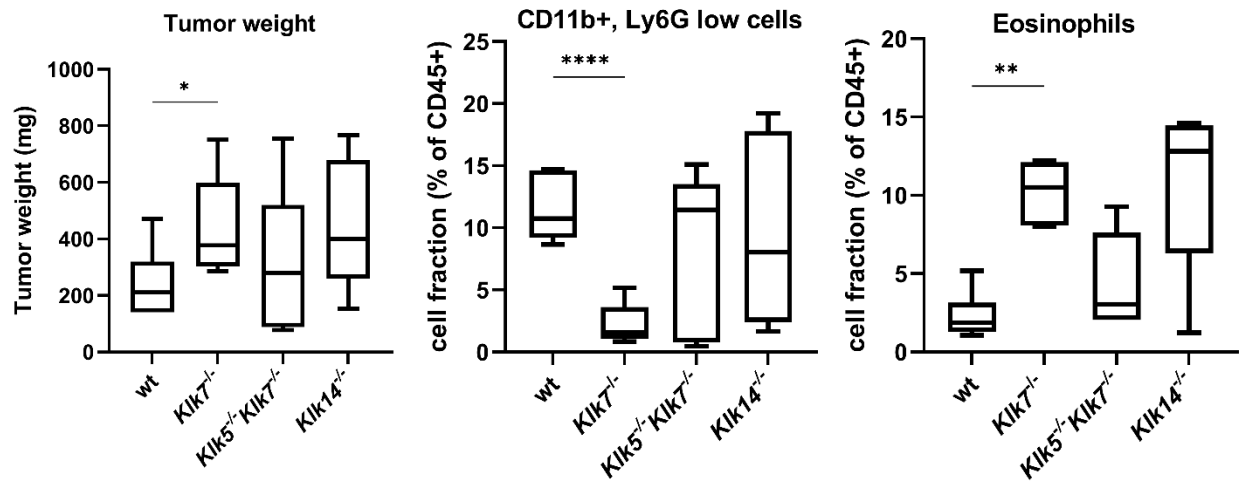


Figure 4.20 Box plots of tumor weight, the fraction of CD11b+, Ly6G low cells, and Eosinophils (% of all CD45+ cells) in tumor tissue from wt, *Klk7*^{-/-}, *Klk5*^{-/-}*Klk7*^{-/-}, and *Klk14*^{-/-} mice with Actb-mCherry E0771 tumors. Calculation of statistical significance was performed by Mann-Whitney test (Eosinophils) and the Unpaired Student's t-test (Tumor weight, CD11b+, Ly6G low cells).

4.5 Generation of *Klk5*, *Klk7*, *Klk14*, *Il1b*, and *F2rl1* deficient E0771 cell lines

To study the role of tumor-derived Klk proteases *in vivo*, we used CRISPR/Cas9 system to generate various E0771 lines deficient for individual *Klk* genes (5, 7, 14) genes that are putatively involved in Klk-mediated inflammation (*F2rl1*, *Il1b*).

4.5.1 Design and preparation of CRISPR/Cas9 vectors

CRISPR guide RNAs were designed using the CRISPOR.org web tool for genome editing experiments with the CRISPR–Cas9 system (Concordet and Haeussler, 2018) and Benchling [Biology Software]. (2020). CRISPR guide RNAs, targeting exons (Fig. 4.21) in selected genes, were then inserted into a pSpCas9(BB)-2A-GFP plasmid as described in the 3.1.5 chapter of this thesis. (Ran et al., 2013)

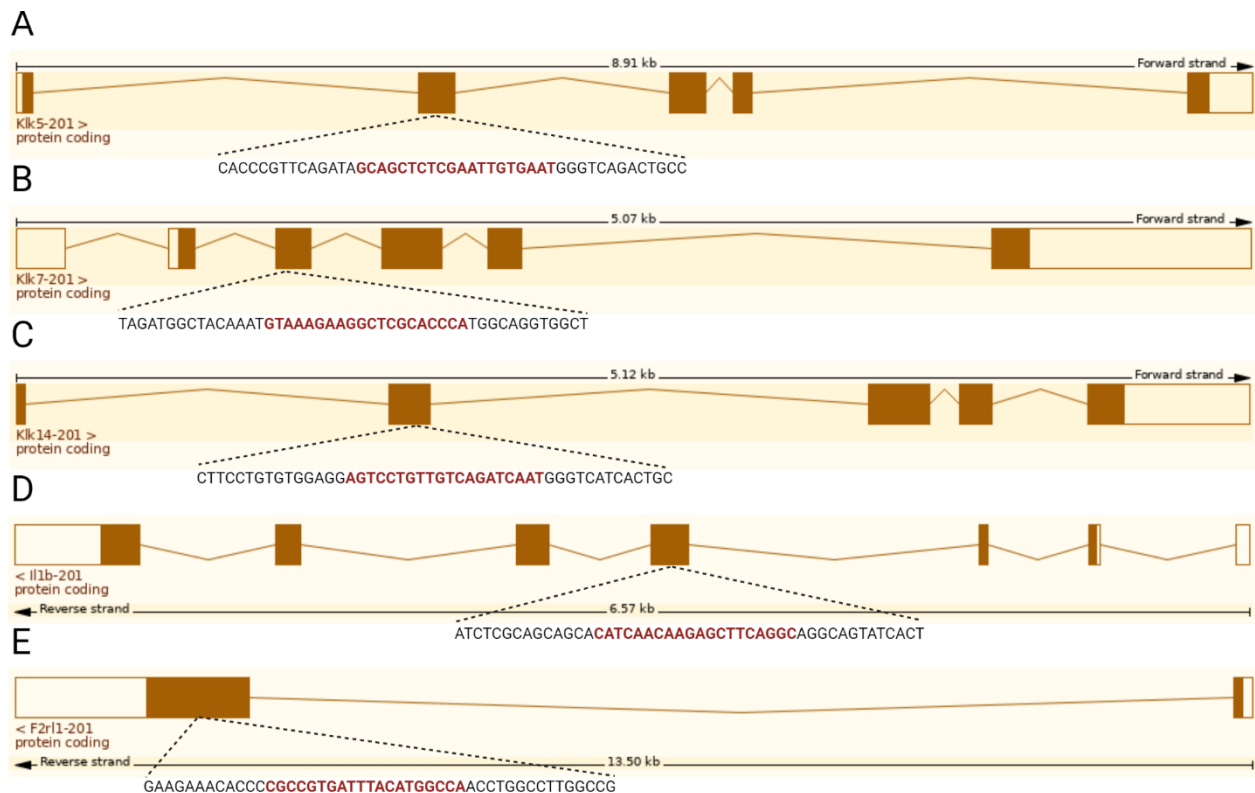


Figure 4.21. CRISPR guide RNAs loci; gRNA locus in exon 2 of *Klk5* gene (A); gRNA locus in exon 3 of *Klk7* gene (B); gRNA locus in exon 2 of *Klk14* gene (C); gRNA locus in exon 4 of *Il1b* gene (D); gRNA locus in exon 2 of *F2rl1* gene (E)

Transfection of the E0771 cell line was performed as described in the 3.2.1 chapter of this thesis. The successfully transfected single clones with transient GFP expression were then sorted by FACS into a conditioned medium in a 96-well plate (Ran et al., 2013). Single clones were further analyzed.

4.5.2 Evaluation of randomly selected knock-out E0771 clones by PCR and PAGE

Clones with mutated target genes were analyzed using agarose and PAGE-based genotyping approaches (Zhu et al., 2015). PCR was performed as described in chapter 3.2.11 with primers in the tab. 3.3. Separation on 2% agarose gel is shown in Fig. 4.22. and 4.23. Clones carrying deletions in target alleles (marked by shifted PCR products upon agarose gel electrophoresis, in red) were further analyzed by PAGE-based genotyping approach, Sanger sequencing, and qPCR to confirm biallelic loss-of-function mutations.

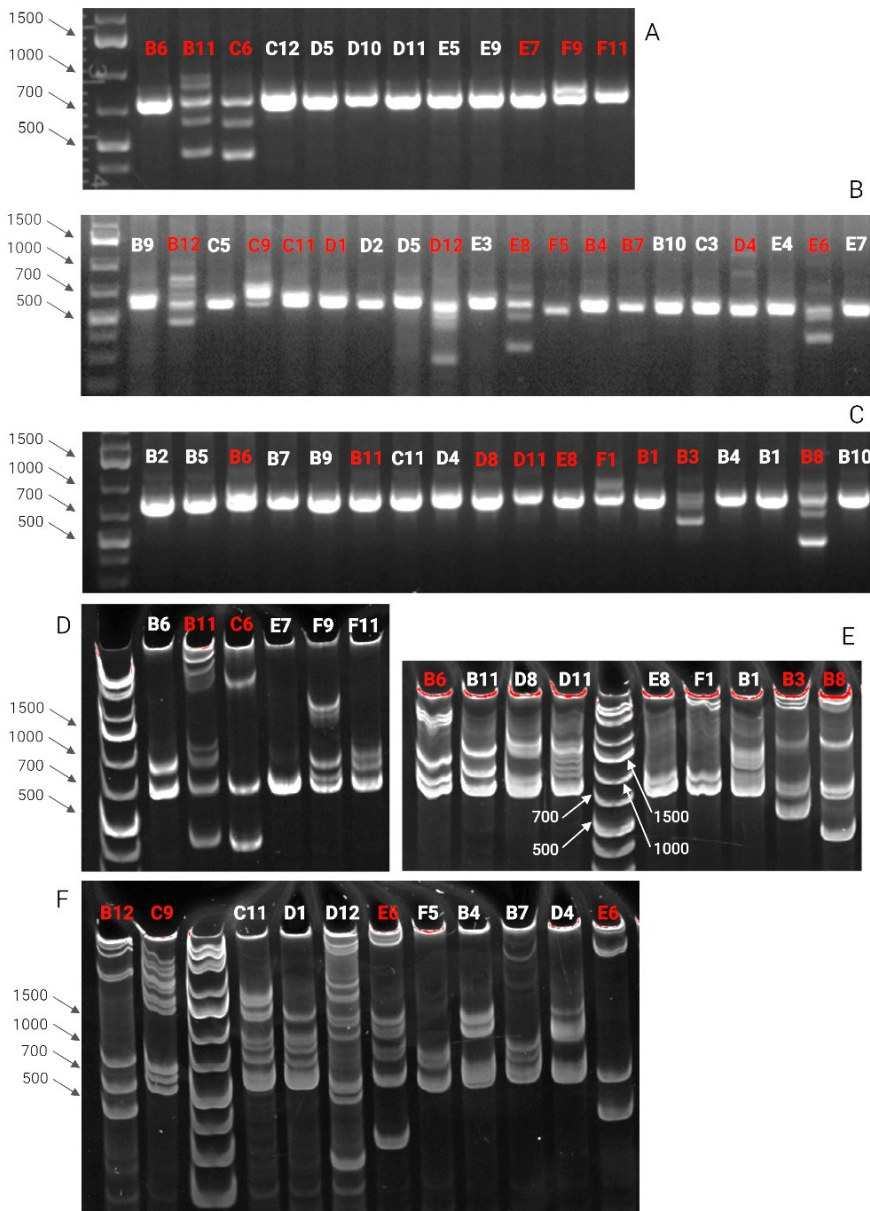


Figure 4.22. Agarose and PAGE-based genotyping approaches for selection of potential *Klk5*, *Klk7*, and *Klk14* KO clones; Agarose separation of PCR products of randomly selected *Klk5* KO clones (A); Agarose separation of PCR products of randomly selected *Klk7* KO clones (B); Agarose separation of PCR products of randomly selected *Klk14* KO clones (C); PAGE separation of PCR products of potential *Klk5* KO clones (D); PAGE separation of PCR products of potential *Klk7* KO clones (E); PAGE separation of PCR products of potential *Klk14* KO clones (F); red-highlighted clones were selected as potential clones for further analysis by PAGE-based genotyping (A, B, C); red-highlighted clones were selected as potential clones for further analysis by sequencing and qRT-PCR (D, E, F)

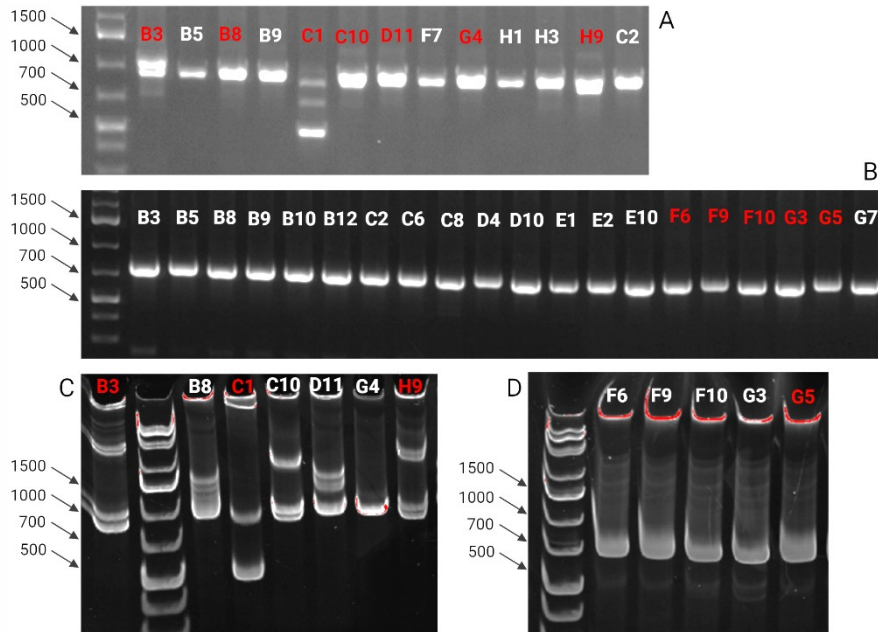


Figure 4.23. Agarose and PAGE-based genotyping approaches for selection of potential *Illb*, and *F2r11* KO clones; Agarose separation of PCR products of randomly selected *Illb* KO clones (A); Agarose separation of PCR products of randomly selected *F2r11* KO clones (B); PAGE separation of PCR products of potential *Illb* KO clones (C); PAGE

separation of PCR products of potential *F2r11* KO clones (D); red-highlighted clones were selected as potential clones for further analysis by PAGE-based genotyping (A, B); red-highlighted clones were selected as potential clones for further analysis by sequencing and qRT-PCR (C, D)

According to PAGE-based genotyping, none of the analyzed clones were mutated in the *F2r11* gene for PAR2 (Fig. 4.23 D). On the contrary, almost all clones analyzed by PAGE-based genotyping were mutated in *Klk5*, *Klk7*, *Klk14* (Fig. 4.22 D–F), and *Illb* (Fig. 4.23 C). The deficiency of the wild-type allele was confirmed as follows.

4.5.3 Evaluation of potential knock-out E0771 clones by sequencing

PCR products of selected clones were further analyzed by Sanger sequencing and chromatograms analyzed by the CRISP-ID web application that allows the detection of insertions, deletions, and location of CRISPR-Cas9 targeted regions (Dehairs et al., 2016). Forward primers pKlk5, pKlk7.2, pKlk14, pF2r11, and pIllb. (Tab. 3.3) were used for sequencing. Sequences of clones with evident deficiency of wild-type allele are shown in Fig. 4.24.

A		
wt	GGACACCCGTTTCAGATAGCAGCTCTCGAATTGTGAATGGGTCAGACTGCCAAAAGGATGCACAGCCATGGCAGGGCG	Klk5
C6	GGACACCCGTTTCAGATAGCAGCTCTCGAATTGTGA-TGGGTCAGACTGCCAAAAGGATGCACAGCCATGGCAGGGCG	-1
B		
wt	TATAGATGGCTACAAATGTAAAGAAGGCTCGCACCCA	TGGCAGGTGGCTCTGCTCAAAGGCAATCAGCTTCACTGTG Klk7
E6	TATAGATGGCTACAAATGTAAAGAAGGC-----CATGGCAGGTGGCTCTGCTCAAAGGCAATCAGCTTCACTGTG	-7
C		
wt	TGTGGAGGAGTCCTGTGTCAGATCAATGGGTCATCACTGCTGCTCATTGTGCCGCCCGTGAGTACTCTTTTTTGT	Klk14
E6	TGTGGAGGAGTCTGTGTCAGATC--TGGGTCATCACTGCTGCTCATTGTGCCGCCCGTGAGTACTCTTTTTTGT	-2
D		
wt	TCCAGCTTCAAATCTCGCAGCAGCATCAACAAGAGCTTCAGGCAGGCAGTATCACTCATTGTGGCTGTGGAGAAG	I11b
H9	TCCAGCTTCAAATCTCGCAGCAGCACATCAACAAG-----GGCAGGCAGTATCACTCATTGTGGCTGTGGAGAAG	-7

Figure 4.24. Sequences of clones with the most apparent deletions in targeted genes; E0771 C6 *Klk5* KO clone (A); E0771 E6 *Klk7* KO clone (B); E0771 E6 *Klk14* KO clone (C); E0771 H9 *Klk7* KO clone (D); the size of deletion on the right side, gRNAs targeting sides are marked yellow

These results confirmed the functionality of designed gRNAs inserted into the pX458 plasmid bearing sequence for the Cas9 protein. Mutated clones selected based on the conclusive results from sequencing were further analyzed by qRT-PCR to evaluate expression levels of mutated genes.

4.5.4 Evaluation of validated *Klk5* and *Klk7* knock-out E0771 clones by qRT-PCR analysis

For qRT-PCR analysis, three *Klk* KO clones were analyzed using primers in tab. 3.4. The three *Klks*' relative mRNA levels were calculated using three housekeeping genes normalization (*Prdx1*, *Actb*, and *GAPDH*) and the $2^{-\Delta Ct}$ analysis method. Expression of *Klk5* and *Klk7* in corresponding KO clones was lowered compared to expression levels in wild-type clones (Fig. 4.25). These results corresponded with the expectation that the expression levels will be reduced due to the determined mutations.

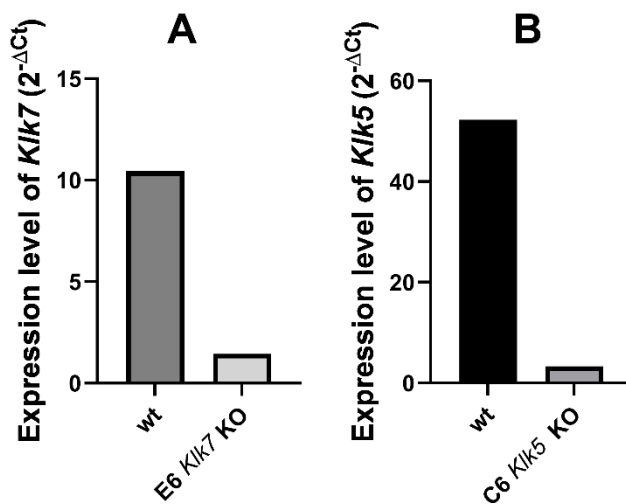


Figure 4.25. Expression levels of *Klk5* and *Klk7* were determined by qRT-PCR using the $2^{-\Delta Ct}$ method; expression level of *Klk5* in E0771 C6 *Klk5* KO clone and wt clone (A); expression level of *Klk7* in E0771 E6 *Klk7* KO clone and wt clone (B)

As a result of this experimental part of the diploma thesis, the E0771 cell lines with mutated *Klk5*, *Klk7*, *Klk14*, and *Il1b* were generated, and various approaches verified their mutations. We assume these generated KO clones can serve as a valuable model for studying KLKs functions in breast cancer

5 Discussion

Immune cells and inflammation significantly influence cancer progression. Most of the results of preclinical *in vivo* studies were obtained using immunodeficient mice. However, such results could be misleading due to an absence of a functional immune system. This may contribute to the low rate of success when introducing anti-cancer drug development into practice.

Using immunocompetent mouse models, C57Bl/6N and BALB/c, our results confirmed that the E0771 cell line is a suitable model for orthotopic cell line-derived allograft experiments in the C57Bl/6N mouse strain. In contrast, the 4T1-Red-FLuc cell line failed to form tumors when used in orthotopic cell line-derived allograft experiments in both C57Bl/6N and BALB/c recipient mouse strains.

Tumor development suppression of the E0771 cell line in BALB/c mice and 4T1-Red-FLuc cell line in C57Bl/6N mice is presumably caused by the allogenic nature of inoculated tumor cells and recipient mouse strain. Whereas there is a publication studying 4T1 cell line inoculation to C57Bl/6 mouse strain (Katsuta et al., 2016), to our knowledge, there is no publication so far with the report of E0771 cell line growth in a BALB/c mouse strain.

The cause of rejection of 4T1-Red-FLuc cells from BALB/c hosts remains unclear. A possible reason could be the insufficient amount of 4T1-Red-FLuc cells injected. Tumor development from this cell line inoculation is reported in Yoo et al., where 5×10^5 4T1-Red-FLuc cells were injected orthotopically into the mammary gland fat pad and evolved into primary tumors (Yoo et al., 2017). Based on our results (chapter 4.1) and literature research, the E0771 cell line was chosen to investigate the role of *Klk* deficiency on the tumor progression in the mouse model based on the C57Bl/6 mouse strain background (Le Naour et al., 2020b).

As a part of this diploma project, optimization of E0771 cells transfection was performed. An optimized transfection protocol allowed us to utilize the NHEJ repair mechanism when generating E0771 “knock-in” clones with various inserted reporter genes under the endogenous *Actb* promoter. Although such an approach is less efficient than homology-

directed repair, it is less laborious, more universal, and even less expensive, as reviewed by Suzuki and Belmonte (Suzuki and Izpisua Belmonte, 2018).

Our *in vitro* experiments with generated fluorescent reporter lines proved that these lines are easily distinguishable when combined with wild-type nonfluorescent cells or when combined with each other (Fig. 4.5). Such an ability provides the potential to use these generated fluorescent reporter lines combined in one experiment. For instance, combining two or more genetically modified clones with different fluorescent markers would allow us to analyze the impact of both of these modifications in uniform conditions, with the ability to distinguish them throughout the whole process (such as metastasizing or preferential growth). However, the differences in the immune response to distinct expressed fluorescent proteins have to be considered during the design of such a project (Day et al., 2014).

The potential of generated fluorescent reporter cell lines as a tool for real-time *in vivo* imaging of breast cancer progression was not fulfilled in this work even though their fluorescence was proved *in vitro*. There are a few possible explanations for this phenomenon. One could be the autofluorescence of mouse skin, disabling the detection of genuinely positive signal, especially in the initial stages of tumor progression (Jun et al., 2017). The second could be the insufficient range of excitation and emission filters provided with the Lago X imaging system in our facility. Filters were set to the closest settings possible for each fluorescent protein used (Tab. 3.6). However, when imperfect filters are combined with the mentioned autofluorescence of mouse tissue, it can be crucial to gaining accurate measurements.

We believe that due to the rapid development of fluorescence imaging methods, the generated fluorescent reporter lines will reach their potential eventually, even in this field of cancer research. Although the generated reporter cell lines could not be used for real-time monitoring of tumor growth, they are still a valuable tool for other *in vivo* experiments. For instance, they can be used to detect metastases in distant organs during autopsy (Fig. 4.8 C), or to evaluate the exact tumor cell fraction in tumor tissue by flow cytometry as described in chapter 4.4.3.

To fulfill our primary intention to prepare an experimental model for real-time *in vivo* imaging, we further focused on luminescent markers. More precisely, classical Firefly Luciferase and the recently developed nanoLuciferase, a small (19 kDa) monomeric enzyme that produces a 100-fold brighter light than Firefly luciferase (England et al., 2016). Although animal tissue strongly absorbs and scatters the light emitted by bioluminescence reactions, the detectable signal is more robust than in the case of fluorescence (Cheong et al., 1990).

Similar to fluorescent proteins, various luciferases can also initiate an immune response, suggesting that the growth of tumors developed from generated Actb-nanoLuc E0771 cells would be inhibited by the immune system of the host (Baklaushev et al., 2017). Surprisingly, our preliminary data show that the tumor growth rate of nanoLuc positive tumors is higher (Fig. 4.12). It is possible that the nanoLuciferase is, unlike its relatives, non-immunogenic, as we found no evidence of it in the literature. However, the anti-tumor immune response is a very complicated, and the heterogeneous field of immunology is full of variable regulatory interactions. Thus, the reason for the higher growth rate is unclear and more samples would need to be evaluated.

Unexpectedly, our data indicate that the size of the tumors (measured with a caliper) did not correlate with their luminescence levels. This was likely caused by suboptimal intraperitoneal administration of luciferase substrate. The luciferase substrate's availability to tumor cells is then dependent on uptake from the peritoneum and distribution via the host's bloodstream. The dynamics of both of these processes can differ between individuals as well.

The horizontal dimensions of tumors reachable by calipers can be precisely measured. However, there is no possibility to measure the depth of the tumors. The third diameter is usually calculated from two horizontal diameters, so the actual tumor size is in fact always estimated. Changes in the luminescence intensity between different measurement time points could provide valuable information about the tumor depth growth.

A unique murine model for studying various KLKs functions was generated in our laboratory by Mgr. Petr Kasparek, Ph.D. These mice are deficient for various *Klks* and their

combinations. These models give a unique opportunity to study KLKs' function in breast cancer and map their crosstalk with the TIME.

According to our results (Fig. 4.13), *Klks* deficient mice developed more extensive tumors than wild types. In the case of KLK5, it corresponds with the report of its reduced concentration in malignant breast tumors (Avgeris et al., 2011). There are contradictory outcomes about the predictive character of *Klk7* mRNA expression levels. However, our results support those of Holzscheiter and Ejaz, who reported it is lower levels of *Klk7* mRNA and KLK7 protein that indicate the worst prognosis for breast cancer patients (Ejaz et al., 2017; Holzscheiter et al., 2006). The increased size of tumors in *Klk14*^{-/-} was surprising because higher expression levels of *Klk14* are associated with the worst cancer disease outcome. The inconsistency can be caused by partial supplementation of one KLKs function by the increased expression of another. This hypothesis corresponds to the results of our qRT-PCR analysis (Fig.4.14), where the relative expression of *Klk7* mRNA is increased in the *Klk14*^{-/-} cohort. A similar phenomenon is seen for *Klk5* and *Klk7* as well.

Il1b expression was not significantly changed in the tumor tissue of KO mice. However, the detection of IL-1 β protein levels in the tumor tissue harbored more relevant results in these experiments. The protein levels in the tumor tissue are partially dependent on the portion of this protein coming from the host. According to the Western blot analysis (Fig. 4.16), IL-1 β was decreased in all KO mice cohorts, and the same trend, although not that significant, is also seen for downstream I κ B ζ protein. IL-1 β activates T-cells and their cytokine production. When generated by activated antigen-presenting cells, it induces type 1 immune response producing CD8⁺ T-lymphocytes, which are the main effectors of the anti-tumorigenic immune response (Acosta-Rodriguez et al., 2007). Thus, lower levels of IL-1 β could be one of the causes of increased tumor size in KO cohorts.

The origin of IL-1 β reduction could be in the role of KLK7 as a pro-IL-1 β activator (Nylander-Lundqvist and Egelrud, 1997). Additionally, KLK5 causes autoactivation of itself and activation of KLK14 and key player KLK7 (Brattsand et al., 2005).

F2r1l mRNA relative expression level was slightly increased in the *Klk14*^{-/-} cohort (Fig. 4.15). The reason for this could be the downregulation of the PAR2 protein level in the same cohort (Fig. 4.16). However, the role of KLK14 in this process remains unclear.

KLK14 and KLK5 can cleave and activate PAR2, initiating its downstream signaling. However, this would, on the contrary, support the opposite trend of PAR2 protein level distribution. This phenomenon, if it turns out to be significant at all, remains to be further elucidated.

The fraction of tumor cells did not correlate with tumor weight in some of the cohorts (Fig. 4.17). On the other hand, in all cohorts, including wild types, the fraction of tumor cells negatively correlated with the immune cell (CD45+) fraction, suggesting the negligibly low fraction of other than a tumor or immune cells present in the tumor samples. All KO cohorts showed a lower fraction of immune cells than wild-type animals, which corresponds to their increased tumor growth. There is an evident difference between the *klk7^{-/-}* cohort and the *Klk5^{-/-}Klk7^{-/-}* cohort heatmap pattern, suggesting opposing roles for KLK5 and KLK7 on the proportion of immune and tumor cells.

There are two types of NKT cells, as previously described. According to data reported by Georgiev et al., it seems that type I NKT cells are more abundant in the C57Bl/6 mouse strain, whereas the level of NKT type II cells is higher in BALB/c mouse strain (Georgiev et al., 2016). This distribution corresponds with the suggestion that the C57Bl/6 mouse strain prevails more to Th1- response and the BALB/c mouse strain towards Th2- (Sellers et al., 2012). Thus, we assume our analyzed NKT cells in C57Bl/6N mouse tumors are mostly NKT type I cells. NKT I cell fraction reported in results is divided into four subpopulations according to Ly6C and CD4 expression. According to Georgiev et al., Ly6C+ cells are NKT1 cells, which are more anti-tumorigenic, and Ly6C- are NKT2 and NKT17 cells, display a more protumorigenic effect.

In our analysis, the fraction of CD4- Ly6C+ NKT cells was significantly increased in the *Klk7^{-/-}* cohort, while the potential increase is seen even in the *Klk5^{-/-}Klk7^{-/-}* cohort. This subpopulation is potent in tumor rejection and produces soluble effector molecules such as IFN γ , perforin, and granzyme a and b (Georgiev et al., 2016). However, Granzyme a may represent a role of endogenous mediator inducing expression of *Il1b* and providing an interesting link to previously mentioned KLK7-dependent activation of pro-IL-1 β (Metkar et al., 2008). Additionally, the more abundant Treg fraction, which possesses a more

significant protumorigenic effect, is increased in both mentioned cohorts. Thus, the antitumorigenic contribution of this subpopulation can be easily smothered.

Ly6C⁻ CD4⁺ and CD4⁻ represent the protumorigenic power of NKT I cells and are significantly elevated in the *Klk5^{-/-}Klk7^{-/-}* cohort and the *Klk7^{-/-}* cohort, respectively. These subpopulations can partially contribute to increased tumor progression in these cohorts. However, their overall low fraction fundamentally lowers their possible effect.

Nonneutrophil myeloid CD11b⁺ Ly6G low cells can be marked as monocytic MDSCs or MDCs (precursors of MDSCs) (Ouzounova et al., 2017). They promote tumor proliferation, stimulate angiogenesis, and suppress anti-tumor immunity. CD11b⁺ Ly6G low cell fraction was significantly lower in the *Klk7^{-/-}* cohort compared to all others, contraindicating with the increased tumor progression in the *Klk7^{-/-}* cohort. Nevertheless, according to Wu and Chiang's publication, this immune cell population's depletion does not impede tumor growth (Wu and Chiang, 2019).

Moreover, looking at CD11b⁺ Ly6G low and eosinophil fractions, there is an opposite trend of these two populations throughout all cohorts. Following the gating strategy, both of these cohorts were determined from the same parental population, and so a possibility of substitution cannot be ruled out. The cytometric panel focusing on myeloid cell populations should be used in the following experiments to answer questions according to these myeloid populations.

The host initiates the antitumor immune response. However, the immune response is highly modulated by the tumor itself. Besides the *Klk* deficient hosts, it would also be valuable to look at the reverse side of the coin, the *Klk* deficient tumor. A combination of both experimental settings would give a more complex view on the KLKs function in the TIME and the possibility to determine the differences between their function on both sides of the immune-tumor crosstalk.

The E0771 cell line was chosen for the preparation of various *Klks* deficient cell lines having the potential to study the KLKs function at the tumor site. Generated *Klk5*, *Klk7*, *Klk14*, and *Il1b* “knock-out” clones were prepared, precisely analyzed, as shown in chapter 4.5, and already inoculated into wild-type female C57Bl/6N mice. Although the

experiment was not finished on the thesis admission date, the grown tumors will be dissected and analyzed following the same protocol as in chapter 4.4. We believe the obtained data will complete the puzzle and help us find answers to the outlined questions.

6 Conclusions, benefits, and prospects for the future

This work aimed to establish an experimental model for studying the crosstalk of selected KLKs (KLK5, KLK7, and KLK14) with breast cancer TIME in the context of their potential utilization as prognostic and predictive biomarkers in this disease.

Following this goal, the murine E0771 breast cancer cell line was used as a background for generating several fluorescent and luminescent reporter cell lines. These were evaluated for their potential to be used as a valuable tool for *in vivo* experiments in the C57Bl/6 mouse model, such as *in vivo* real-time tumor progression imaging or flow cytometry experiments. Upon our preliminary results, it was assumed the Actb-mCherry E0771, the Actb-EGFP E0771, the Actb-NLSsfEGFP E0771, and the Actb-mTBFP2 E0771 are suitable fluorescent reporter cell lines for identification of tumor cells at experimental end point but not for real-time imaging of tumor growth *in vivo*. In contrast to fluorescent markers, nano-Luciferase (used in Actb-nanoLuc E0771 cells) enabled efficient real-time *in vivo* monitoring of cancer progression.

The Actb-mCherry E0771 cell line was used in the following experiments, allowing us to identify tumor cells precisely. It was concluded that compared to the wt cohort, tumors of the *Klk14*^{-/-} cohort had a significantly elevated fraction of tumor cells. On the contrary, the *Klk7*^{-/-} cohort had the same proportion of tumor and immune cells as the wt cohort, although the tumors were significantly more progressive.

Downregulation of IL-1 β on protein levels in tumors derived from individual *Klk*-deficient strains support its role in KLK-mediated immunogenic effects on cancer progression. The ongoing experiments with generated *Klk* knock-out cell clones to evaluate the role of KLKs at the tumor site will provide missing elements of data to allow us to draw conclusions with improved confidence.

Taken together, this diploma project brings various valuable tools for studying the function of selected KLKs in breast cancer progression in the immunocompetent C57Bl/6N mouse model. This is supported with the analysis of the first set of *in vivo* experiments, suggesting that all three examined KLKs (KLK5, KLK7, and KLK14) seem to affect the tumor

progression in E0771 cell line-derived orthotopic allografts with strong suspicions that the activation of the IL-1 β pathway is involved. These findings support the idea of using *Klks* expression as a prognostic marker in breast cancer.

7 References

Acosta-Rodriguez, E.V., Napolitani, G., Lanzavecchia, A., and Sallusto, F. (2007). Interleukins 1 β and 6 but not transforming growth factor- β are essential for the differentiation of interleukin 17–producing human T helper cells. *Nat. Immunol.* 8, 942–949.

Agerberth, B., Gunne, H., Odeberg, J., Kogner, P., Boman, H.G., and Gudmundsson, G.H. (1995). FALL-39, a putative human peptide antibiotic, is cysteine-free and expressed in bone marrow and testis. *Proc. Natl. Acad. Sci.* 92, 195–199.

*Anderson, E., and Clarke, R.B. (2004). Steroid Receptors and Cell Cycle in Normal Mammary Epithelium. *J. Mammary Gland Biol. Neoplasia* 9, 3–13.

Aoyama, N., Miyoshi, H., Miyachi, H., Sonoshita, M., Okabe, M., and Taketo, M.M. (2018). Transgenic mice that accept Luciferase- or GFP-expressing syngeneic tumor cells at high efficiencies. *Genes Cells* 23, 580–589.

Armogida, S.A., Yannaras, N.M., Melton, A.L., and Srivastava, M.D. (2004). Identification and quantification of innate immune system mediators in human breast milk. *Allergy Asthma Proc.* 25, 297–304.

Avgeris, M., Papachristopoulou, G., Polychronis, A., and Scorilas, A. (2011). Down-regulation of kallikrein-related peptidase 5 (KLK5) expression in breast cancer patients: a biomarker for the differential diagnosis of breast lesions. *Clin. Proteomics* 8, 5.

Bajgain, P., Tawinwung, S., D’Elia, L., Sukumaran, S., Watanabe, N., Hoyos, V., Lulla, P., Brenner, M.K., Leen, A.M., and Vera, J.F. (2018). CAR T cell therapy for breast cancer: harnessing the tumor milieu to drive T cell activation. *J. Immunother. Cancer* 6, 34.

Baklaushev, V.P., Kilpeläinen, A., Petkov, S., Abakumov, M.A., Grinenko, N.F., Yusubalieva, G.M., Latanova, A.A., Gubskiy, I.L., Zabozaev, F.G., Starodubova, E.S., et al. (2017). Luciferase Expression Allows Bioluminescence Imaging But Imposes Limitations on the Orthotopic Mouse (4T1) Model of Breast Cancer. *Sci. Rep.* 7, 7715.

*Balkwill, F.R., Capasso, M., and Hagemann, T. (2012). The tumor microenvironment at a glance. *J. Cell Sci.* 125, 5591–5596.

Belham, C.M., Tate, R.J., Scott, P.H., Pemberton, A.D., Miller, H.R.P., Wadsworth, R.M., Gould, G.W., and Plevin, R. (1996). Trypsin stimulates proteinase-activated receptor-2-dependent and -independent activation of mitogen-activated protein kinases. *Biochem. J.* 320, 939–946.

Ben-Sasson, S.Z., Wang, K., Cohen, J., and Paul, W.E. (2013). IL-1 Strikingly Enhances Antigen-Driven CD4 and CD8 T-Cell Responses. *Cold Spring Harb. Symp. Quant. Biol.* 78, 117–124.

Benzekry, S., Lamont, C., Beheshti, A., Tracz, A., Ebos, J.M.L., Hlatky, L., and Hahnfeldt, P. (2014). Classical Mathematical Models for Description and Prediction of Experimental Tumor Growth. *PLOS Comput. Biol.* *10*, e1003800.

Bolton, S.J., McNulty, C.A., Thomas, R.J., Hewitt, C.R.A., and Wardlaw, A.J. (2003). Expression of and functional responses to protease-activated receptors on human eosinophils. *J. Leukoc. Biol.* *74*, 60–68.

Brattsand, M., Stefansson, K., Lundh, C., Haasum, Y., and Egelrud, T. (2005). A Proteolytic Cascade of Kallikreins in the Stratum Corneum. *J. Invest. Dermatol.* *124*, 198–203.

Bresser, K., Dijkgraaf, F.E., Pritchard, C.E.J., Huijbers, I.J., Song, J.-Y., Rohr, J.C., Scheeren, F.A., and Schumacher, T.N. (2020). A mouse model that is immunologically tolerant to reporter and modifier proteins. *Commun. Biol.* *3*, 273.

Briot, A., Deraison, C., Lacroix, M., Bonnart, C., Robin, A., Besson, C., Dubus, P., and Hovnanian, A. (2009). Kallikrein 5 induces atopic dermatitis-like lesions through PAR2-mediated thymic stromal lymphopoietin expression in Netherton syndrome. *J. Exp. Med.* *206*, 1135–1147.

Brisken, C., Park, S., Vass, T., Lydon, J.P., O'Malley, B.W., and Weinberg, R.A. (1998). A paracrine role for the epithelial progesterone receptor in mammary gland development. *Proc. Natl. Acad. Sci. U. S. A.* *95*, 5076–5081.

Buddenkotte, J., Stroh, C., Engels, I.H., Moormann, C., Shpacovitch, V.M., Seeliger, S., Vergnolle, N., Vestweber, D., Luger, T.A., Schulze-Osthoff, K., et al. (2005). Agonists of Proteinase-Activated Receptor-2 Stimulate Upregulation of Intercellular Cell Adhesion Molecule-1 in Primary Human Keratinocytes via Activation of NF-kappa B. *J. Invest. Dermatol.* *124*, 38–45.

*Carmeliet, P., and Jain, R.K. (2011). Molecular mechanisms and clinical applications of angiogenesis. *Nature* *473*, 298–307.

Carvalho, É., Hugo de Almeida, V., Rondon, A.M.R., Possik, P.A., Viola, J.P.B., and Monteiro, R.Q. (2018). Protease-activated receptor 2 (PAR2) upregulates granulocyte colony stimulating factor (G-CSF) expression in breast cancer cells. *Biochem. Biophys. Res. Commun.* *504*, 270–276.

Casey, A.E., Laster, W.R., and Ross, G.L. (1951). Sustained Enhanced Growth of Carcinoma EO771 in C57 Black Mice. *Exp. Biol. Med.* *77*, 358–362.

*Cha, Y.J., and Koo, J.S. (2020). Role of Tumor-Associated Myeloid Cells in Breast Cancer. *Cells* *9*, 1785.

Cha, H.-R., Lee, J.H., Hensel, J.A., Sawant, A.B., Davis, B.H., Lee, C.M., Deshane, J.S., and Ponnazhagan, S. (2016). Prostate cancer-derived cathelicidin-related antimicrobial peptide facilitates macrophage differentiation and polarization of immature myeloid

progenitors to protumorigenic macrophages: The Role of CRAMP in Prostate Cancer. *The Prostate* 76, 624–636.

Chang, A., Yousef, G.M., Scorilas, A., Grass, L., Sismondi, P., Ponzzone, R., and Diamandis, E.P. (2002). Human kallikrein gene 13 (KLK13) expression by quantitative RT–PCR: an independent indicator of favourable prognosis in breast cancer. *Br. J. Cancer* 86, 1457–1464.

*Chen, D.S., and Mellman, I. (2013). Oncology Meets Immunology: The Cancer-Immunity Cycle. *Immunity* 39, 1–10.

*Chen, X., Zou, X., Qi, G., Tang, Y., Guo, Y., Si, J., and Liang, L. (2018). Roles and Mechanisms of Human Cathelicidin LL-37 in Cancer. *Cell. Physiol. Biochem.* 47, 1060–1073.

*Cheong, W.F., Prahl, S.A., and Welch, A.J. (1990). A review of the optical properties of biological tissues. *IEEE J. Quantum Electron.* 26, 2166–2185.

Concordet, J.-P., and Haeussler, M. (2018). CRISPOR: intuitive guide selection for CRISPR/Cas9 genome editing experiments and screens. *Nucleic Acids Res.* 46, W242–W245.

*Costa, E., Ferreira-Gonçalves, T., Chasqueira, G., Cabrita, A.S., Figueiredo, I.V., and Reis, C.P. (2020). Experimental Models as Refined Translational Tools for Breast Cancer Research. *Sci. Pharm.* 88, 32.

Cowland, J.B., Muta, T., and Borregaard, N. (2006). IL-1 β -Specific Up-Regulation of Neutrophil Gelatinase-Associated Lipocalin Is Controlled by I κ B- ζ . *J. Immunol.* 176, 5559–5566.

Csernok, E., Ai, M., Gross, W.L., Wicklein, D., Petersen, A., Lindner, B., Lamprecht, P., Holle, J.U., and Hellmich, B. (2006). Wegener autoantigen induces maturation of dendritic cells and licenses them for Th1 priming via the protease-activated receptor-2 pathway. *Blood* 107, 4440–4448.

Cui, Z., Cui, Y., Luo, G., Yang, S., Ling, X., Lou, Y., and Sun, X. (2017). Kallikrein-related peptidase 4 contributes to the tumor metastasis of oral squamous cell carcinoma. *Biosci. Biotechnol. Biochem.* 81, 1768–1777.

*Dai, X., Cheng, H., Bai, Z., and Li, J. (2017). Breast Cancer Cell Line Classification and Its Relevance with Breast Tumor Subtyping. *J. Cancer* 8, 3131–3141.

D’andrea, M.R., Rogahn, C.J., and Andrade-Gordon, P. (2000). Localization of Protease-Activated Receptors -1 and -2 in Human Mast Cells: Indications for an Amplified Mast Cell Degranulation Cascade. *Biotech. Histochem.* 75, 85–90.

Day, C.-P., Carter, J., Ohler, Z.W., Bonomi, C., El Meskini, R., Martin, P., Graff-Cherry, C., Feigenbaum, L., Tüting, T., Van Dyke, T., et al. (2014). “Glowing Head” Mice: A

Genetic Tool Enabling Reliable Preclinical Image-Based Evaluation of Cancers in Immunocompetent Allografts. *PLoS ONE* 9, e109956.

DeFea, K.A., Zalevsky, J., Thoma, M.S., Déry, O., Mullins, R.D., and Bunnett, N.W. (2000). β -Arrestin-Dependent Endocytosis of Proteinase-Activated Receptor 2 Is Required for Intracellular Targeting of Activated Erk1/2. *J. Cell Biol.* 148, 1267–1282.

Dehairs, J., Talebi, A., Cherifi, Y., and Swinnen, J.V. (2016). CRISP-ID: decoding CRISPR mediated indels by Sanger sequencing. *Sci. Rep.* 6, 28973.

Deraison, C., Bonnart, C., Lopez, F., Besson, C., Robinson, R., Jayakumar, A., Wagberg, F., Brattsand, M., Hachem, J.P., Leonardsson, G., et al. (2007). LEKTI fragments specifically inhibit KLK5, KLK7, and KLK14 and control desquamation through a pH-dependent interaction. *Mol. Biol. Cell* 18, 3607–3619.

Dexter, D.L., Kowalski, H.M., Blazar, B.A., Fligiel, Z., Vogel, R., and Heppner, G.H. (1978). Heterogeneity of Tumor Cells from a Single Mouse Mammary Tumor. *Cancer Res.* 38, 3174–3181.

*Dinarello, C.A. (2009). Immunological and Inflammatory Functions of the Interleukin-1 Family. *Annu. Rev. Immunol.* 27, 519–550.

*Dinarello, C.A. (2011). Interleukin-1 in the pathogenesis and treatment of inflammatory diseases. *Blood* 117, 3720–3732.

*Dinarello, C.A. (2018). Overview of the IL-1 family in innate inflammation and acquired immunity. *Immunol. Rev.* 281, 8–27.

*Dinarello, C.A., Simon, A., and van der Meer, J.W.M. (2012). Treating inflammation by blocking interleukin-1 in a broad spectrum of diseases. *Nat. Rev. Drug Discov.* 11, 633–652.

Dunne, A., and O’Neill, L.A.J. (2003). The Interleukin-1 Receptor/Toll-Like Receptor Superfamily: Signal Transduction During Inflammation and Host Defense. *Sci. Signal.* 2003, re3–re3.

Ejaz, S., Nasim, F.-H., Ashraf, M., and Ahmad, G. (2017). Down-regulation of hK7 in the sera of breast cancer and benign breast disease patients. *Heliyon* 3, e00356.

England, C.G., Ehlerding, E.B., and Cai, W. (2016). NanoLuc: A Small Luciferase Is Brightening Up the Field of Bioluminescence. *Bioconjug. Chem.* 27, 1175–1187.

*Esteva, F.J., and Hortobagyi, G.N. (2004). Prognostic molecular markers in early breast cancer. *Breast Cancer Res.* 6, 109.

Ferlay, J., Colombet, M., Soerjomataram, I., Mathers, C., Parkin, D.M., Piñeros, M., Znaor, A., and Bray, F. (2019). Estimating the global cancer incidence and mortality in 2018: GLOBOCAN sources and methods. *Int. J. Cancer* 144, 1941–1953.

Filippou, P.S., Karagiannis, G.S., Musrap, N., and Diamandis, E.P. (2016). Kallikrein-related peptidases (KLKs) and the hallmarks of cancer. *Crit. Rev. Clin. Lab. Sci.* *53*, 277–291.

*Franchi, L., Eigenbrod, T., Muñoz-Planillo, R., and Nuñez, G. (2009). The inflammasome: a caspase-1-activation platform that regulates immune responses and disease pathogenesis. *Nat. Immunol.* *10*, 241–247.

Fridlender, Z.G., Sun, J., Kim, S., Kapoor, V., Cheng, G., Ling, L., Worthen, G.S., and Albelda, S.M. (2009). Polarization of Tumor-Associated Neutrophil Phenotype by TGF- β : “N1” versus “N2” TAN. *Cancer Cell* *16*, 183–194.

Gambotto, A., Dworacki, G., Cicinnati, V., Kenniston, T., Steitz, J., Tüting, T., Robbins, P., and DeLeo, A. (2000). Immunogenicity of enhanced green fluorescent protein (EGFP) in BALB/c mice: identification of an H2-Kd-restricted CTL epitope. *Gene Ther.* *7*, 2036–2040.

Georgiev, H., Ravens, I., Benarafa, C., Förster, R., and Bernhardt, G. (2016). Distinct gene expression patterns correlate with developmental and functional traits of iNKT subsets. *Nat. Commun.* *7*, 13116.

Girnita, A., Zheng, H., Grönberg, A., Girnita, L., and Stähle, M. (2012). Identification of the cathelicidin peptide LL-37 as agonist for the type I insulin-like growth factor receptor. *Oncogene* *31*, 352–365.

Gossa, S., Nayak, D., Zinselmeyer, B.H., and McGavern, D.B. (2015). Development of an Immunologically Tolerated Combination of Fluorescent Proteins for In vivo Two-photon Imaging. *Sci. Rep.* *4*, 6664.

Gratio, V., Lorient, C., Virca, G.D., Oikonomopoulou, K., Walker, F., Diamandis, E.P., Hollenberg, M.D., and Darmoul, D. (2011). Kallikrein-Related Peptidase 14 Acts on Proteinase-Activated Receptor 2 to Induce Signaling Pathway in Colon Cancer Cells. *Am. J. Pathol.* *179*, 2625–2636.

Grohar, P.J., Woldemichael, G.M., Griffin, L.B., Mendoza, A., Chen, Q.-R., Yeung, C., Currier, D.G., Davis, S., Khanna, C., Khan, J., et al. (2011). Identification of an Inhibitor of the EWS-FLI1 Oncogenic Transcription Factor by High-Throughput Screening. *JNCI J. Natl. Cancer Inst.* *103*, 962–978.

Guesdon, W., Pezier, T., Menard, S., Nicolosi, A., Le Vern, Y., Silvestre, A., Diana, J., Laurent, F., and Lacroix-Lamandé, S. (2020). *Cryptosporidium parvum* Subverts Antimicrobial Activity of CRAMP by Reducing Its Expression in Neonatal Mice. *Microorganisms* *8*, 1635.

*Gutierrez, C., and Schiff, R. (2011). HER 2: Biology, Detection, and Clinical Implications. *Arch. Pathol. Lab. Med.* *135*, 55–62.

Haddada, M., Draoui, H., Deschamps, L., Walker, F., Delaunay, T., Brattsand, M., Magdolen, V., and Darmoul, D. (2018). Kallikrein-related peptidase 7 overexpression in melanoma cells modulates cell adhesion leading to a malignant phenotype. *Biol. Chem.* *399*, 1099–1105.

*Han, Y., Zhang, Y., Jia, T., and Sun, Y. (2015). Molecular mechanism underlying the tumor-promoting functions of carcinoma-associated fibroblasts. *Tumor Biol.* *36*, 1385–1394.

*Harper, J., and Sainson, R.C.A. (2014). Regulation of the anti-tumour immune response by cancer-associated fibroblasts. *Semin. Cancer Biol.* *25*, 69–77.

Heilborn, J.D., Nilsson, M.F., Jimenez, C.I.C., Sandstedt, B., Borregaard, N., Tham, E., Sørensen, O.E., Weber, G., and Ståhle, M. (2005). Antimicrobial protein hCAP18/LL-37 is highly expressed in breast cancer and is a putative growth factor for epithelial cells. *Int. J. Cancer* *114*, 713–719.

*Hirenallur-Shanthappa, D.K., Ramírez, J.A., and Iritani, B.M. (2017). Immunodeficient Mice. In *Patient Derived Tumor Xenograft Models*, (Elsevier), pp. 57–73.

Holzschneider, L., Biermann, J.C., Kotzsch, M., Prezas, P., Farthmann, J., Baretton, G., Luther, T., Tjan-Heijnen, V.C., Talieri, M., Schmitt, M., et al. (2006). Quantitative Reverse Transcription-PCR Assay for Detection of mRNA Encoding Full-Length Human Tissue Kallikrein 7: Prognostic Relevance of KLK7 mRNA Expression in Breast Cancer 3. *Clin. Chem.* *52*, 1070–1079.

Horn, M., Zbodakova, O., Kasperek, P., Srp, J., Haneckova, R., Hradilek, M., Mares, M., and Sedlacek, R. (2018). Profiling system for skin kallikrein proteolysis applied in gene-deficient mouse models. *Biol. Chem.* *399*, 1085–1089.

Hughes, T., Becknell, B., Freud, A.G., McClory, S., Briercheck, E., Yu, J., Mao, C., Giovenzana, C., Nuovo, G., Wei, L., et al. (2010). Interleukin-1 β Selectively Expands and Sustains Interleukin-22+ Immature Human Natural Killer Cells in Secondary Lymphoid Tissue. *Immunity* *32*, 803–814.

Jean-Quartier, C., Jeanquartier, F., Jurisica, I., and Holzinger, A. (2018). In silico cancer research towards 3R. *BMC Cancer* *18*, 408.

Jin, L., Yuan, R.Q., Fuchs, A., Yao, Y., Joseph, A., Schwall, R., Schnitt, S.J., Guida, A., Hastings, H.M., Andres, J., et al. (1997). Expression of interleukin-1beta in human breast carcinoma. *Cancer* *80*, 421–434.

Johnstone, C.N., Smith, Y.E., Cao, Y., Burrows, A.D., Cross, R.S.N., Ling, X., Redvers, R.P., Doherty, J.P., Eckhardt, B.L., Natoli, A.L., et al. (2015). Functional and molecular characterisation of EO771.LMB tumours, a new C57BL/6-mouse-derived model of spontaneously metastatic mammary cancer. *Dis. Model. Mech.* *8*, 237–251.

Jun, Y.W., Kim, H.R., Reo, Y.J., Dai, M., and Ahn, K.H. (2017). Addressing the autofluorescence issue in deep tissue imaging by two-photon microscopy: the significance of far-red emitting dyes. *Chem Sci* 8, 7696–7704.

Kakarala, K.K., and Jamil, K. (2016). Biased signaling: potential agonist and antagonist of PAR2. *J. Biomol. Struct. Dyn.* 34, 1363–1376.

*Kalluri, R. (2016). The biology and function of fibroblasts in cancer. *Nat. Rev. Cancer* 16, 582–598.

*Kalluri, R., and Weinberg, R.A. (2009). The basics of epithelial-mesenchymal transition. *J. Clin. Invest.* 119, 1420–1428.

Kaplanov, I., Carmi, Y., Kornetsky, R., Shemesh, A., Shurin, G.V., Shurin, M.R., Dinarello, C.A., Voronov, E., and Apte, R.N. (2019). Blocking IL-1 β reverses the immunosuppression in mouse breast cancer and synergizes with anti-PD-1 for tumor abrogation. *Proc. Natl. Acad. Sci.* 116, 1361–1369.

*Kaskova, Z.M., Tsarkova, A.S., and Yampolsky, I.V. (2016). 1001 lights: luciferins, luciferases, their mechanisms of action and applications in chemical analysis, biology and medicine. *Chem. Soc. Rev.* 45, 6048–6077.

Kasperek, P., Ileninova, Z., Zbodakova, O., Kanchev, I., Benada, O., Chalupsky, K., Brattsand, M., Beck, I.M., and Sedlacek, R. (2017). KLK5 and KLK7 Ablation Fully Rescues Lethality of Netherton Syndrome-Like Phenotype. *PLoS Genet.* 13.

Katsuta, E., DeMasi, S.C., Terracina, K.P., Spiegel, S., Phan, G.Q., Bear, H.D., and Takabe, K. (2016). Modified breast cancer model for preclinical immunotherapy studies. *J. Surg. Res.* 204, 467–474.

Kin, N.W., Chen, Y., Stefanov, E.K., Gallo, R.L., and Kearney, J.F. (2011). Cathelin-related antimicrobial peptide differentially regulates T- and B-cell function. *Eur. J. Immunol.* 41, 3006–3016.

Koo, B.-H., Chung, K.-H., Hwang, K.-C., and Kim, D.-S. (2002). Factor Xa induces mitogenesis of coronary artery smooth muscle cell via activation of PAR-2. *FEBS Lett.* 523, 85–89.

*Krijgsman, D., Hokland, M., and Kuppen, P.J.K. (2018). The Role of Natural Killer T Cells in Cancer—A Phenotypical and Functional Approach. *Front. Immunol.* 9, 367.

Kryza, T., Achard, C., Parent, C., Marchand-Adam, S., Guillon-Munos, A., Iochmann, S., Korkmaz, B., Respaud, R., Courty, Y., and Heuzé-Vourc'h, N. (2014). Angiogenesis stimulated by human kallikrein-related peptidase 12 acting *via* a platelet-derived growth factor B-dependent paracrine pathway. *FASEB J.* 28, 740–751.

*Kryza, T., Silva, M.L., Loessner, D., Heuzé-Vourc'h, N., and Clements, J.A. (2016). The kallikrein-related peptidase family: Dysregulation and functions during cancer progression. *Biochimie* 122, 283–299.

Lasfargues, E.Y., and Ozzello, L. (1958). Cultivation of human breast carcinomas. *J. Natl. Cancer Inst.* 21, 1131–1147.

*Lawrence, M.G., Lai, J., and Clements, J.A. (2010). Kallikreins on steroids: structure, function, and hormonal regulation of prostate-specific antigen and the extended kallikrein locus. *Endocr. Rev.* 31, 407–446.

Le Naour, A., Koffi, Y., Diab, M., Le Guennec, D., Rougé, S., Aldekwer, S., Goncalves-Mendes, N., Talvas, J., Farges, M.-C., Caldefie-Chezet, F., et al. (2020a). EO771, the first luminal B mammary cancer cell line from C57BL/6 mice. *Cancer Cell Int.* 20, 328.

Le Naour, A., Rossary, A., and Vasson, M. (2020b). EO771, is it a well-characterized cell line for mouse mammary cancer model? Limit and uncertainty. *Cancer Med.* 9, 8074–8085.

Levental, K.R., Yu, H., Kass, L., Lakins, J.N., Egeblad, M., Erler, J.T., Fong, S.F.T., Csiszar, K., Giaccia, A., Weninger, W., et al. (2009). Matrix Crosslinking Forces Tumor Progression by Enhancing Integrin Signaling. *Cell* 139, 891–906.

Li, X., Liu, J., Wang, Y., Zhang, L., Ning, L., and Feng, Y. (2009). Parallel underexpression of kallikrein 5 and kallikrein 7 mRNA in breast malignancies. *Cancer Sci.* 100, 601–607.

*Lin, H., Liu, A.P., Smith, T.H., and Trejo, J. (2013). Cofactoring and Dimerization of Proteinase-Activated Receptors. *Pharmacol. Rev.* 65, 1198–1213.

Lindner, J.R., Kahn, M.L., Coughlin, S.R., Sambrano, G.R., Schauble, E., Bernstein, D., Foy, D., Hafezi-Moghadam, A., and Ley, K. (2000). Delayed Onset of Inflammation in Protease-Activated Receptor-2-Deficient Mice. *J. Immunol.* 165, 6504–6510.

*Loessner, D., Goettig, P., Preis, S., Felber, J., Bronger, H., Clements, J.A., Dorn, J., and Magdolen, V. (2018). Kallikrein-related peptidases represent attractive therapeutic targets for ovarian cancer. *Expert Opin. Ther. Targets* 22, 745–763.

Lowry, M.B., Guo, C., Borregaard, N., and Gombart, A.F. (2014). Regulation of the human cathelicidin antimicrobial peptide gene by $1\alpha,25$ -dihydroxyvitamin D₃ in primary immune cells. *J. Steroid Biochem. Mol. Biol.* 143, 183–191.

*Lu, P., Takai, K., Weaver, V.M., and Werb, Z. (2011). Extracellular Matrix Degradation and Remodeling in Development and Disease. *Cold Spring Harb. Perspect. Biol.* 3, a005058–a005058.

Ludeman, M.J., Zheng, Y.W., Ishii, K., and Coughlin, S.R. (2004). Regulated Shedding of PAR1 N-terminal Exodomain from Endothelial Cells. *J. Biol. Chem.* 279, 18592–18599.

Madhukar, N.S., Khade, P.K., Huang, L., Gayvert, K., Galletti, G., Stogniew, M., Allen, J.E., Giannakakou, P., and Elemento, O. (2019). A Bayesian machine learning approach for drug target identification using diverse data types. *Nat. Commun.* *10*, 5221.

Mallepell, S., Krust, A., Chambon, P., and Brisken, C. (2006). Paracrine signaling through the epithelial estrogen receptor α is required for proliferation and morphogenesis in the mammary gland. *Proc. Natl. Acad. Sci.* *103*, 2196–2201.

Mangé, A., Dimitrakopoulos, L., Soosaipillai, A., Coopman, P., Diamandis, E.P., and Solassol, J. (2016). An integrated cell line-based discovery strategy identified follistatin and kallikrein 6 as serum biomarker candidates of breast carcinoma. *J. Proteomics* *142*, 114–121.

*Mantovani, A., Barajon, I., and Garlanda, C. (2018). IL-1 and IL-1 regulatory pathways in cancer progression and therapy. *Immunol. Rev.* *281*, 57–61.

Mashkoo, F.C., Al-Asadi, J.N., and Al-Naama, L.M. (2013). Serum level of prostate-specific antigen (PSA) in women with breast cancer. *Cancer Epidemiol.* *37*, 613–618.

Matsumura, M., Bhatt, A.S., Andress, D., Clegg, N., Takayama, T.K., Craik, C.S., and Nelson, P.S. (2005). Substrates of the prostate-specific serine protease prostase/KLK4 defined by positional-scanning peptide libraries. *The Prostate* *62*, 1–13.

Meraz, I.M., Majidi, M., Meng, F., Shao, R., Ha, M.J., Neri, S., Fang, B., Lin, S.H., Tinkey, P.T., Shpall, E.J., et al. (2019). An improved patient-derived xenograft humanized mouse model for evaluation of lung cancer immune responses. *Cancer Immunol. Res.* *7*, 1267–1279.

Metkar, S.S., Mena, C., Pardo, J., Wang, B., Wallich, R., Freudenberg, M., Kim, S., Raja, S.M., Shi, L., Simon, M.M., et al. (2008). Human and Mouse Granzyme A Induce a Proinflammatory Cytokine Response. *Immunity* *29*, 720–733.

Michael, I.P., Sotiropoulou, G., Pampalakis, G., Magklara, A., Ghosh, M., Wasney, G., and Diamandis, E.P. (2005). Biochemical and enzymatic characterization of human kallikrein 5 (hK5), a novel serine protease potentially involved in cancer progression. *J. Biol. Chem.* *280*, 14628–14635.

Mihara, K., Ramachandran, R., Saifeddine, M., Hansen, K.K., Renaux, B., Polley, D., Gibson, S., Vanderboor, C., and Hollenberg, M.D. (2016). Thrombin-Mediated Direct Activation of Proteinase-Activated Receptor-2: Another Target for Thrombin Signaling. *Mol. Pharmacol.* *89*, 606–614.

Miloud, T., Henrich, C., and Hämmerling, G.J. (2007). Quantitative comparison of click beetle and firefly luciferases for in vivo bioluminescence imaging. *J. Biomed. Opt.* *12*, 054018.

*Mocellin, S., Pooley, K.A., and Nitti, D. (2013). Telomerase and the search for the end of cancer. *Trends Mol. Med.* *19*, 125–133.

Morris, D.R., Ding, Y., Ricks, T.K., Gullapalli, A., Wolfe, B.L., and Trejo, J. (2006). Protease-Activated Receptor-2 Is Essential for Factor VIIa and Xa-Induced Signaling, Migration, and Invasion of Breast Cancer Cells. *Cancer Res.* *66*, 307–314.

*Motz, G.T., and Coukos, G. (2013). Deciphering and Reversing Tumor Immune Suppression. *Immunity* *39*, 61–73.

Nakao, S., Kuwano, T., Tsutsumi-Miyahara, C., Ueda, S., Kimura, Y.N., Hamano, S., Sonoda, K., Saijo, Y., Nukiwa, T., Strieter, R.M., et al. (2005). Infiltration of COX-2-expressing macrophages is a prerequisite for IL-1 β -induced neovascularization and tumor growth. *J. Clin. Invest.* *115*, 2979–2991.

*Netea, M.G., van de Veerdonk, F.L., van der Meer, J.W.M., Dinarello, C.A., and Joosten, L.A.B. (2015). Inflammasome-Independent Regulation of IL-1-Family Cytokines. *Annu. Rev. Immunol.* *33*, 49–77.

Niu, Y., Yeh, S., Miyamoto, H., Li, G., Altuwajiri, S., Yuan, J., Han, R., Ma, T., Kuo, H.-C., and Chang, C. (2008). Tissue Prostate-Specific Antigen Facilitates Refractory Prostate Tumor Progression via Enhancing ARA70-Regulated Androgen Receptor Transactivation. *Cancer Res.* *68*, 7110–7119.

*Noy, R., and Pollard, J.W. (2014). Tumor-Associated Macrophages: From Mechanisms to Therapy. *Immunity* *41*, 49–61.

Nylander-Lundqvist, E., and Egelrud, T. (1997). Formation of active IL-1 beta from pro-IL-1 beta catalyzed by stratum corneum chymotryptic enzyme in vitro. *Acta Derm. Venereol.* *77*, 203–206.

Nystedt, S., Emilsson, K., Larsson, A.-K., Strombeck, B., and Sundelin, J. (1995). Molecular Cloning and Functional Expression of the Gene Encoding the Human Proteinase-Activated Receptor 2. *Eur. J. Biochem.* *232*, 84–89.

*Oikonomopoulou, K., Hansen, K.K., Saifeddine, M., Vergnolle, N., Tea, I., Blaber, M., Blaber, S.I., Scarisbrick, I., Diamandis, E.P., and Hollenberg, M.D. (2006). Kallikrein-mediated cell signalling: targeting proteinase-activated receptors (PARs). *Biol. Chem.* *387*.

Oikonomopoulou, K., DeAngelis, R.A., Chen, H., Diamandis, E.P., Hollenberg, M.D., Ricklin, D., and Lambris, J.D. (2013). Induction of Complement C3a Receptor Responses by Kallikrein-Related Peptidase 14. *J. Immunol.* *191*, 3858–3866.

*Oldham, W.M., and Hamm, H.E. (2008). Heterotrimeric G protein activation by G-protein-coupled receptors. *Nat. Rev. Mol. Cell Biol.* *9*, 60–71.

Ombrato, L., Nolan, E., Kurelac, I., Mavousian, A., Bridgeman, V.L., Heinze, I., Chakravarty, P., Horswell, S., Gonzalez-Gualda, E., Maticchione, G., et al. (2019). Metastatic-niche labelling reveals parenchymal cells with stem features. *Nature* *572*, 603–608.

Ouzounova, M., Lee, E., Piranlioglu, R., El Andaloussi, A., Kolhe, R., Demirci, M.F., Marasco, D., Asm, I., Chadli, A., Hassan, K.A., et al. (2017). Monocytic and granulocytic myeloid derived suppressor cells differentially regulate spatiotemporal tumour plasticity during metastatic cascade. *Nat. Commun.* *8*, 14979.

*Palucka, K., and Banchereau, J. (2013). Dendritic-Cell-Based Therapeutic Cancer Vaccines. *Immunity* *39*, 38–48.

Pan, W.L., Wang, Y., Hao, Y., Wong, J.H., Chan, W.C., Wan, D.C.-C., and Ng, T.B. (2018). Overexpression of CXCR4 synergizes with LL-37 in the metastasis of breast cancer cells. *Biochim. Biophys. Acta BBA - Mol. Basis Dis.* *1864*, 3837–3846.

Pantschenko, A.G., Pushkar, I., Anderson, K.H., Wang, Y., Miller, L.J., Kurtzman, S.H., Barrows, G., and Kreutzer, D.L. (2003). The interleukin-1 family of cytokines and receptors in human breast cancer: implications for tumor progression. *Int. J. Oncol.* *23*, 269–284.

Papachristopoulou, G., Avgeris, M., and Scorilas, A. (2009). Expression analysis and study of KLK4 in benign and malignant breast tumours. *Thromb. Haemost.* *101*, 381–387.

Papachristopoulou, G., Avgeris, M., Charlaftis, A., and Scorilas, A. (2011). Quantitative expression analysis and study of the novel human kallikrein-related peptidase 14 gene (KLK14) in malignant and benign breast tissues. *Thromb. Haemost.* *105*, 131–137.

Pestonjamas, V.K., Huttner, K.H., and Gallo, R.L. (2001). Processing site and gene structure for the murine antimicrobial peptide CRAMP. *Peptides* *22*, 1643–1650.

*Piktel, E., Niemirowicz, K., Wnorowska, U., Wątek, M., Wollny, T., Głuszek, K., Gózdź, S., Levental, I., and Bucki, R. (2016). The Role of Cathelicidin LL-37 in Cancer Development. *Arch. Immunol. Ther. Exp. (Warsz.)* *64*, 33–46.

*Pio, R., Ajona, D., Ortiz-Espinosa, S., Mantovani, A., and Lambris, J.D. (2019). Complementing the Cancer-Immunity Cycle. *Front. Immunol.* *10*, 774.

*Potenta, S., Zeisberg, E., and Kalluri, R. (2008). The role of endothelial-to-mesenchymal transition in cancer progression. *Br. J. Cancer* *99*, 1375–1379.

Ramani, V.C., and Haun, R.S. (2008). The extracellular matrix protein fibronectin is a substrate for kallikrein 7. *Biochem. Biophys. Res. Commun.* *369*, 1169–1173.

Ramelli, G., Fuertes, S., Narayan, S., Busso, N., Acha-Orbea, H., and So, A. (2010). Protease-activated receptor 2 signalling promotes dendritic cell antigen transport and T-cell activation *in vivo*. *Immunology* *129*, 20–27.

Ran, F.A., Hsu, P.D., Wright, J., Agarwala, V., Scott, D.A., and Zhang, F. (2013). Genome engineering using the CRISPR-Cas9 system. *Nat. Protoc.* *8*, 2281–2308.

*Rayees, S., Rochford, I., Joshi, J.C., Joshi, B., Banerjee, S., and Mehta, D. (2020). Macrophage TLR4 and PAR2 Signaling: Role in Regulating Vascular Inflammatory Injury and Repair. *Front. Immunol.* *11*, 2091.

*R  b  , C., and Ghiringhelli, F. (2020). Interleukin-1   and Cancer. *Cancers* *12*, 1791.

Schenk, M., Fabri, M., Krutzik, S.R., Lee, D.J., Vu, D.M., Sieling, P.A., Montoya, D., Liu, P.T., and Modlin, R.L. (2014). Interleukin-1   triggers the differentiation of macrophages with enhanced capacity to present mycobacterial antigen to T cells. *Immunology* *141*, 174–180.

*Schmitt, M., Magdolen, V., Yang, F., Kiechle, M., Bayani, J., Yousef, G.M., Scorilas, A., Diamandis, E.P., and Dorn, J. (2013). Emerging clinical importance of the cancer biomarkers kallikrein-related peptidases (KLK) in female and male reproductive organ malignancies. *Radiol. Oncol.* *47*, 319–329.

*Sellers, R.S., Clifford, C.B., Treuting, P.M., and Brayton, C. (2012). Immunological Variation Between Inbred Laboratory Mouse Strains: Points to Consider in Phenotyping Genetically Immunomodified Mice. *Vet. Pathol.* *49*, 32–43.

Shaner, N.C., Steinbach, P.A., and Tsien, R.Y. (2005). A guide to choosing fluorescent proteins. *Nat. Methods* *2*, 905–909.

Shaw, J.L., and Diamandis, E.P. (2007). Distribution of 15 Human Kallikreins in Tissues and Biological Fluids. *Clin. Chem.* *53*, 1423–1432.

Shpacovitch, V.M., Varga, G., Strey, A., Gunzer, M., Mooren, F., Buddenkotte, J., Vergnolle, N., Sommerhoff, C.P., Grabbe, S., Gerke, V., et al. (2004). Agonists of proteinase-activated receptor-2 modulate human neutrophil cytokine secretion, expression of cell adhesion molecules, and migration within 3-D collagen lattices. *J. Leukoc. Biol.* *76*, 388–398.

Shpacovitch, V.M., Feld, M., Holzinger, D., Kido, M., Hollenberg, M.D., Levi-Schaffer, F., Vergnolle, N., Ludwig, S., Roth, J., Luger, T., et al. (2011). Role of proteinase-activated receptor-2 in anti-bacterial and immunomodulatory effects of interferon-   on human neutrophils and monocytes: PAR2 and anti-microbial defence of human leucocytes. *Immunology* *133*, 329–339.

Skelton, D., Satake, N., and Kohn, D. (2001). The enhanced green fluorescent protein (eGFP) is minimally immunogenic in C57BL/6 mice. *Gene Ther.* *8*, 1813–1814.

Slamon, D.J., Clark, G.M., Wong, S.G., Levin, W.J., Ullrich, A., and McGuire, W.L. (1987). Human breast cancer: correlation of relapse and survival with amplification of the HER-2/neu oncogene. *Science* *235*, 177–182.

*Solinas, C., Gombos, A., Latifyan, S., Piccart-Gebhart, M., Kok, M., and Buisseret, L. (2017). Targeting immune checkpoints in breast cancer: an update of early results. *ESMO Open* *2*, e000255.

Sørensen, O.E., Follin, P., Johnsen, A.H., Calafat, J., Tjabringa, G.S., Hiemstra, P.S., and Borregaard, N. (2001). Human cathelicidin, hCAP-18, is processed to the antimicrobial peptide LL-37 by extracellular cleavage with proteinase 3. *Blood* 97, 3951–3959.

*Sotiropoulou, G., and Pampalakis, G. (2010). Kallikrein-related peptidases: bridges between immune functions and extracellular matrix degradation. *Biol. Chem.* 391.

Soule, H.D., Vazquez, J., Long, A., Albert, S., and Brennan, M. (1973). A Human Cell Line From a Pleural Effusion Derived From a Breast Carcinoma 2. *JNCI J. Natl. Cancer Inst.* 51, 1409–1416.

Spinetti, G., Fortunato, O., Cordella, D., Portararo, P., Kränkel, N., Katare, R., Sala-Newby, G.B., Richer, C., Vincent, M.-P., Alhenc-Gelas, F., et al. (2011). Tissue Kallikrein Is Essential for Invasive Capacity of Circulating Proangiogenic Cells. *Circ. Res.* 108, 284–293.

*Stefanini, A.C.B., da Cunha, B.R., Henrique, T., and Tajara, E.H. (2015). Involvement of Kallikrein-Related Peptidases in Normal and Pathologic Processes. *Dis. Markers* 2015, 1–17.

*Steinhoff, M., Buddenkotte, J., Shpacovitch, V., Rattenholl, A., Moormann, C., Vergnolle, N., Luger, T.A., and Hollenberg, M.D. (2005). Proteinase-Activated Receptors: Transducers of Proteinase-Mediated Signaling in Inflammation and Immune Response. *Endocr. Rev.* 26, 1–43.

Stripecke, R., del Carmen Villacres, M., Skelton, D.C., Satake, N., Halene, S., and Kohn, D.B. (1999). Immune response to green fluorescent protein: implications for gene therapy. *Gene Ther.* 6, 1305–1312.

Su, S., Li, Y., Luo, Y., Sheng, Y., Su, Y., Padia, R., Pan, Z., Dong, Z., and Huang, S. (2009). Proteinase-Activated Receptor 2 Expression in Breast Cancer and Its Role in Breast Cancer Cell Migration. *Oncogene* 28, 3047–3057.

Suetsugu, A., Osawa, Y., Nagaki, M., Moriwaki, H., Saji, S., Bouvet, M., and Hoffman, R.M. (2010). Simultaneous color-coded imaging to distinguish cancer “stem-like” and non-stem cells in the same tumor. *J. Cell. Biochem.* 111, 1035–1041.

Sun, Y., Fan, X., Zhang, Q., Shi, X., Xu, G., and Zou, C. (2017). Cancer-associated fibroblasts secrete FGF-1 to promote ovarian proliferation, migration, and invasion through the activation of FGF-1/FGFR4 signaling. *Tumor Biol.* 39, 101042831771259.

Sutkowski, D.M., Goode, R.L., Baniel, J., Teater, C., Cohen, P., McNulty, A.M., Hsiung, H.M., Becker, G.W., and Neubauer, B.L. (1999). Growth regulation of prostatic stromal cells by prostate-specific antigen. *J. Natl. Cancer Inst.* 91, 1663–1669.

Suzuki, K., and Izpisua Belmonte, J.C. (2018). In vivo genome editing via the HITI method as a tool for gene therapy. *J. Hum. Genet.* 63, 157–164.

*Swartz, M.A., and Lund, A.W. (2012). Lymphatic and interstitial flow in the tumour microenvironment: linking mechanobiology with immunity. *Nat. Rev. Cancer* 12, 210–219.

Takács, L., Kovacs, E.J., Smith, M.R., Young, H.A., and Durum, S.K. (1988). Detection of IL-1 alpha and IL-1 beta gene expression by in situ hybridization. Tissue localization of IL-1 mRNA in the normal C57BL/6 mouse. *J. Immunol. Baltim. Md 1950* 141, 3081–3095.

Talieri, M., Diamandis, E., Gourgiotis, D., Mathioudaki, K., and Scorilas, A. (2004). Expression analysis of the human kallikrein 7 (KLK7) in breast tumors: a new potential biomarker for prognosis of breast carcinoma. *Thromb. Haemost.* 91, 180–186.

*Testa, U., Castelli, G., and Pelosi, E. (2020). Breast Cancer: A Molecularly Heterogenous Disease Needing Subtype-Specific Treatments. *Med. Sci.* 8, 18.

*Tian, T., Olson, S., Whitacre, J.M., and Harding, A. (2011). The origins of cancer robustness and evolvability. *Integr Biol* 3, 17–30.

Tsang, J.Y.S., and Tse, G.M. (2020). Molecular Classification of Breast Cancer. *Adv. Anat. Pathol.* 27, 27–35.

Tulotta, C., Lefley, D.V., Freeman, K., Gregory, W.M., Hanby, A.M., Heath, P.R., Nutter, F., Wilkinson, J.M., Spicer-Hadlington, A.R., Liu, X., et al. (2019). Endogenous Production of IL1B by Breast Cancer Cells Drives Metastasis and Colonization of the Bone Microenvironment. *Clin. Cancer Res. Off. J. Am. Assoc. Cancer Res.* 25, 2769–2782.

Turner, J., Cho, Y., Dinh, N.-N., Waring, A.J., and Lehrer, R.I. (1998). Activities of LL-37, a Cathelin-Associated Antimicrobial Peptide of Human Neutrophils. *Antimicrob. Agents Chemother.* 42, 2206–2214.

Tyan, S.-W., Kuo, W.-H., Huang, C.-K., Pan, C.-C., Shew, J.-Y., Chang, K.-J., Lee, E.Y.-H.P., and Lee, W.-H. (2011). Breast Cancer Cells Induce Cancer-Associated Fibroblasts to Secrete Hepatocyte Growth Factor to Enhance Breast Tumorigenesis. *PLoS ONE* 6, e15313.

Untergasser, A., Nijveen, H., Rao, X., Bisseling, T., Geurts, R., and Leunissen, J.A.M. (2007). Primer3Plus, an enhanced web interface to Primer3. *Nucleic Acids Res.* 35, W71–W74.

Van Damme, J., De Ley, M., Opdenakker, G., Billiau, A., De Somer, P., and Beeumen, J.V. (1985). Homogeneous interferon-inducing 22K factor is related to endogenous pyrogen and interleukin-1. *Nature* 314, 266–268.

*Vandamme, D., Landuyt, B., Luyten, W., and Schoofs, L. (2012). A comprehensive summary of LL-37, the factotum human cathelicidin peptide. *Cell. Immunol.* 280, 22–35.

*Velonas, V., Woo, H., Remedios, C., and Assinder, S. (2013). Current Status of Biomarkers for Prostate Cancer. *Int. J. Mol. Sci.* 14, 11034–11060.

Versteeg, H.H., Schaffner, F., Kerver, M., Petersen, H.H., Ahamed, J., Felding-Habermann, B., Takada, Y., Mueller, B.M., and Ruf, W. (2008). Inhibition of tissue factor signaling suppresses tumor growth. *Blood* *111*, 190–199.

Vu, T.-K.H., Hung, D.T., Wheaton, V.I., and Coughlin, S.R. (1991). Molecular cloning of a functional thrombin receptor reveals a novel proteolytic mechanism of receptor activation. *Cell* *64*, 1057–1068.

Wang, H.Y., and Wang, R.-F. (2007). Regulatory T cells and cancer. *Curr. Opin. Immunol.* *19*, 217–223.

Weber, G., Chamorro, C.I., Granath, F., Liljegren, A., Zreika, S., Saidak, Z., Sandstedt, B., Rotstein, S., Mentaverri, R., Sánchez, F., et al. (2009). Human antimicrobial protein hCAP18/LL-37 promotes a metastatic phenotype in breast cancer. *Breast Cancer Res.* *11*, R6.

Weichand, B., Popp, R., Dziumbila, S., Mora, J., Strack, E., Elwakeel, E., Frank, A.-C., Scholich, K., Pierre, S., Syed, S.N., et al. (2017). S1PR1 on tumor-associated macrophages promotes lymphangiogenesis and metastasis via NLRP3/IL-1 β . *J. Exp. Med.* *214*, 2695–2713.

Wu, S.-Y., and Chiang, C.-S. (2019). Distinct Role of CD11b+Ly6G–Ly6C– Myeloid-Derived Cells on the Progression of the Primary Tumor and Therapy-Associated Recurrent Brain Tumor. *Cells* *9*, 51.

*Wu, Q., Li, B., Li, Z., Li, J., Sun, S., and Sun, S. (2019). Cancer-associated adipocytes: key players in breast cancer progression. *J. Hematol. Oncol.* *J Hematol Oncol* *12*, 95.

*Wu, S.-Y., Fu, T., Jiang, Y.-Z., and Shao, Z.-M. (2020). Natural killer cells in cancer biology and therapy. *Mol. Cancer* *19*, 120.

Xiang, Y., Yao, X., Chen, K., Wang, X., Zhou, J., Gong, W., Yoshimura, T., Huang, J., Wang, R., Wu, Y., et al. (2016). The G-protein coupled chemoattractant receptor FPR2 promotes malignant phenotype of human colon cancer cells. *Am. J. Cancer Res.* *6*, 2599–2610.

Yamasaki, K., Schaubert, J., Coda, A., Lin, H., Dorschner, R.A., Schechter, N.M., Bonnart, C., Descargues, P., Hovnanian, A., and Gallo, R.L. (2006). Kallikrein-mediated proteolysis regulates the antimicrobial effects of cathelicidins in skin. *FASEB J.* *20*, 2068–2080.

*Yang, B., Good, D., Mosaiab, T., Liu, W., Ni, G., Kaur, J., Liu, X., Jessop, C., Yang, L., Fadhil, R., et al. (2020). Significance of LL-37 on Immunomodulation and Disease Outcome. *BioMed Res. Int.* *2020*, 1–16.

Yang, D., Chen, Q., Schmidt, A.P., Anderson, G.M., Wang, J.M., Wooters, J., Oppenheim, J.J., and Chertov, O. (2000). LL-37, the Neutrophil Granule–And Epithelial Cell–Derived Cathelicidin, Utilizes Formyl Peptide Receptor–Like 1 (Fprl1) as a Receptor to

Chemoattract Human Peripheral Blood Neutrophils, Monocytes, and T Cells. *J. Exp. Med.* *192*, 1069–1074.

Yoo, B., Kavishwar, A., Wang, P., Ross, A., Pantazopoulos, P., Dudley, M., Moore, A., and Medarova, Z. (2017). Therapy targeted to the metastatic niche is effective in a model of stage IV breast cancer. *Sci. Rep.* *7*, 45060.

Yoon, H., Laxmikanthan, G., Lee, J., Blaber, S.I., Rodriguez, A., Kogot, J.M., Scarisbrick, I.A., and Blaber, M. (2007). Activation Profiles and Regulatory Cascades of the Human Kallikrein-related Peptidases*. *J. Biol. Chem.* *282*, 31852–31864.

Yousef, G.M., and Diamandis, E.P. (2001). The New Human Tissue Kallikrein Gene Family: Structure, Function, and Association to Disease. *Endocr. Rev.* *22*, 184–204.

Yousef, G.M., Polymeris, M.-E., Grass, L., Soosaipillai, A., Chan, P.-C., Scorilas, A., Borgoño, C., Harbeck, N., Schmalfeldt, B., Dorn, J., et al. (2003a). Human kallikrein 5: a potential novel serum biomarker for breast and ovarian cancer. *Cancer Res.* *63*, 3958–3965.

Yousef, G.M., Scorilas, A., Nakamura, T., Abd Ellatif, M., Ponzzone, R., Biglia, N., Maggiorotto, F., Roagna, R., Sismondi, P., and Diamandis, E.P. (2003b). The Prognostic Value of the Human Kallikrein Gene 9 (KLK9) in Breast Cancer. *Breast Cancer Res. Treat.* *78*, 149–158.

Yousef, G.M., Yacoub, G.M., Polymeris, M.-E., Popalis, C., Soosaipillai, A., and Diamandis, E.P. (2004). Kallikrein gene downregulation in breast cancer. *Br. J. Cancer* *90*, 167–172.

Yu, Y., Xiao, C.-H., Tan, L.-D., Wang, Q.-S., Li, X.-Q., and Feng, Y.-M. (2014). Cancer-associated fibroblasts induce epithelial–mesenchymal transition of breast cancer cells through paracrine TGF- β signalling. *Br. J. Cancer* *110*, 724–732.

*Zeng, L., Li, W., and Chen, C.-S. (2020). Breast cancer animal models and applications. *Zool. Res.* *41*, 477–494.

*Zhang, Y., Bhat, I., Zeng, M., Jayal, G., Wazer, D.E., Band, H., and Band, V. (2006). Human kallikrein 10, a predictive marker for breast cancer. *Biol. Chem.* *387*, 715–721.

Zhu, X., Xu, Y., Yu, S., Lu, L., Ding, M., Cheng, J., Song, G., Gao, X., Yao, L., Fan, D., et al. (2015). An Efficient Genotyping Method for Genome-modified Animals and Human Cells Generated with CRISPR/Cas9 System. *Sci. Rep.* *4*, 6420.

*Zitvogel, L., Galluzzi, L., Smyth, M.J., and Kroemer, G. (2013). Mechanism of Action of Conventional and Targeted Anticancer Therapies: Reinstating Immunosurveillance. *Immunity* *39*, 74–88.

Zoudilova, M., Kumar, P., Ge, L., Wang, P., Bokoch, G.M., and DeFea, K.A. (2007). β -Arrestin-dependent Regulation of the Cofilin Pathway Downstream of Protease-activated Receptor-2. *J. Biol. Chem.* *282*, 20634–20646.

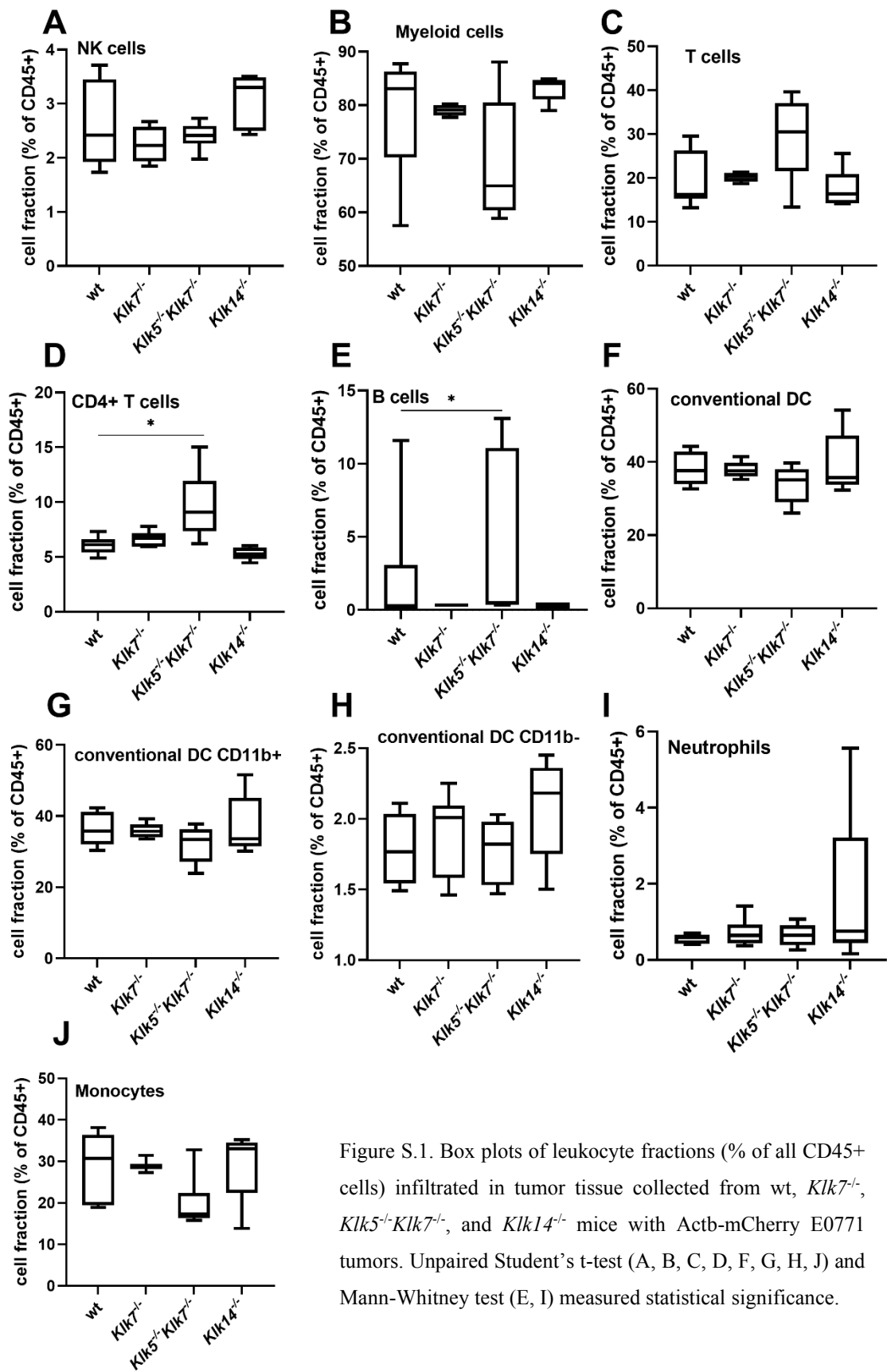


Figure S.1. Box plots of leukocyte fractions (% of all CD45+ cells) infiltrated in tumor tissue collected from wt, *Kik7*^{-/-}, *Kik5*^{-/-}*Kik7*^{-/-}, and *Kik14*^{-/-} mice with Actb-mCherry E0771 tumors. Unpaired Student's t-test (A, B, C, D, F, G, H, J) and Mann-Whitney test (E, I) measured statistical significance.